Variability of the polar stratospheric vortex and its impact on surface climate patterns

by

Aditi Sheshadri

B. E. Mechanical Engineering, R. V. College of Engineering, Bangalore, India

S. M. Aeronautics and Astronautics, Massachusetts Institute of Technology, Cambridge, MA

Submitted to the Department of Earth, Atmospheric and Planetary Sciences

In partial fulfilment of the requirements for the degree of

Doctor of Philosophy

At the

MASSACHUSETTS INSTITUTE OF TECHNOLOGY

June 2015

Signature redacted

Author.....
Department of Earth, Atmospheric and Planetary Sciences
May 26, 2015

Signature redacted

Certified by.....
R. Alan Plumb
Professor of Meteorology
Thesis supervisor

Signature redacted

Accepted by.....
Robert van der Hilst
Schlumberger Professor of Earth Sciences
Head, Department of Earth, Atmospheric and Planetary Sciences

Variability of the polar stratospheric vortex and its impact on surface climate patterns

by

Aditi Sheshadri

Submitted to the Department of Earth, Atmospheric and Planetary Sciences on May 26, 2015 in partial fulfilment of the requirements for the degree of Doctor of Philosophy

Abstract

This thesis investigates various aspects of the variability of the stratospheric polar vortex and the effect of this variability on tropospheric weather and climate patterns on various timescales. In the first part of this work, an improved idealized model was developed to study the coupled stratosphere-troposphere system. The model is forced by relaxation to a specified equilibrium temperature profile, which varies seasonally only in the stratosphere. This model setup permits the investigation of stratosphere-troposphere interactions on seasonal timescales, without the complication of an internal tropospheric seasonal cycle. The model is forced with different shapes and amplitudes of simple bottom topography, resulting in a range of stratospheric climates. The effect of these different kinds of topography on the seasonal variability of the strength of the polar vortex, the average timing and variability in timing of the final breakup of the vortex (final warming events), the conditions of occurrence and frequency of midwinter warming events, and the impact of the stratospheric seasonal cycle on the troposphere are explored. The inclusion of wavenumber 1 and wavenumber 2 topographies results in very different stratospheric seasonal variability. Hemispheric differences in stratospheric seasonal variability are recovered in the model with appropriate choices of wave-2 topography. In the model experiment with a realistic Northern Hemisphere-like frequency of midwinter warming events, the distribution of the intervals between these events suggest that the model has no year to year memory. When forced with wave-1 topography, the gross features of seasonal variability are similar to those forced with wave-2 topography, but the dependence on forcing magnitude is weaker. Further, the frequency of major warming events has a non-monotonic dependence on forcing magnitude, and never reaches the frequency observed in the northern hemisphere.

In the second part of the thesis, the impact of stratospheric ozone depletion on the Antarctic polar vortex and its subsequent influences on southern hemisphere surface climate patterns is investigated. It is verified that stratospheric final warming events have an impact on tropospheric circulation in a simplified GCM with seasonal variations in the stratosphere only. The model produces qualitatively realistic final warming events whose influence extends down to the surface, much like what has been reported in observational analyses. The hypothesis that recent observed trends in surface westerlies in the Southern Hemisphere are directly consequent on observed trends in the timing of stratospheric final warming events is tested. It is confirmed that there is a statistically significant shift towards later final warming events in the years with large ozone depletion. However it is found that the observed trends in surface westerlies cannot be attributed simply to this shift towards later final warming events.

Finally, responses of the idealized AGCM to polar stratospheric cooling that mimics the radiative effects of stratospheric ozone depletion are studied. It is found that there are two factors that play a role in setting the magnitude and persistence of the model's surface response to cooling: the seasonal cycle of tropospheric annular mode timescales, and whether or not the imposed cooling leads to the presence of stratospheric westerlies at a time when easterlies were prevalent in the control run. That is, the surface response is sensitive to the timing of the imposed polar stratospheric cooling.

Thesis supervisor: R. Alan Plumb

Title: Professor of Meteorology

Acknowledgements

I have thoroughly enjoyed the last few years working on my Ph.D. in PAOC, and the completion of this degree would not have occurred without the support of many people, whom I acknowledge below. I got very lucky in my choice of advisor and I begin by thanking him. Alan Plumb is a wonderful research advisor, very calm, kind, and perceptive, and also a very clear teacher. I'm very grateful for the many times that he's suggested a way forward conceptually, and for reading and helping me improve manuscript drafts multiple times. It has been a pleasure working with Alan.

I thank John Marshall, for persuading me to come to PAOC for my Ph.D., for including me in the activities of his own group, and for his general encouragement. His enthusiasm for research is infectious. I'm also very grateful to Susan Solomon for all her support, for many useful discussions, for inviting me to her group meetings, and for trying to teach me some chemistry. I really appreciate Paul O'Gorman's help with answering questions on statistics that came up periodically during my work. Finally, I thank Ed Gerber, for serving as my external committee member even though he was on sabbatical. I have had numerous very useful e-mail exchanges about my research with him and he has patiently dealt with bad internet connections to remotely attend a number of committee meetings and even my defense. I'm also grateful to Tiffany Shaw and Gang Chen for useful discussions at conferences and for their general support.

I greatly appreciate all the help I've had from Greg and Linda with regard to elorenz. Many students and postdocs have contributed in both professional and personal ways to my development over the last few years. I thank Daniela Domeisen, Lantao Sun, and Eric Leibensperger for clarifying various questions over e-mail. Marianna Linz and Brian Green have

patiently proof read and provided useful comments on various drafts. I thank Yavor Kostov, Emily Zakem and Brian for a very friendly office environment, and Yavor, Jareth Holt and Kat Saad, for studying with me for the general examination. I'm also grateful to the other members of Alan's research group – Daniela, Eric, Andy Miller, Marianna Linz, Erik Lindgren, and recently Casey Hilgenbrink, for listening to many practice talks. Martha Buckley and Ryan Abernathey were supportive student mentors in my first year, as were Morgan O'Neill and Marty Singh in my second. Tim Cronin has been a great source of general advice. The Houghton fund and Alan have funded many trips to conferences and summer schools.

On a more personal note, I am deeply grateful to my parents (particularly my father, who has helped me get through every challenge), for their tremendous and constant support for everything I ever wanted to accomplish. This thesis is dedicated to them. My husband and I got married while we were graduate students at MIT, and this campus has been a special place for us. I think our mutual calm acceptance and encouragement of each other's goals and sometimes crazy schedules has contributed to keeping me sane and happy for the last few years, and I am grateful for his companionship.

Contents

List of figures

composite for the time series of polar-cap averaged geopotential height (60°N-90°N), normalized by its standard deviation at each level. (Taken from Kushner, 2010).

Figure 2-1: Snapshot of the equilibrium temperature profile (K) at northern hemisphere winter solstice. The contour interval is 10 K.

Figure 2-2: Seasonal cycle of zonal mean zonal winds (ms^{-1}) at 10 hPa and 50 hPa from the model (h_0=0), with the equilibrium temperature specifications of Kushner and Polvani (2002) in the top panel, from the model with the new equilibrium specifications used in this study in the middle panel, and from ERA-Interim (Southern Hemisphere) in the bottom panel. The contour interval is 2 m/s for the 50hPa winds and 4 m/s for the 10 hPa winds.

Figure 2-3: Latitude pressure structure of DJF winds (ms^{-1}) for Experiment 1 (no topography, top row, left), Experiment 4 (4000 m wave-2, top row, right), and Experiment 6 (4000 m wave-1, bottom row). The white patch at the bottom indicates the extent of topography. The contour interval is 5 m/s.

Figure 2-4: Histogram of 10 hPa zonal mean zonal wind at 60°S in the left panel and 60°N in the right panel for 30 years from the ERA-Interim Reanalysis. Midwinter (June and July for the Southern Hemisphere and December and January for the Northern Hemisphere) is in the center of both histograms. The ordinate shows the number of occurrences of a specific value of zonal mean zonal wind.

Figure 2-5: Histograms of 10 hPa zonal mean zonal wind at 60°N for Experiments 1 (top left), 2 (top right), 3(bottom left), and 4(bottom right). The ordinate shows the number of occurrences of a specific value of zonal mean zonal wind.

Figure 2-6: The climatological evolution of the wave-2 geopotential height amplitude (m) at 10 hPa, 60°N for Experiments 1 (no topography), 2 (2000 m wave-2), 3(3000 m wave-2) and 4 (4000 m wave-2).

Figure 2-7: The climatological evolution of the wave-2 geopotential height amplitude (m) at 95 hPa, 60°N for Experiments 1 (no topography), 2 (2000 m wave-2), 3(3000 m wave-2) and 4 (4000 m wave-2).

Figure 2-8: The seasonal cycle (calendar average) of 50 hPa heat fluxes (mKs^{-1}) for Experiments 1 (no topography, top row, left), 2 (2000 m wave-2, top row, right), 3 (3000 m wave-2, bottom row, left), and 4 (4000 m wave-2, bottom row, right).

Figure 2-9: Evolution of weak vortex events, from Experiment 4 (4000 m wave-2). The top row shows geopotential height anomalies averaged from 65-90°N, normalized by their standard deviations and composited on weak vortex events. The left and right panels of the top row show events that are chosen based on 1σ and 2σ or greater annular mode anomalies at 10 hPa. The contour interval is .25. The bottom row shows heat flux anomalies at 95 hPa normalized by their standard deviations and composited on all 50 weak vortex events. The contour interval is 0.1. The zero level is shown by the heavy black contour in all panels.

Figure 2-10: Evolution of strong vortex events from Experiment 4 (4000 m wave-2). The top panel shows geopotential height anomalies averaged from 65-90°N, normalized by their standard deviations and composited on strong vortex events, defined as 1σ annular mode anomalies at 10 hPa. The contour interval is 0.25. The bottom panel shows heat flux anomalies at 95 hPa, normalized by their standard deviations and composited on strong vortex events. The contour interval is 0.1. The zero level is shown by the heavy black contour in both panels.

Figure 2-11: Histograms of the distribution of the interval (in years) between midwinter warming events from the idealized model (from the experiment with 4000 m wave-2 topography, which had a realistic Northern Hemisphere-like frequency of midwinter warming events) in the left panel and from the ERA Reanalyses in the right panel. Blue bars show the actual distribution of intervals between midwinter warming events in the model run/reanalysis. Grey bars show the distribution of intervals between midwinter warming events from the random time series of 0s and 1s with a given probability. The grey dots are the 95^{th} and 5^{th} percentiles of the samplings from the random sequences of 0s and 1s.

Figure 2-12: Examples of the evolution of 50 hPa geopotential height (m) leading up to and immediately after final warming events. 50 hPa geopotential height is shown 5 days before, the day of, and 5 days after the final warming. These are examples of final warming events from Experiment 1 (no topography, top row), Experiment 2 (2000 m wave-2 topography, second row) and Experiment 3 (3000 m wave-2 topography, bottom row). Experiment 4 (4000 m wave-2 topography) is similar to Experiment 3. The contour interval is 53 m.

Figure 2-13: 50 hPa zonal mean zonal wind at 60°N (ms^{-1}) composited on the final warming for Experiments 1 (no topography), 2 (2000 m wave-2), 3 (3000 m wave-2), and 4 (4000 m wave-2).

Figure 2-14: 50 hPa heat fluxes (mKs^{-1}) composited on final warming events for Experiment 1 (no topography, top row, left), 2 (2000 m wave-2, top row, right), 3 (3000 m wave-2, bottom row, left) and 4(4000 m wave-2, bottom row, right). The white contour indicates the 95% confidence interval for a two sided t-test.

Figure 2-15: Histograms of 10 hPa zonal mean zonal wind at 60°N for Experiments 5 (top left),

6 (top right), 7 (bottom left) and 8 (bottom right). The ordinate shows the number of occurrences of a specific value of zonal mean zonal wind.

Figure 2-16: The climatological evolution of the wave-1 geopotential height amplitude (m) at 10 hPa, 60°N for Experiments 1 (no topography), 5 (2000 m wave-1), 6 (3000 m wave-1), 7 (4000 m wave-1), 4500 m wave-1, Experiment 8 (5000 m wave-1), 5250 m wave-1, 5500 m wave-1 and 6000 m wave-1.

Figure 2-17: Evolution of 50 hPa geopotential height (m) leading up to and immediately after final warming events. 50 hPa geopotential height is shown 5 days before, the day of, and 5 days after the final warming. These are examples of final warming events from Experiment 1 (no topography, top row) and Experiment 5 (3000 m wave-1 topography, bottom row). Experiment 6 (4000 m wave-1 topography) is similar to Experiment 5 (not shown). The contour interval is 53 m.

Figure 2-18: Seasonal cycle of 515 hPa winds (ms^{-1}) from Experiments 1 (top row, left, no topography), 2 (top row, right, 2000 m wave-2), 3 (middle row, left, 3000 m wave-2), 5 (middle row, right, 2000 m wave-1) and 6 (bottom row, 3000 m wave-1) shown as calendar averages. The tropospheric annular mode timescale for the experiment is also indicated. Experiments with higher heights of topography of both wavenumbers are similar to Experiment 3 (not shown).

Figure 3-1: Timing of SFW events from the 28 years simulated in the model run.

Figure 3-2: Top panel: Transition in zonal mean zonal wind averaged from 60°S to 70°S for a 60 day period centered on SFW events for 28 years from the GCM run. The contour interval is 2 m/s. Bottom panel: Time evolution of zonal mean zonal wind averaged from 60°S to 70°S for a 60 day period centered on SFW events for 28 years from the GCM run, as differences from day -

30. The contour interval is 0.25 m/s up to -2 m/s (shown as filled colored contours) and 5 m/s thereafter (shown as unfilled black contours). Magenta and brown contours denote the 90% and 95% confidence intervals for a two-sided t test.

Figure 3-3: Panel a: Latitude-pressure structure of the change in zonal mean zonal winds between days -10 and +10. The contour interval is 0.5 m/s. Panel b: First EOF of zonal mean zonal winds at 585 mb. Panel c: Vertically integrated tropospheric (from the surface to 200 mb) horizontal momentum flux divergence as anomalies from the climatology averaged over a 21 day period centered on the final warming (same time period as shown in panel a). Panel d: Vertically integrated tropospheric (from the surface to 200 mb) horizontal momentum flux divergence regressed on the first EOF of zonal mean zonal winds at 585 mb. These figures are from the model run, and the white patch in the top panel shows the extent of the bottom topography.

Figure 3-4: Latitude pressure structure of the zonal mean zonal wind regressed on the first EOF of geopotential height at 585 mb (the first model level above the extent of the topography). Latitude pressure structure shown for all data in the left panel and for a 90 day period centered on final warming events in the right panel. These figures are from the model run, and the white patch at the bottom of both figures shows the extent of bottom topography.

Figure 3-5: Timing of warming for SFW events from 1960-2010, determined from NCEP/NCAR Reanalysis data.

Figure 3-6: Transition in zonal mean zonal wind anomalies averaged from 60°S to 70°S for a 60 day period centered on SFW events, averaged for 49 SFW events from the NCEP/NCAR Reanalysis data. The contour interval is .3 m/s.

Figure 3-7: Polar mean (averaged from 65°S-90°S) geopotential height, shown as anomalies from an average seasonal cycle (defined as the sum of the first six Fourier harmonics of a seasonal cycle derived from an annual time series of long-term daily averages), difference between the late and early years, centered on the mean warming day in panel a and on the SFW event in panel b. The contour interval is 30 m. Magenta and white contours denote the 90% and 95% confidence intervals for a two sided t test.

Figure 3-8: Difference between the late and early years 850 mb zonal mean zonal wind anomaly from time mean at a) 60^0S and b) 40^0S.

Figure 4-1: The vertical and horizontal extents of the imposed polar stratospheric diabatic cooling (K day^{-1}). (Top) vertical extent shown averaged over the polar cap (65-90°S), and (Bottom) latitudinal cross-section at 50 hPa.

Figure 4-2: Temperature response to the imposed polar stratospheric cooling averaged over the polar cap (65-90°S). The magenta contour denotes 95% statistical significance. The contour interval is 1 K.

Figure 4-3: Zonal mean zonal wind response to the imposed polar stratospheric cooling averaged over 40-60°S. The magenta contour denotes 95% statistical significance. The contour interval is 1 m/s.

Figure 4-4: Geopotential height changes averaged over the polar cap (65-90°S). The magenta contour denotes 95% statistical significance. The contour interval is 25 m.

Figure 4-5: Polar plot of the December changes in geopotential height at 850 hPa.

Figure 4-6: Change in eddy heat fluxes (Km/s). The magenta contour denotes 95% statistical significance. The contour interval is 0.5.

Figure 4-7: (Left panel) 850 hPa zonal mean zonal wind response. The magenta contour denotes 95% statistical significance. The contour interval is 0.5 m/s. (Right panel) First EOF of zonal mean zonal winds at 850 hPa.

Figure 4-8: 850 hPa zonal mean zonal wind response for polar stratospheric cooling that peaks August 20. The magenta contour denotes 95% statistical significance. The contour interval is 0.5 m/s.

Figure 4-9: 850 hPa zonal mean zonal wind response for polar stratospheric cooling that peaks September 20. The magenta contour denotes 95% statistical significance. The contour interval is 0.5 m/s.

Figure 4-10: 850 hPa zonal mean zonal wind response for polar stratospheric cooling that peaks November 20. The magenta contour denotes 95% statistical significance. The contour interval is 0.5 m/s.

Figure 4-11: 850 hPa zonal mean zonal wind response for polar stratospheric cooling uniformly applied through the entire year. The magenta contour denotes 95% statistical significance. The contour interval is 0.5 m/s.

Figure 4-12: The seasonal cycle of 850 hPa annular mode timescale (days).

Figure 4-13: The seasonal cycle of 50 hPa zonal mean zonal winds for the model experiment with doubled cooling peaking (top row, left) all year around, (top row, right), August 20, (middle row, left) September 20, (middle row, right), October 20, and (bottom row, left), November 20.

The control run is shown in the right panel of the bottom row for comparison. The final warming is delayed in all the perturbed runs.

Figure 4-14: 850 hPa zonal mean zonal wind response for doubled polar stratospheric cooling uniformly applied through the entire year. The magenta contour denotes 95% statistical significance. The contour interval is 0.5 m/s.

Figure 4-15: 850 hPa zonal mean zonal wind response for doubled polar stratospheric cooling that peaks August 20. The magenta contour denotes 95% statistical significance. The contour interval is 0.5 m/s.

Figure 4-16: 850 hPa zonal mean zonal wind response for doubled polar stratospheric cooling that peaks September 20. The magenta contour denotes 95% statistical significance. The contour interval is 0.5 m/s.

Figure 4-17: 850 hPa zonal mean zonal wind response for doubled polar stratospheric cooling that peaks October 20. The magenta contour denotes 95% statistical significance. The contour interval is 0.5 m/s.

Figure 4-18: 850 hPa zonal mean zonal wind response for doubled polar stratospheric cooling that peaks November 20. The magenta contour denotes 95% statistical significance. The contour interval is 0.5 m/s.

1. Introduction

In the lowest several kilometers of the atmosphere, temperature falls almost monotonically with latitude and height, and this region is called the troposphere. Above the troposphere is the stratosphere, and here temperature typically increases with height (e.g. Vallis, 2006). Historically, interest in the stratosphere was motivated by concerns regarding the stratospheric ozone layer, which plays a crucial role in shielding the surface of the earth from harmful ultraviolet light. Over the last several decades there has been intensive research into the earth's stratosphere, which has resulted in major advances in our understanding of its dynamics, transport and chemistry, and its coupling with other parts of the atmosphere.

A prominent feature of the circulation of the stratosphere is the seasonal formation and decay of an intense cyclonic vortex over the winter pole, known as the stratospheric polar vortex, or the polar night jet. The strong circumpolar westerly winds at the edge of the polar vortex are in stark contrast to the weak easterlies that occur in the summer hemisphere (e.g. Waugh and Polvani, 2010). The structure and dynamics of these polar vortices play an important role in setting the circulation of the stratosphere and are key to determining the distributions of trace gases, in particular ozone. Because the polar vortices act as containment vessels (transport barriers) and allow for the occurrence of extremely low temperatures, they play a critical role in polar ozone depletion and the annual formation of the Antarctic ozone hole (e.g. Newman, 2010, Solomon, 1999). Interest in the polar vortices has further intensified in recent years as numerous modeling and observational studies have shown that the polar vortices can influence weather and climate patterns in the troposphere. In this chapter, we briefly review the observed structure of polar vortices, their variability, and aspects of their coupling to tropospheric circulation. In our

discussion we borrow from Waugh and Polvani (2010), Kushner (2010), and the introduction sections of two papers that are based on the results presented in chapters 2 and 3 (Sheshadri et al. 2014 and Sheshadri et al. 2015).

1.1. Climatological structure of the stratospheric polar vortices

The general characteristics of stratospheric polar vortices can be seen in plots of zonal mean zonal winds. Figure 1-1 shows the latitude-pressure variations of climatological zonal winds for July in the Southern Hemisphere and January in the Northern Hemisphere in the top panel. For both hemispheres, there is a strong westerly jet in midwinter. Radiative cooling during the long polar night leads to extremely low temperatures in the polar stratosphere in the winter, and these westerly jets shown in Figure 1-1 form because of the resulting strong equator to pole temperature gradients.

These stratospheric polar vortices form in fall when solar heating of the polar regions is cut off, reach maximum strength in midwinter, and then decay in later winter to spring as sunlight returns to the pole. This is illustrated in the bottom panel of Figure 1-1, which shows the latitude-seasonal variations of the zonal winds in the middle stratosphere (10 hPa), and in which the seasonal formation and decay of the Arctic and Antarctic vortices is evident. In both hemispheres, there are weak easterlies during summer months (June-August in the NH and December-February in the SH), which are replaced by westerlies in fall that grow in strength until there is a strong zonal flow in midwinter. These strong westerlies then decay through spring, and the flow returns to easterlies in the summer.

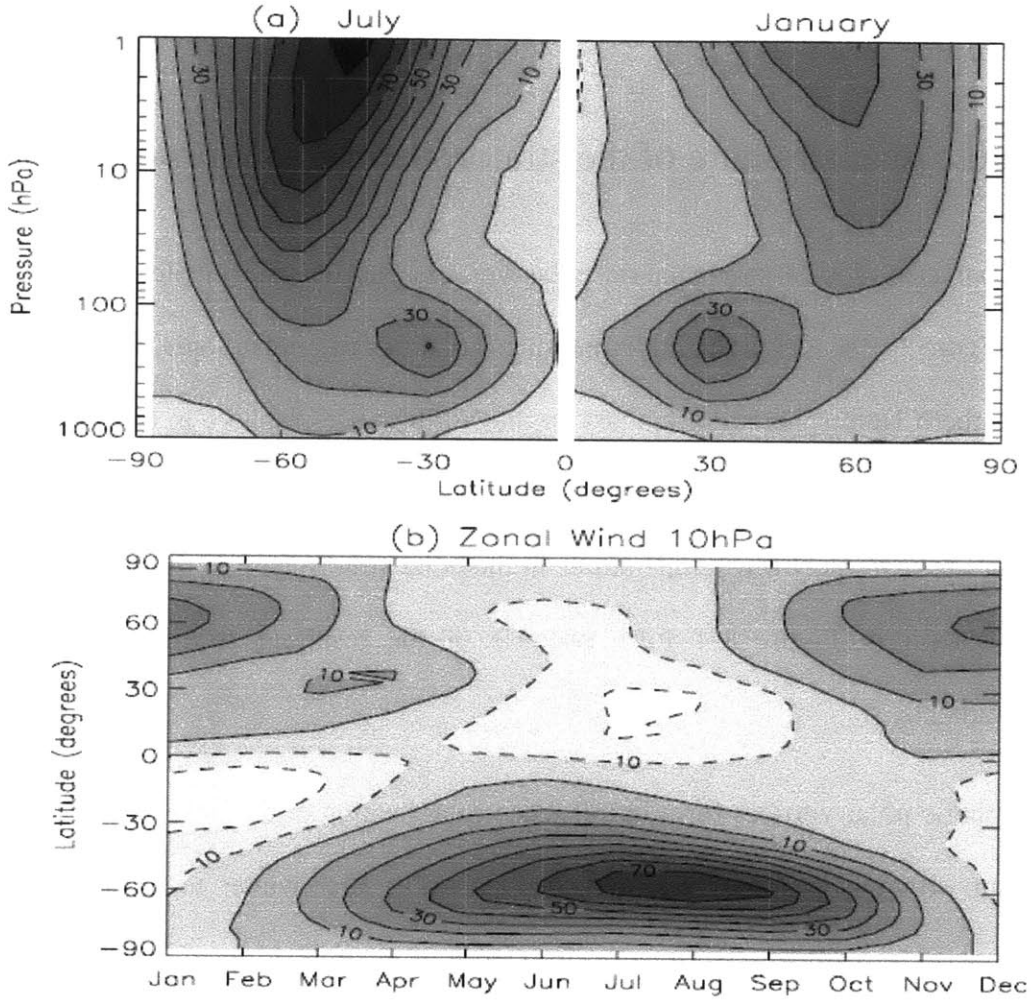

Figure 1-1: (top panel) Latitude-height variation of climatological mean zonal mean zonal winds for (left) SH in July and (right) NH in January. (Bottom panel) Latitude-month variation of climatological mean zonal mean zonal winds at 10 hPa. Figure from Waugh and Polvani (2010).

Although radiative processes (e.g. heating by absorption of solar radiation by ozone and cooling by thermal emission by carbon dioxide) play the forcing role in setting up the large scale latitudinal temperature gradients and resulting zonal flow, the winter stratosphere is not in thermal equilibrium. Waves excited in the troposphere (e.g. by topography, land-sea heating contrasts, or the nonlinear interactions of synoptic scale eddies) propagate up into the stratosphere and perturb it away from radiative equilibrium, and the zonal winds shown in Figure 1 are weaker than predicted by radiative equilibrium (e.g. Andrews et al. 1987). Additionally, the propagation of such waves into the stratosphere varies with conditions in the stratosphere itself. Charney and Drazin (1961) showed that Rossby waves propagate upward only if their horizontal scale is large and if the flow is weakly eastward relative to their phase speed; that is, stationary waves only propagate through weak westerlies. As a result, stationary Rossby waves propagate up into the stratosphere in the winter (when westerlies are prevalent) and not in the summer (when easterlies are prevalent), and the stratospheric flow is consequently more disturbed in the winter than in the summer.

Large hemispheric differences in the polar vortices can be seen in Figure 1-1: the Antarctic vortex is larger, stronger, and has a longer lifespan than its Arctic counterpart. These differences are caused by hemispheric differences in wave generation and propagation. The larger topography and land-sea contrasts in the NH excite more/larger planetary scale Rossby waves that disturb the polar vortex and push it further from radiative equilibrium than in the SH.

There are also significant hemispheric differences in the variability of the vortices, with the Antarctic vortex being less variable on both intraseasonal and interannual timescales. These differences can be seen in the evolution of minimum polar temperatures at 50 hPa, shown in Figure 1-2 (Waugh and Polvani, 2010). Similar features are observed in other temperature

diagnostics and in high latitude winds (e.g. Yoden et al. 2002). The climatological mean temperatures (thick curves) in the Antarctic are lower than in the Arctic. The duration of cold temperatures is also longer. Additionally, there is much larger variability in the Arctic temperatures than in the Antarctic. As evident from Figure 1-2, a large range of temperatures can be observed from fall to spring, whereas in the Antarctic there is a fairly narrow range of values except during late spring. The range and quartiles in Figure 1-2 show that the distribution of Arctic temperatures is non-Gaussian and highly skewed (Yoden et al. 2002).

The large variability of the Arctic occurs on varying timescales (interannual, intraseasonal, and weekly timescales). Within a single winter, there can be periods with extremely low temperatures as well as periods with extremely high temperatures, and the transitions between these events can occur very rapidly. These extreme events, and, in particular, the so called stratospheric "sudden warmings" will be discussed in detail subsequently.

The differences in polar temperatures shown in Figure 1-2 explain hemispheric differences in polar ozone depletion. In the Antarctic, midwinter minimum temperatures are lower than threshold temperatures for the formation of polar stratospheric clouds (PSCs) every year (horizontal lines in Figure 1-2), and formation of PSCs and widespread ozone depletion occur every year (e.g. Newman, 2010). In contrast, Arctic temperatures fall below the threshold for PSC formation less frequently, and, as a consequence, ozone depletion in the Arctic is much less frequent and widespread.

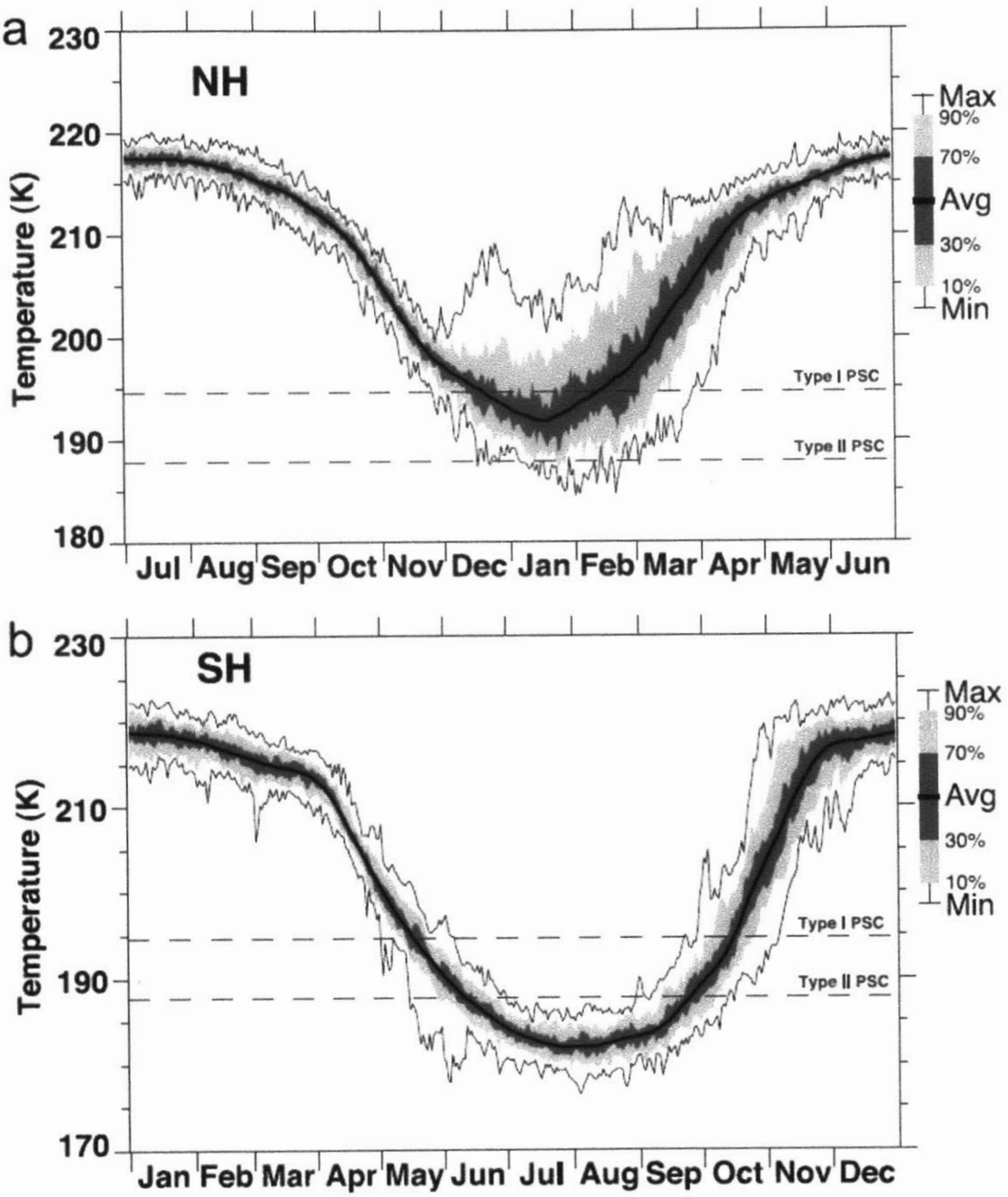

Figure 1-2: Time series of climatological daily minimum polar temperatures at 50 hPa for the a) Arctic (50-90°N) and b) Antarctic (50-90°S). The daily climatology is determined from the 1979-2008 period. The black line shows the average for each day of the climatology. The grey shading shows the percentage range of the values (taken from Waugh and Polvani, 2010).

Maps of potential vorticity (PV) on isentropic surfaces provide useful information on the structure and evolution of the polar vortices and the associated transport of trace gases. McIntyre and Palmer (1983, 1984) examined maps of PV and interpreted features in terms of Rossby waves. They associated reversible distortions of the vortex with propagating Rossby waves and contrasted these with irrevsersible deformations where air with high PV is pulled off the vortex and stirred into midlatitudes. They referred to the latter process as Rossby wave breaking, which is very common at the vortex edge.

1.2. Extreme events

As was discussed in the previous section, there is large variability in the Arctic vortex from fall to spring, and there are periods when the vortex is anomalously strong and periods when it is weak or even nonexistent, with rapid transitions between these states. The principal modes of variability of the extratropical circulation of the stratosphere and troposphere are usually referred to as the annular modes (Thompson and Wallace, 1998, 2000). They are derived using empirical orthogonal function analysis of meteorological fields such as zonal mean zonal wind and geopotential height. The annular modes of the two hemispheres are referred to as the Northern Annular Mode (NAM) and the Southern Annular Mode (SAM). The variability of the Arctic vortex and the existence of extreme events is illustrated in Figure 1-3, which shows the time series of the Northern Annular Mode (NAM) index for 24 years (taken from Polvani and Waugh, 2004). Since the polar vortex dominates the variability of the stratospheric circulation, the NAM index at 10 hPa is a rough measure of the strength of the polar vortex, with a positive NAM index corresponding to a strong vortex and a negative index to a weak one.

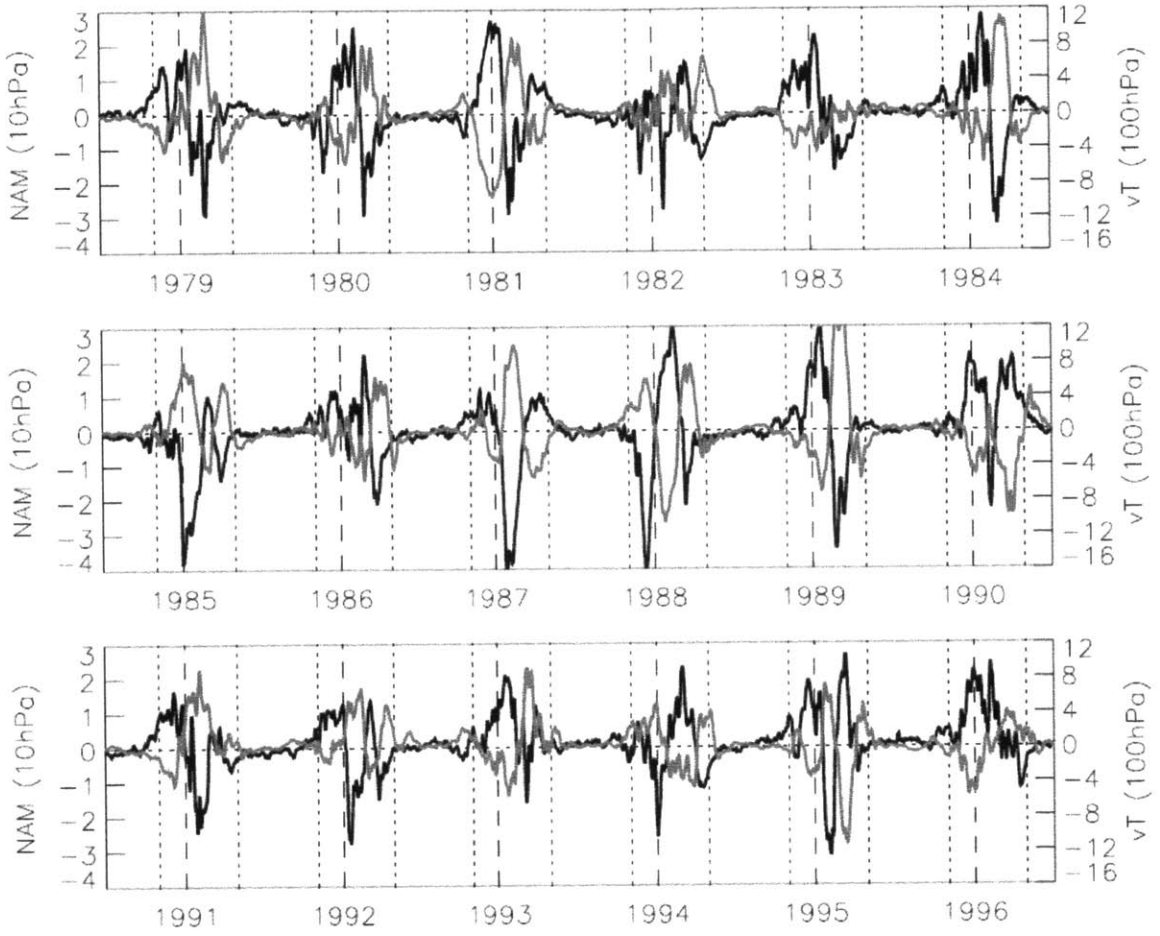

Figure 1-3: Daily values of the NAM index at 10 hPa (black) and 40 day averaged heat flux anomalies at 100 hPa (grey) for 1 July 1978 to 31 December 1996. From Waugh and Polvani (2010).

There is virtually no variability in the NAM index during the summer months but large variability during winter and spring, with rapid transitions between strong and weak vortices. Extremely strong and weak events occur on average around once every other winter, although the occurrence of extreme events is not evenly spread: two weak vortex events can occur in one winter (e.g. the 1998/1999 winter), and there can be extended periods when there are few weak events but frequent strong events (e.g. early to the mid-1990s, studied in Manney et al. 2005). The probability distribution function of the NAM index in winter is close to Gaussian (Polvani and Waugh 2004).

The occurrence of strong and weak vortex events has been linked to the upward wave activity entering the stratosphere. Case studies and composite analyses have shown that anomalously strong wave activity nearly always precedes weak vortex events, with strong vortex events being similarly preceded by weak wave activity. This is also seen in Figure 1-3, which also shows the time series of eddy heat flux at 100 hPa integrated over the prior 40 days (a measure of the time-integrated wave activity entering the stratosphere) in grey. This time series is shown to be anticorrelated with the NAM index at 10 hPa, with a correlation coefficient of -0.8.

Periods when the NAM index is less than -2.7 are generally associated with what are known as stratospheric sudden warming (SSW) events, which are traditionally, and more simply, defined by the reversal of the zonal mean zonal winds at 60°N and 10 hPa. There has been considerable research into SSWs since they were first reported by Scherhag (1952). Using the simple definition of a reversal of zonal mean zonal wind at 60°N and 10 hPa, Charlton and Polvani (2007) reported an average of around six SSWs every decade (29 SSWs in the 44 winters between 1957/58 and 2001/2001). This study and those of Limpasuvan et al. (2004) and Matthewmann et al. (2009) also used composite-based analysis to examine the climatological

nature of SSWs, including the evolution of temperature, zonal flow, and eddy fluxes during warming events as well as the three-dimensional structure of the vortices. (The climatological nature of strong vortex events has also been examined by Limpasuvan et al., 2005.) Traditionally, SSWs were classified into wave 1 or wave 2 events depending on the amplitude of the longitudinal wave numbers. However, given the nonlinearity of the flow, such a classification can be misleading (Waugh, 1997), and it might be more appropriate to use a vortex-oriented classification. Charlton and Polvani (2007) and Matthewman et al. (2009) used such a classification and divided the SSWs into either "vortex displacement" or "vortex split" events. Figure 1-4 (from Charlton and Polvani 2007), shows an example each of a vortex split and a vortex displacement. Both panels show polar stereographic projections of geopotential height on the 10 hPa pressure surface, with the top panel showing the vortex displaced off its climatological position and the bottom panel showing the vortex split into two segments.

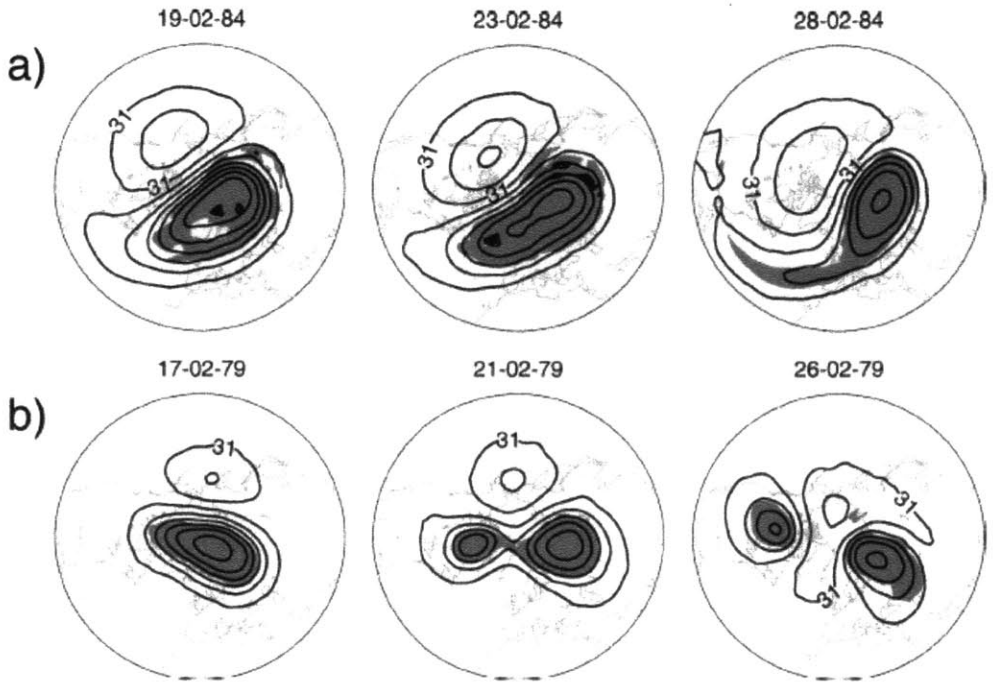

Figure 1-4: Examples of a vortex displacement in the top panel, and a vortex split in the bottom panel (from Charlton and Polvani, 2007). ©American Meteorological Society. Used with permission.

These studies showed that the two types of events are dynamically different, with differences in the stratospheric and tropospheric flows before the events and in vortex evolution during the event. Although the life cycles of the displacement and split events are very different, there is much less variation between individual events of each class, both in terms of vertical structure and longitudinal orientation, and characteristics are well captured by the composite events (e.g. Matthewman et al., 2009). In particular, during splitting events the vortex deformations are highly barotropic, while for displacement events the vortex tilts westward with height.

The basic understanding of the dynamics of SSWs, based on the seminal Matsuno (1970 and 1971) studies, involves the anomalous growth of upward propagating planetary-scale Rossby waves originating in the troposphere. However, the cause of the rapid amplification of the Rossby wave and the role of the initial state of the stratospheric vortex are not fully understood. There is evidence that the vortex needs to be preconditioned for SSWs to occur (e.g., McIntyre, 1982; Limpasuvan et al., 2004). While most analyses of SSWs have focused on upward propagating Rossby waves, alternate theories include resonant excitation of free modes (Tung and Lindzen, 1979; Plumb, 1981; Esler and Scott, 2005; Esler et al., 2006) and vortex interactions, in particular interactions between the polar vortex and Aleutian anticyclone (O'Neill and Pope, 1988; Scott and Dritschel, 2006).

Until recently, it was thought that sudden warming events were exclusively a NH phenomenon. However, a dramatic event occurred in the SH in September 2002, when the Antarctic vortex elongated and split into two. This is the only known SSW in the SH, and there has been considerable research into this event, some of which is summarized in the March 2005 special issue of the Journal of the Atmospheric Sciences. Although there have been many studies into the dynamics of this event (see the above mentioned special issue), the exact cause remains unknown. Most of the focus has been on upward propagating Rossby waves, but Esler et al. (2006) provide evidence that the event may have been the result of a self-tuned resonance. Kushner and Polvani (2005) documented the spontaneous occurrence of a sudden warming, resembling the observed SH event, in a long numerical simulation of a simple troposphere-stratosphere general circulation model with no stationary forcing, suggesting that the 2002 event may have been just a rare, random event.

There is large interannual variability not only in the midwinter vortices but also in the timing and characteristics of the final breakdown of the vortices (so called "final warming") (e.g., Waugh and Rong, 2002, Black and McDaniel, 2007a, b). These stratospheric final warming events influence not only the stratospheric circulation (i.e., a transition from winter stratospheric westerlies to summer easterlies) but also strongly organize the tropospheric circulation, with a rapid weakening of high latitude tropospheric westerlies occurring for both NH and SH final warmings (e.g., Black and McDaniel, 2007a, 2007b).

1.3. Stratosphere-troposphere coupling

Increasing observational and modeling evidence in the last decade suggests that polar stratospheric vortices can have a significant influence on the tropospheric flow for a range of time scales (e.g., Baldwin and Dunkerton, 2001; Thompson and Solomon, 2002; Polvani and Kushner, 2002; Gillett and Thompson, 2003; Charlton et al., 2004).

Much of the evidence for a stratospheric impact on the troposphere is described using the so-called annular modes: the Northern Annular Mode (NAM) and Southern Annular Mode (SAM) (e.g., Thompson and Wallace, 2000). As discussed above, these modes are the dominant patterns of variability in the extra tropical troposphere and stratosphere, and the NAM/ SAM index in the stratosphere is a measure of the vortex strength. Baldwin and Dunkerton (1999) showed that anomalous values in the NAM index are found to appear in the stratosphere first and subsequently progress downward over periods of several weeks. Moreover, subsequent studies showed that extreme stratospheric events can be followed by anomalous weather regimes at the surface that persist for up to 2 months (Baldwin and Dunkerton, 2001; Thompson et al., 2002). Figure 1-5 shows composites of weak vortex events from the NCEP-NCAR Reanalysis taken

from Kushner (2010). It is evident that anomalous values of the NAM are evident in the troposphere and at the surface for up to two months after they first appear in the stratosphere.

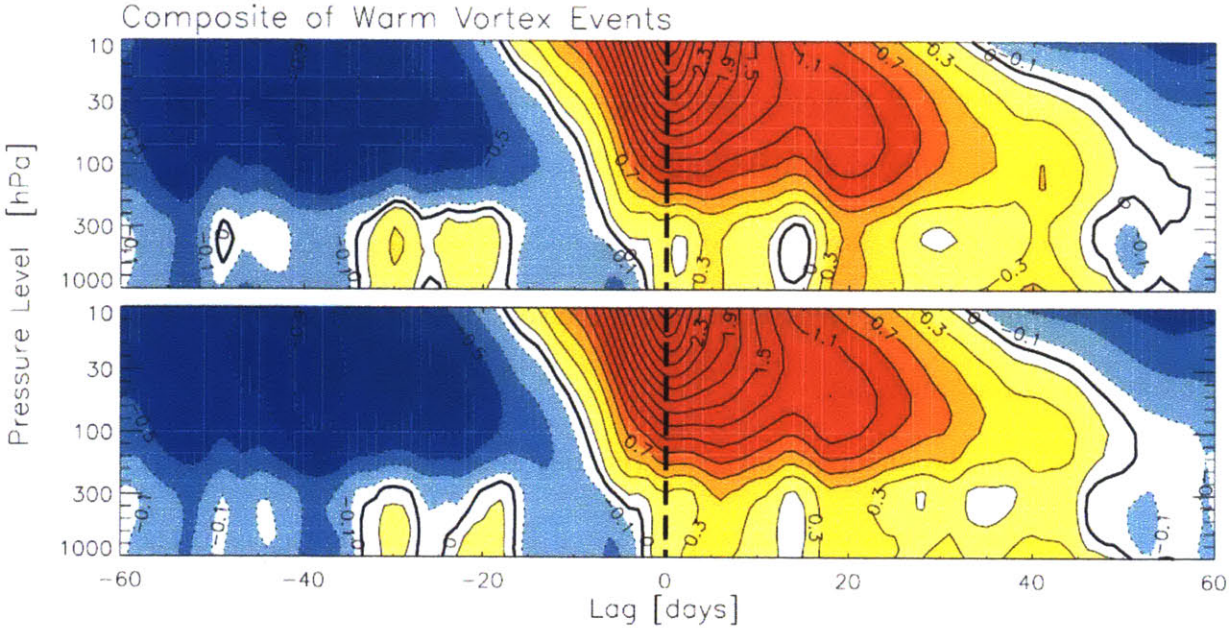

Figure 1-5: Composites of 50 warm vortex events from NCEP Reanalysis from 1958 to 2007. For each winter season (November to March inclusive), the strongest geopotential height anomaly at 10 hPa was used. Contour intervals are spaced by 0.2. Index values between -0.1 and 0.1 are unshaded. The zero level is shown by the heavy black contour. The top plot shows a composite of nondimensional NAM index (based on geopotential height anomalies and using the

zonal-mean EOF method described by Baldwin and Dunkerton (2009)). The bottom plot shows a composite for the time series of polar-cap averaged geopotential height (60°N-90°N), normalized by its standard deviation at each level. (Taken from Kushner, 2010).

The exact dynamical mechanism by which the stratosphere influences the troposphere is unknown, but there are several proposed theories, the most discussed being the "downward control" of the extratropical meridional circulation (Haynes et al. 1991). This can be explained as follows (e.g. Plumb, 2010): when dissipating waves act as a drag on the westerly mean flow in the stratosphere, the wave drag drives a mean flow poleward. Continuity then requires corresponding vertical motion – at the poleward side of the wave drag, the flow must turn upward or downward. It cannot actually go upward, since then it would have to turn back equatorward at some higher altitude, and there is no reverse wave drag at higher altitudes to allow it to do so. So, the flow turns downward, and is able to return at lower altitude by virtue either of frictional or topographic form drag at the surface or of a region of divergent EP flux if the waves are forced internally.

Other theories include direct PV inversion (Hartley et al., 1998; Ambaum and Hoskins, 2002; Black, 2002), changes in refractive properties and Rossby wave propagation (Hartmann et al., 2000) or wave reflection (Perlwitz and Harnick, 2004). The tropospheric response to stratospheric perturbations has been described as being influenced by eddy-mediated feedbacks (Kushner and Polvani, 2004; Song and Robinson, 2004; Chen and Held, 2007).

Although anomalous values of the annular mode index appear first in the upper stratosphere, it should be noted, as discussed earlier, that these the extreme events are preceded by anomalous wave activity entering the stratosphere. While the fact that stratospheric extreme events are

preceded by anomalous wave activity might indicate that the stratosphere is slave to the troposphere, this is not necessarily the case. Numerous studies, using a hierarchy of models, have shown that internal variability can be generated within the stratosphere, with vacillation cycles of strong (westerly) and weak (easterly) polar winds (e.g., Holton and Mass, 1976; Yoden, 1987; Scott and Haynes, 2000; Rong and Waugh, 2003; Scott and Polvani, 2004).

Furthermore, the Scott and Polvani (2004) simulations show cycles in wave activity entering the stratosphere that resemble those in observations (e.g., Figure 3) even though all forcings in their simple model are completely time-independent. This therefore suggests that the stratosphere plays a role in determining the wave activity entering from the troposphere.

Couplings between the stratospheric vortices and tropospheric circulation have also been found in the southern hemisphere. Observations show a strengthening of westerlies (and corresponding increase in the SAM) in both the stratosphere and troposphere over the past 2–3 decades. The largest stratospheric trends occur in spring months, whereas the largest tropospheric trends occur in the summer. This is consistent with Antarctic ozone depletion strengthening the stratospheric vortex and a time lag for stratospheric anomalies to descend to the surface (Thompson and Solomon, 2002; Gillett and Thompson, 2003). By modifying the SAM, a strengthening Antarctic vortex also has the potential to impact other aspects of the tropospheric circulation, including subtropical jets, storm tracks, and the Hadley cell width (e.g. Son et al. 2009).

In this thesis, a number of issues related to the variability of the stratospheric polar vortices, and the impact of this variability on surface climate patterns on various timescales are considered. In Chapter 2, we build on previous modeling work and develop an improved idealized model to study the circulation of the stratosphere and its impacts on the tropospheric circulation. This model is used to study how the strength of the stratospheric polar vortices changes with the

seasons in various model configurations with different tropospheric wave forcing. We focus particularly on the timing of maximum variability of zonal mean zonal wind, geopotential height amplitude and eddy heat fluxes as the wave forcing from the troposphere is increased. The model is found to have qualitatively different stratospheric seasonal variability when forced with wavenumber-1 bottom topography than when it is forced with wavenumber-2 bottom topography, in terms of the frequency and type of sudden warming events. We also study how the frequency of major sudden warming events and the timing and variability of the seasonal breakup of the stratospheric polar vortex, (i.e. final warming events), changes with tropospheric wave forcing. In addition, since the model configuration includes a seasonal cycle in equilibrium temperatures that is confined to the stratosphere, it is possible to study the impact of stratospheric variability on the tropospheric circulation on seasonal timescales. It is found that the stratospheric seasonal cycle impacts the tropospheric jet continuously, in addition to the more local (in time) effects of 'events' such as stratospheric sudden warming and final warming events. In Chapters 3 and 4, we study the impacts of stratospheric ozone depletion on the variability of the Antarctic polar vortex, and the impact of these stratospheric trends on tropospheric climate. As previously mentioned in this section, polar stratospheric ozone depletion is considered to be the primary driver of southern hemisphere tropospheric circulation changes over the second half of the twentieth century (e.g. Polvani et al. 2011). Stratospheric ozone depletion cools the polar stratosphere, changing the equator to pole temperature gradient (e.g. Thompson et al. 2011). In Chapter 3, we begin by showing that stratospheric "final warming" events induce a coherent circulation change in the tropospheric circulation in a model that is forced with a seasonal cycle of equilibrium temperatures that is confined to the stratosphere. The surface impacts of final warming events are then studied in a reanalysis

product. We find a statistically significant trend in the reanalysis towards a delay in the timing of the final seasonal breakdown of the Antarctic polar vortex (final warming events). We then test the hypothesis that the observed trends in surface westerlies in the era of large ozone depletion are directly consequent on this shift towards later final warming events. In Chapter 4, tropospheric circulation changes brought about in the idealized model described in Chapter 2 because of imposed polar stratospheric diabatic cooling (that mimics the effects of ozone depletion) are studied. It is found that the tropospheric response depends on several factors, including the seasonal cycle of tropospheric annular mode timescales, and whether or not the imposed cooling induces westerlies at a time when easterlies were prevalent in the control run. Each chapter will begin with a review of previous literature relevant to the chapter.

2. Seasonal variability of the polar stratospheric vortex in an idealized AGCM with varying tropospheric wave forcing[1]

2. 1. Introduction

One of the most obvious characteristics of the winter stratosphere, aside from the dominance of planetary scale waves, is its high degree of variability, on both intraseasonal and interannual time scales. The most dramatic manifestations of this variability are the major stratospheric sudden warmings (SSWs) that occur on average about 0.6 times per winter in the Northern Hemisphere (e.g. Charlton and Polvani 2007), but only once in the observational era in the Southern Hemisphere, though similar events that fail to meet the 'major' criterion are common in both hemispheres. Major SSW events can be classified into 'displacement' and 'splitting' events, in approximately equal numbers (Charlton and Polvani 2007). Similar 'final warmings' (FWs), which occur at the end of winter at the final transition into the summertime circulation, occur in both hemispheres. These events show many similarities to SSWs, especially in being characterized by planetary wave amplification; their timing is variable around or after spring equinox (being delayed by around 2 months with respect to equinox in the southern hemisphere), with the early events being the most active (Black and McDaniel 2007a,b; Hu et al., 2014b).

While some part of this wintertime variability is undoubtedly a reflection of variability in tropospheric wave forcing, it is clear from modeling studies that such variability can arise spontaneously as a consequence of the dynamical interaction between waves and the zonal flow

[1] This chapter is based on Sheshadri, A., R. A. Plumb, and E. P. Gerber, 2015: Seasonal variability of the polar stratospheric vortex in an idealized AGCM with varying tropospheric wave forcing, *J. Atmos. Sci.*, doi: 10.1175/JAS-D-14-0191.1, in press, with some changes.

in the deep stratosphere-troposphere system. Even the one-dimensional Holton-Mass model (Holton and Mass 1976) exhibits such behavior; depending on the amplitude of steady wave forcing at the bottom boundary, the system can exhibit steady solutions or, at larger forcing amplitude, quasi-periodic or chaotic behavior (e.g. Yoden 1990). More realistic global models have revealed similar behavior (Christiansen, 2000; Taguchi et al., 2001; Gray et al. 2003; Scott and Polvani, 2004, 2006) and have demonstrated that a realistic degree of variability can be generated even when the tropospheric wave forcing is fixed in time.

Some full GCMs exhibit reasonable stratospheric variability, but shortcomings still exist. Full GCMs tend to underestimate the wave forcing in the Northern Hemisphere, but slightly overestimate the wave forcing in the Southern Hemisphere (Eyring et al., 2010, Chapter 4), while many such models underestimate the frequency of major warming events (Charlton et al., 2007). Experiments with idealized GCMs permit an investigation of parameter dependence that have proved useful to better understand stratospheric dynamics in models as well as the real atmosphere.

In mechanistic studies with global dynamical models run in 'perpetual solstice' mode with simple planetary-scale surface topography and with the stratospheric state determined by Newtonian relaxation to a specified equilibrium temperature distribution, Taguchi et al. (2001) and Gerber and Polvani (2009) documented the dependence of their model's climatology on the amplitude of the specified topography. Taguchi et al. (2001) found SSW-like variability appearing at modest topographic amplitude, becoming more frequent and more intense, with a weaker vortex, with greater amplitudes. Gerber and Polvani (2009), who also explored the role

of different stratospheric vortex strengths, found similar behavior with forcing at zonal wavenumber 2, and were able to identify cases with a realistic (for the Northern Hemisphere) frequency of major SSW events. Unlike Taguchi et al., however, they were unable to find a realistic regime with wave 1 forcing; rather, at forcings below a certain value, variability was found to be too weak, with no SSWs, while at larger forcings, the vortex was completely destroyed and the model climatology was highly unrealistic.

Greater realism and, especially, the key aspects of the observed differences between variability in the northern and southern hemispheres, has been achieved by imposing a seasonal cycle in the imposed equilibrium temperature distribution. Using a one-dimensional Holton-Mass-like model, Plumb (1989) found a transition from a cycle like that of the southern stratosphere, with greatest wave amplitudes in early and, especially, late winter with weak topographic amplitudes, to one like that of the northern hemisphere, with peak amplitudes throughout winter. Taguchi and Yoden (2002), using wavenumber 1 forcing, found similar behavior in a global model, highlighting the shift of maximum wave amplitudes and of zonal wind variability from late winter to mid-winter as topographic amplitude was increased.

In fact, Scott and Haynes (2002), in similar calculations in which geopotential wave amplitude rather than topographic height was specified at the surface, found threshold behavior, with rather modest changes to the zonal winds below some critical forcing amplitude, changing suddenly to a state with large variability in early winter, followed by a complete collapse of the vortex, and of its variability, throughout late winter. This finding raises a question as to whether this transition corresponds to that found by Gerber and Polvani (2009) with wave 1 forcing: in

'perpetual solstice' mode, if such a vortex collapse occurred during the early part of the run, the collapse may be sustained indefinitely whereas, in the presence of an annual cycle the vortex may be reinitialized every winter and thus produce a seasonal cycle like that found by Scott and Haynes.

The simulation of FWs has also been assessed in such models with seasonal forcing. Scott and Haynes (2002) did not find realistic final warmings in their strongly-forced cases. However, Sun and Robinson (2009) and Sun et al. (2011) reported realistic FW events in a global model running from mid-winter into summer. Like observed FWs, these events were associated with bursts of amplified planetary waves which were demonstrated to play a major role in the events' dynamics. Increasing tropospheric forcing in such models led to FWs becoming earlier on average, but with greater variability in their timing.

Both SSWs and FWs have clear impacts on the tropospheric circulation. Fluctuations in vortex strength are followed by persistent perturbations to surface winds, manifesting themselves as "annular mode" anomalies (Thompson and Wallace, 1998; Baldwin and Dunkerton 1999, 2001). Model studies indicate that synoptic-scale tropospheric eddies appear to play an important role in organizing and amplifying the stratospheric response into this form (e.g. Song and Robinson, 2004; Kushner and Polvani 2004). Gerber and Polvani (2009) explicitly demonstrated a realistic tropospheric signal associated with SSWs in their global model. FWs are also observed to have a similar tropospheric impact, although its latitudinal structure differs somewhat from annular mode form (Black et al., 2006; Black and McDaniel, 2007a,b; Hu et al., 2014), and upper tropospheric planetary scale waves may play a role (Sun et al. 2011). Similar results have been

found in simplified global models (Sun and Robinson, 2009; Sun et al., 2011, Sheshadri et al., 2014).

In this section, we revisit the seasonal behavior of the stratosphere in a global model, paying particular attention to the dependence of seasonal and interannual variability on the amplitude and wavenumber of topographic forcing. The model is essentially the same as that used by Gerber and Polvani (2009), with modifications to the imposed equilibrium temperature distributions; the model setup is described in Section 2. With wavenumber 2 topography (Section 3) the model reproduces the essential characteristics of the observed stratosphere in the two hemispheres: with weak topographic forcing, maximum zonal wind variability occurs in late winter, with a late FW, while both of these characteristics shift towards earlier in the winter as the forcing is increased. Moreover, like Gerber and Polvani (2009) we find a range of topographic forcing amplitudes for which a realistic frequency of SSWs is generated. Unlike Scott and Haynes' (2002) results with wave 1 forcing, however, we find that the evolution varies smoothly with the wave forcing amplitude; there is no evidence of threshold behavior. Interestingly we do find, consistent with the results of Taguchi and Yoden (2002), evidence for saturation of wave amplitudes with stronger forcings, i.e. stratospheric wave amplitudes do not increase, once topographic forcing reaches a certain value.

As we shall describe in Section 2.4, the story with wavenumber 1 forcing is somewhat different. The shift, with increased forcing, of the dynamical evolution toward early winter, though present, is weaker than in the wavenumber 2 case. Realistic FWs are produced, but we are unable to find any regime with realistic frequency of major SSW events. While Gerber and Polvani

(2009) could find no such events, some major SSWs do occur within a range of forcing amplitudes in these experiments, but never with the observed frequency.

Since the imposed equilibrium temperature in this model varies seasonally only in the stratosphere, any seasonal variations in the tropospheric circulation are obviously of stratospheric origin. As discussed in Section 5, in some experiments we find a substantial tropospheric signal not only of SSWs and FWs, but also of the seasonal cycle itself. Just as found by Chan and Plumb (2009) we find this to be a consequence of the unrealistically long tropospheric annular mode time scale in some experiments; in experiments with more reasonable time scales, this tropospheric signal disappears. Conclusions are presented in Section 2.6.

2. 2. Model setup

The model is dry and hydrostatic, solving the global primitive equations with T42 resolution. We use 40 hybrid levels, transitioning from a terrain-following $\sigma = p / p_s$ coordinate at the surface to pure pressure levels by 115 hPa. The hybrid levels are located at the same mean position as the levels in Polvani and Kushner (2002). We include bottom topography specified as in Gerber and Polvani (2009) in the Northern Hemisphere of the model in all experiments. The topography is specified by setting the surface geopotential height as follows:

$$\Phi_0(\lambda,\phi) = \begin{cases} gh_0 \sin^2\left(\dfrac{\phi-\phi_0}{\phi_1-\phi_0}\pi\right)\cos(m\lambda), \phi_0 < \phi < \phi_1 \\ 0, otherwise \end{cases} \quad (1)$$

where λ and ϕ refer to longitude and latitude, and m and h_0 refer to the wavenumber and height of topography. ϕ_0 and ϕ_1 are set to 25°N and 65°N, so that the topography is centered at 45°N.

Linear damping of the horizontal winds is applied in the planetary boundary layer and in a sponge above 0.5 hPa, exactly as in Polvani and Kushner (2002).

Newtonian relaxation forces temperatures towards a zonally symmetric equilibrium temperature T_{eq}. In the stratosphere, the radiative relaxation timescale is 40 days. Within the troposphere there is no imposed seasonal variation; T_{eq} is specified as in Polvani and Kushner (2002):

$$T_{eq}^{trop}(p,\phi) = \max\left[T_T, (T_0 - \delta T)(p/p_0)^{\kappa}\right] \tag{3}$$

Where T_0=*315 K,* p_0=*1000 hPa,* and κ=*2/7*, with

$$\delta T = \delta_y \sin^2\phi + \varepsilon \sin\phi + \delta_z \log(p/p_0)\cos^2\phi$$

Where $\delta_y = 60K$, $\delta_z = 10K$, with the nonzero parameter $\varepsilon = 10K$ providing an asymmetry between the two hemispheres (our setup makes the Northern Hemisphere colder). Within the stratosphere, a seasonal cycle in T_{eq} is prescribed following Kushner and Polvani (2006) as follows:

$$T_{eq}^{strat}(\phi, p, t) = [1 - W(\phi,t)]T_{US}(p) + W(\phi,t)T_{PV}(p) \tag{4}$$

where ϕ is latitude, p is pressure, $T_{US}(p)$ is the temperature defined by the U. S. Standard Atmosphere (U.S. Committee on the Extension to the Standard Atmosphere, 1976) expressed as a function of pressure and $T_{PV}(p)$ is the polar vortex T_{eq} prescription of Polvani and Kushner (2002). The lapse rate of $T_{PV}(p)$ is γ, which can be varied to produce different strengths of the polar vortex. Here we use a fixed lapse rate of 4K/km in all experiments. The weighting function is

$$W(\phi,t) = \frac{1}{2}\left\langle A_S(t)\{1 + \tanh[(\phi - \phi_{0S})/\delta\phi_S]\} + A_N(t)\{1 + \tanh[(\phi - \phi_{0N})/\delta\phi_N]\}\right\rangle \tag{5}$$

where $A_S(t) = \max\{0.0, \sin[2\pi(t - t_0)/\Delta T]\}$ and $A_N(t) = \max\{0.0, \sin(2\pi t/\Delta T)\}$,

with

$t_0 = 180$ days, $\Delta T = 360$ days, $\phi_{0S} = -50°$, $\phi_{0N} = 50°$, $\delta\phi_S = -10°$ and $\delta\phi_N = 10°$. Thus, at a given polar latitude, T_{eq}^{strat} varies between polar summer and polar winter over a 360 day year. In the original Polvani and Kushner (2002) study, there is a smooth transition from tropospheric to stratospheric specifications of T_{eq} across 100 hPa. Hung and Gerber (2013) reported a number of problems that result from the use of the Polvani and Kushner (2002) equilibrium temperature profile. They concluded that the culprit was a bias in the lower stratospheric equilibrium temperatures, which were too warm. In this study, we deviate slightly from the Polvani and Kushner (2002) equilibrium temperature profile, in that we cause T_{eq} to transition from tropospheric to stratospheric specifications at 200 hPa, rather than at 100 hPa. Thus, the cold anomaly that is the representation of the stratospheric polar vortex in this model comes into effect lower down in the stratosphere and addresses the bias in lower stratospheric equilibrium temperatures reported by Hung and Gerber (2013). Figure 2-1 shows a snapshot of T_{eq} at northern hemisphere winter solstice, and can be compared with Figure 1 in Kushner and Polvani (2006).

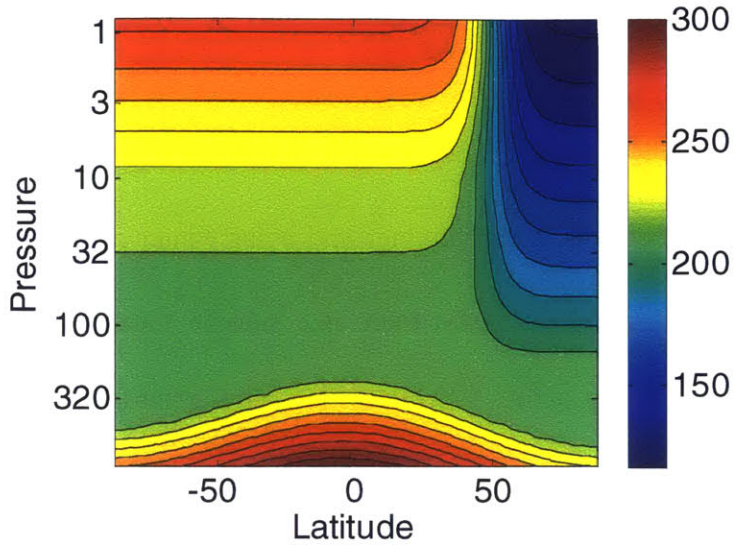

Figure 2-1: Snapshot of the equilibrium temperature profile (K) at northern hemisphere winter solstice. The contour interval is 10 K.

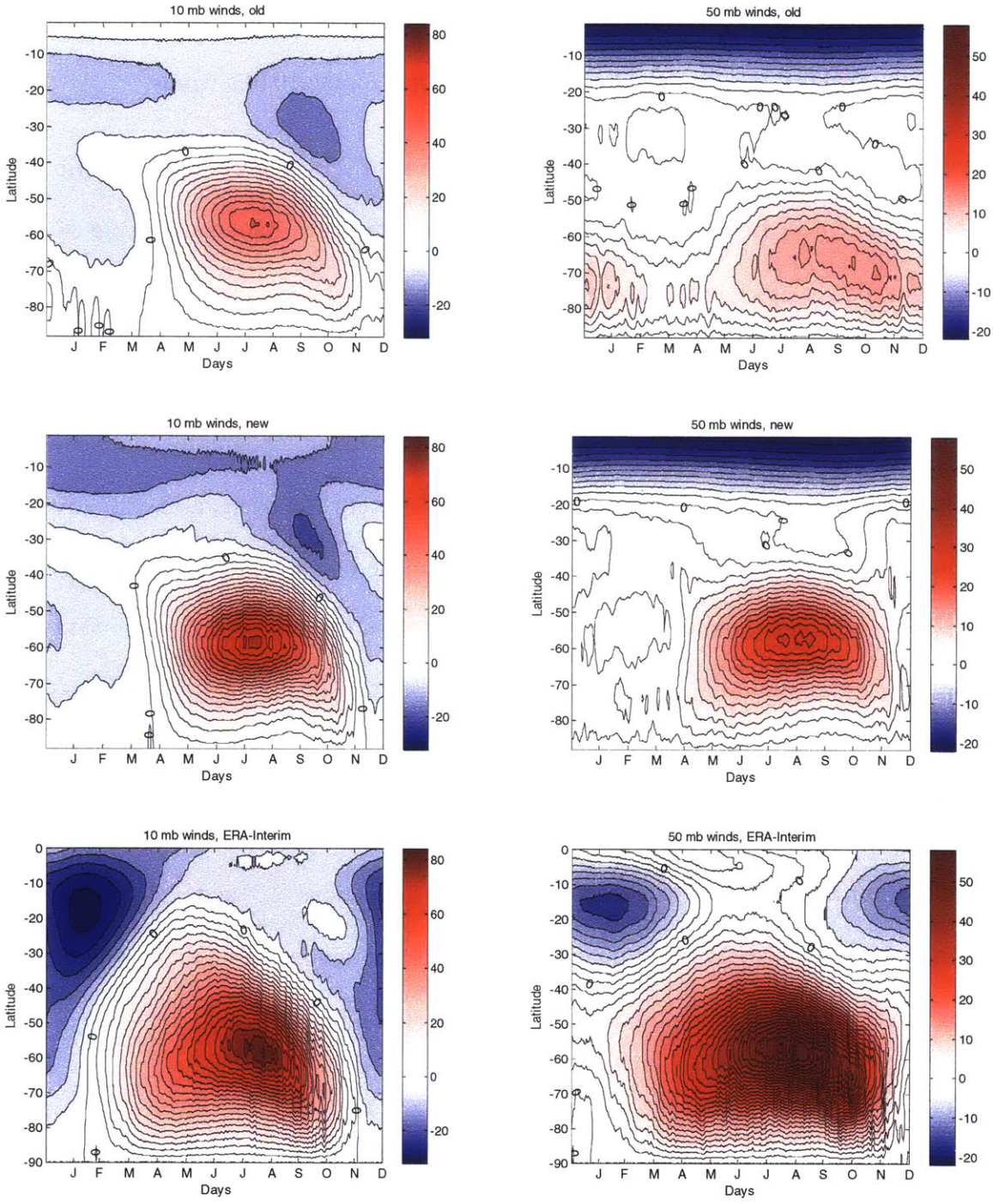

Figure 2-2: Seasonal cycle of zonal mean zonal winds (ms^{-1}) at 10 hPa and 50 hPa from the model (h_0=0), with the equilibrium temperature specifications of Kushner and Polvani (2002) in the top panel, from the model with the new equilibrium specifications used in this study in the

middle panel, and from ERA-Interim (Southern Hemisphere) in the bottom panel. The contour interval is 2 m/s for the 50hPa winds and 4 m/s for the 10 hPa winds.

This change leads to a marked improvement in the seasonal cycle of lower stratospheric zonal winds. The improvement is evident in Figure 2-2, which compares the annual cycle of zonal mean zonal winds at 10 hPa and 50 hPa generated from the model using the T_{eq} specifications of Polvani and Kushner (2002) in the top panel with the new T_{eq} specifications that we use in the middle panel. These figures are from a model configuration without topography, and, as will be described in Section 2.3, this configuration results in a Southern Hemisphere-like stratospheric seasonal variability. The bottom panel shows the annual cycle of zonal mean zonal winds at 10 hPa and 50 hPa for the Southern Hemisphere from ERA-Interim (Dee et al. 2011), for comparison. The new equilibrium temperature specifications lead to a stronger polar vortex both at 10 hPa and 50 hPa. In addition, the persistence of westerly winds in the summer at 50 hPa is reduced, so that the new T_{eq} specifications result in a sharper seasonal cycle, with a clear seasonal formation and breakup of the polar vortex. In sections 2.3 and 2.4, we use this improved model setup to explore the climatology and seasonal and interannual variability of the polar vortex forced by different amplitudes of wave-1 and wave-2 topography.

Table 1 summarizes results from the experiments analyzed here. We integrated every model experiment for 35 years and analyzed the last 30 years. Experiment 4 (with 4000 m wave-2 topography), which resulted in the most Northern Hemisphere-like stratospheric variability, i.e. a frequency of sudden warming events that matches the observations, was run for a further 20 years, giving us a larger dataset for the analysis of sudden warming events. Figure 2-3 compares the latitude-pressure structure of the wintertime (averaged from December to February) winds

for the experiments without topography and wave-1 and wave-2 topography with h_0=4000 m. Increasing the tropospheric wave forcing from the inclusion of increasing heights of topography of either wavenumber reduces the strength of midwinter westerlies.

Experiment	Topography	Peak 50 hPa wind at 60°N (m/s)	Mean SFW timing (day of year)	Standard deviation of SFW timing (days)	SSWs/year
1	None	28	160	19.4	0
2	2000 m wave-2	32	141	21.3	.17
3	3000 m wave-2	19	98	20.5	.2
4	4000 m wave-2	13	88	31	.62[1]
5	2000 m wave-1	30	155	21.2	0
6	3000 m wave-1	28	149	17.5	0
7	4000 m wave-1	23	114	10.6	0.033
8	5000 m wave-1	13	97	15	0.1
NH		24	103 (April 13)	15.1	0.61[2]
SH		55	335 (December 1) Or 155 days after July 1	12.9	0.033

Table 1: Bottom topography used, the annual maximum of 50 hPa winds at 60°N, mean timing of final warming events, standard deviation in their timing, and the frequency of midwinter warming events from 30 years in the model experiments. The corresponding statistics for the years 1979-2008 (30 years) from ERA-Interim are included in the bottom two rows for comparison. While comparing the final warming date in the model experiments with that in reanalysis, it should be noted that the model year has 360 days.

[1]This value is from a 50 year integration, 20 years longer than the other experiments.

[2]This value is from a larger set of years, 1958-2013.

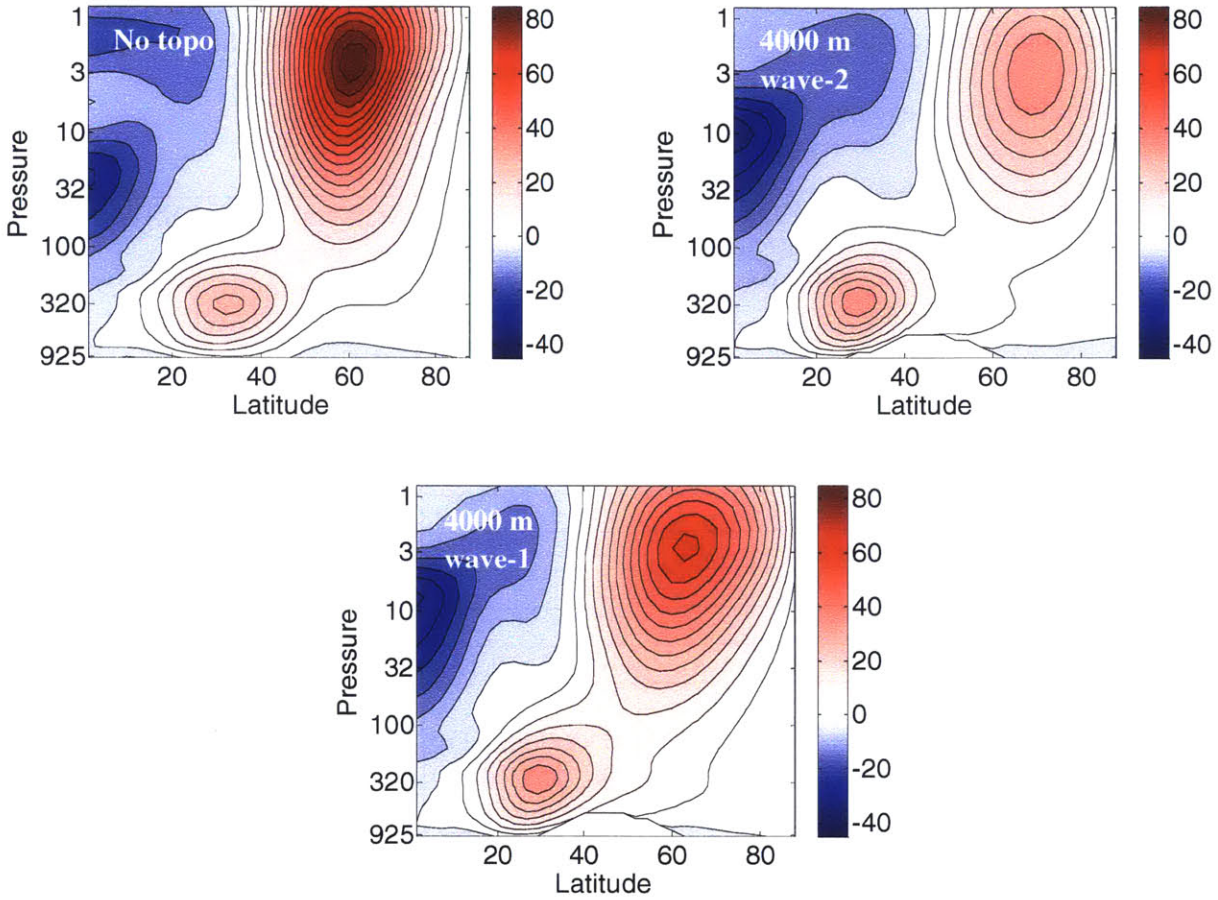

Figure 2-3: Latitude pressure structure of DJF winds (ms^{-1}) for Experiment 1 (no topography, top row, left), Experiment 4 (4000 m wave-2, top row, right), and Experiment 6 (4000 m wave-1, bottom row). The white patch at the bottom indicates the extent of topography. The contour interval is 5 m/s.

2. 3. Stratospheric seasonal variability in the presence of wave-2 topography

Stratospheric seasonal variability is illustrated here with histograms of the 10 hPa monthly mean zonal mean zonal wind at 60° (*cf.* similar figures of Naujokat (1981) and Taguchi and Yoden (2002) showing frequency distributions of polar temperature). The seasonal variability of the observed Southern and Northern Hemisphere stratospheres (1979-2008 from ERA-Interim) is shown in Figure 2-4 for reference. The summertime winds are similar in both hemispheres: winds are weakly easterly and show little variability. Significant differences between the hemispheres, however, appear in the winter winds. The midwinter westerlies in the Antarctic polar vortex are much stronger than those in the Arctic, and most of the variability in the Antarctic winds occurs at the end of the winter and into spring, in contrast to the midwinter variability evident in the Arctic.

Zonal wind histograms for Experiment 1 (without topography) and Experiments, 2, 3 and 4 (with increasing amplitudes h_o of wave-2 topography) are shown in Figure 2-5. The strength of the midwinter westerlies in the model experiments reduces with increased h_o. The experiment without topography most resembles the observed southern stratosphere, with most of the variability occurring after spring equinox, and little variability through the winter. Although the maximum winds do not reduce significantly between the experiments with h_0=*0*m and h_0=*2000*m, the latter exhibits somewhat more wintertime variability. The experiments with 3000 m and 4000 m topography begin to resemble the real Northern Hemisphere, with weaker westerlies and significant variability in the strength of westerlies around midwinter. These experiments also show reduced mean westerlies and much less variability in late winter and early

spring, similar to the results of Taguchi and Yoden (2002) with wave-1 forcing. However, unlike the threshold behavior reported by Scott and Haynes (2002), also with wave-1 forcing, this shift toward early winter occurs rather smoothly as h_0 is increased.

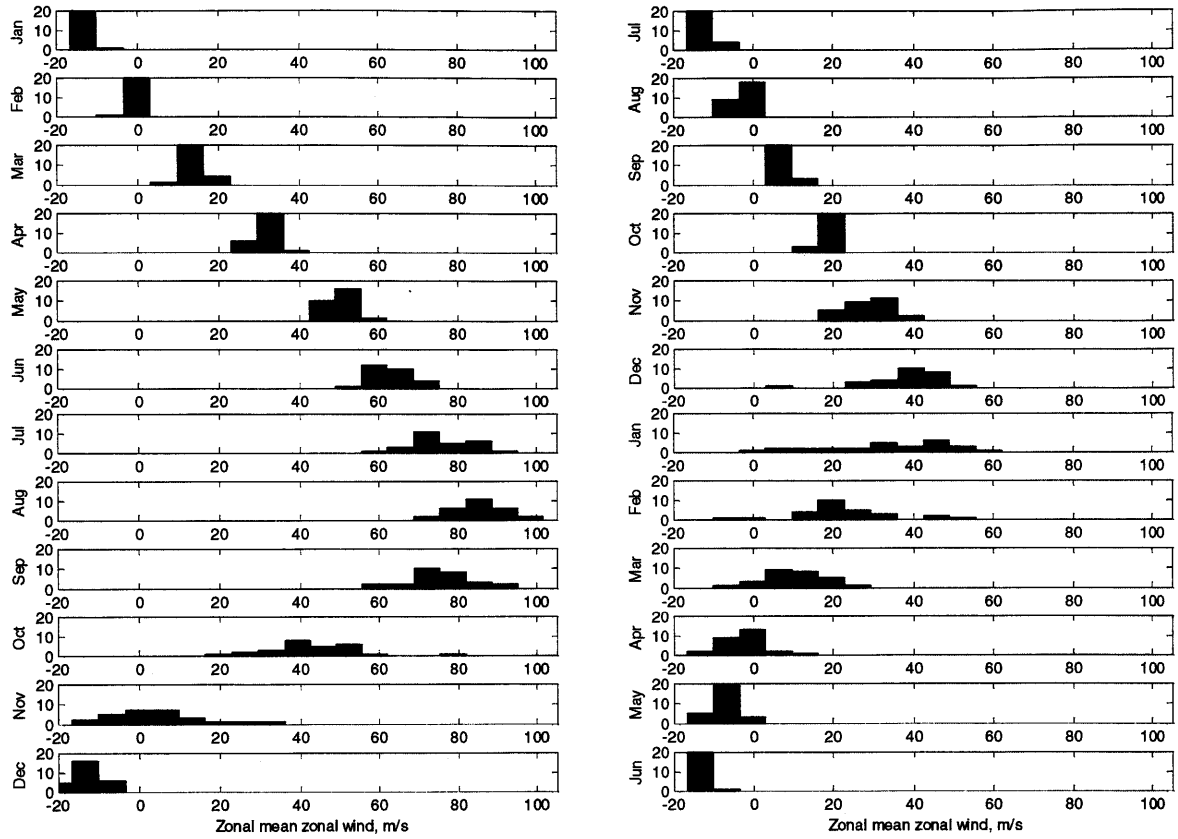

Figure 2-4: Histogram of 10 hPa zonal mean zonal wind at 60°S in the left panel and 60°N in the right panel for 30 years from the ERA-Interim Reanalysis. Midwinter (June and July for the Southern Hemisphere and December and January for the Northern Hemisphere) is in the center of both histograms. The ordinate shows the number of occurrences of a specific value of zonal mean zonal wind.

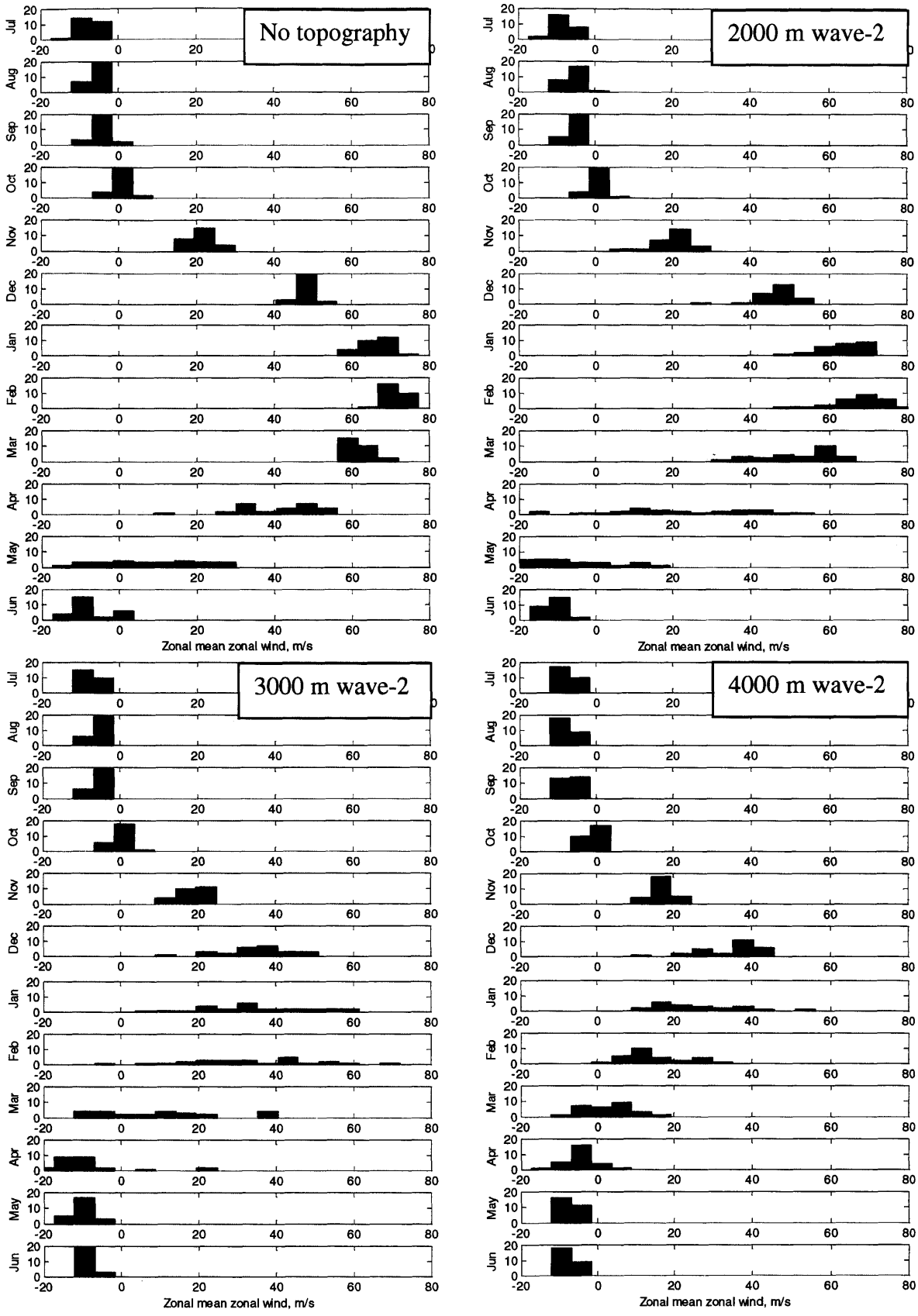
No topography
2000 m wave-2
3000 m wave-2
4000 m wave-2
Jul
Aug
Sep
Oct
Nov
Dec
Jan
Feb
Mar
Apr
May
Jun
Zonal mean zonal wind, m/s

Figure 2-5: Histograms of 10 hPa zonal mean zonal wind at 60°N for Experiments 1 (top left), 2 (top right), 3(bottom left), and 4(bottom right). The ordinate shows the number of occurrences of a specific value of zonal mean zonal wind.

The climatological evolution of the geopotential height amplitude of wave-2 in the middle stratosphere for these experiments is shown in Figure 2-6. Even without topographic forcing the amplitudes reach 500m, forced presumably by the nonlinear interaction of baroclinic, synoptic-scale eddies in the troposphere (Scinocca and Haynes, 1998). However, note that the broad peak in wave amplitudes, occurring between winter solstice and spring equinox, does not coincide with the peak in zonal wind variability for this case of $h_0=0$ (*cf.*, Figure 5). With topographic forcing, the amplitudes are greater; while wave growth occurs at about the same time (*i.e.*, about one month before winter solstice), the timing of peak amplitudes, and of their subsequent collapse, drifts systematically earlier as h_0 is increased, now mirroring the similar shift in mean zonal wind behavior seen in Figure 2-5. One remarkable feature of Figure 2-6, which is also evident in the results of Taguchi and Yoden (2002), is the apparent saturation of wave amplitudes, which do not show any marked increase as h_0 is increased from 2000m to 4000m. At small h_0 there is no evidence of the early winter resonance described by Scott and Haynes (2002), nor of the springtime peak seen in observations and found in models both by Scott and Haynes and by Taguchi and Yoden. This saturation of wave amplitudes that is seen at 10 hPa is not evident in the troposphere, as shown in Figure 2-7 (which shows the climatological evolution of geopotential height amplitude of wave-2 for the four experiments at 95 hPa). Attempts to identify a saturation limit on wave amplitudes have been made in the past (Lindzen and Schoeberl 1982, Schoeberl 1982). Our saturated amplitudes do not come close to the limits calculated by Lindzen and Schoeberl. An open question is whether this saturation can be related to the distribution of PV gradients in winter.

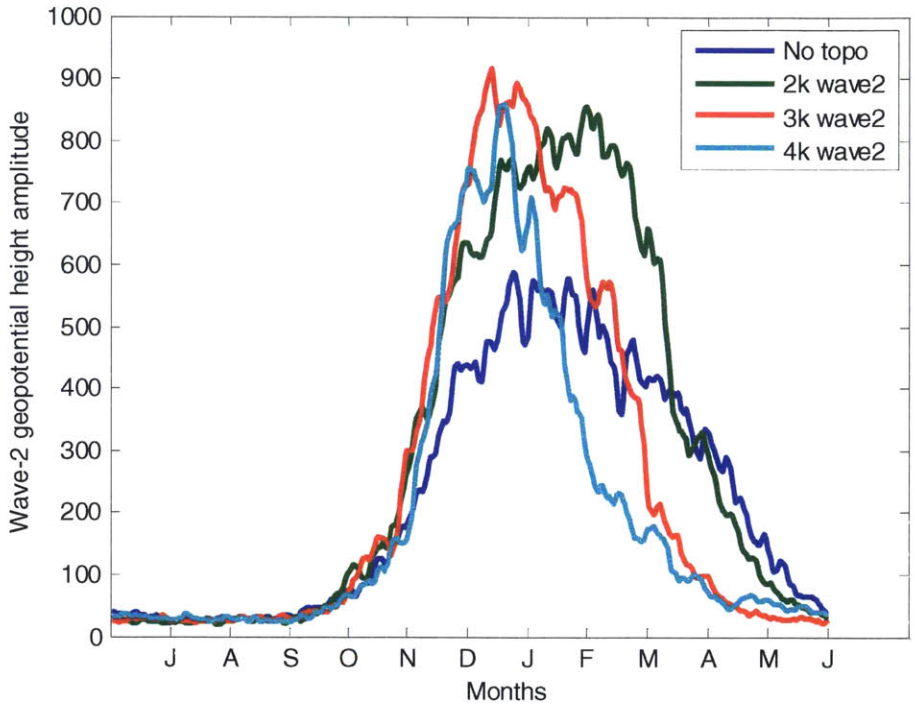

Figure 2-6: The climatological evolution of the wave-2 geopotential height amplitude (m) at 10 hPa, 60°N for Experiments 1 (no topography), 2 (2000 m wave-2), 3(3000 m wave-2) and 4 (4000 m wave-2).

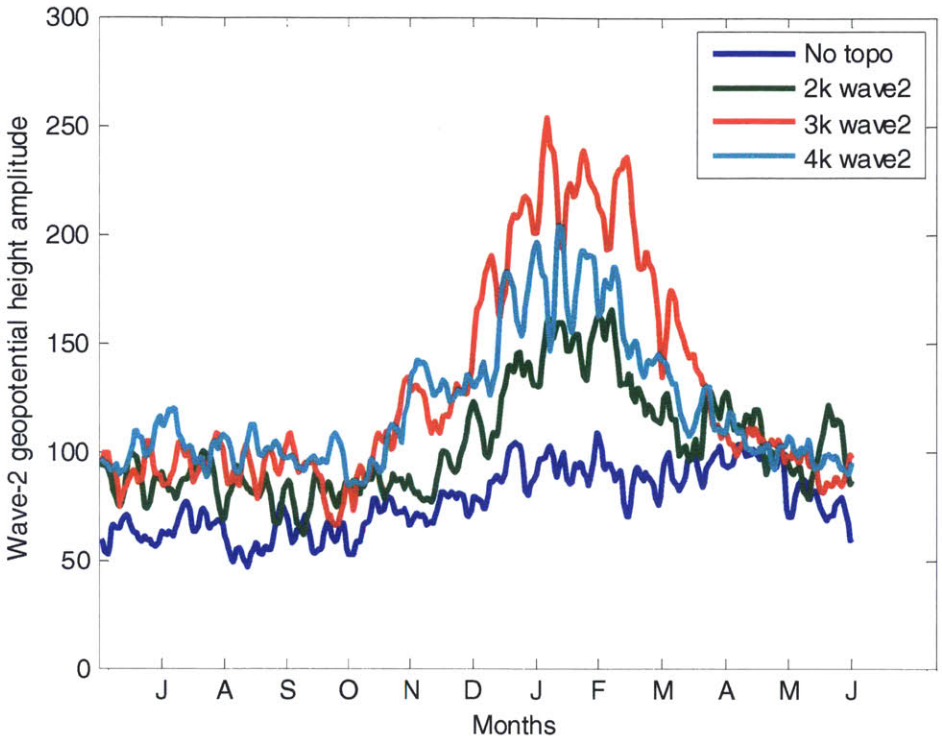

Figure 2-7: The climatological evolution of the wave-2 geopotential height amplitude (m) at 95 hPa, 60°N for Experiments 1 (no topography), 2 (2000 m wave-2), 3(3000 m wave-2) and 4 (4000 m wave-2).

This temporal shift of wave behavior from the end of winter to midwinter is also evident in the magnitude of wave activity propagation into the stratosphere. Figure 2-8 shows the mean seasonal cycle of eddy heat flux $\overline{v'T'}$ at 50 hPa, a measure of the vertical component of Eliassen-Palm flux in the lower stratosphere, for the same four wavenumber 2 experiments. Unlike what is seen in geopotential height amplitudes in Figure 2-6, here we do see a clear late winter/spring peak in the heat fluxes for $h_0=0$; the peak shifts systematically towards midwinter with

increasing h_0. It is also evident that the latitude of the maximum heat fluxes migrates with the seasonal cycle; we will revisit this in the section on final warming events.

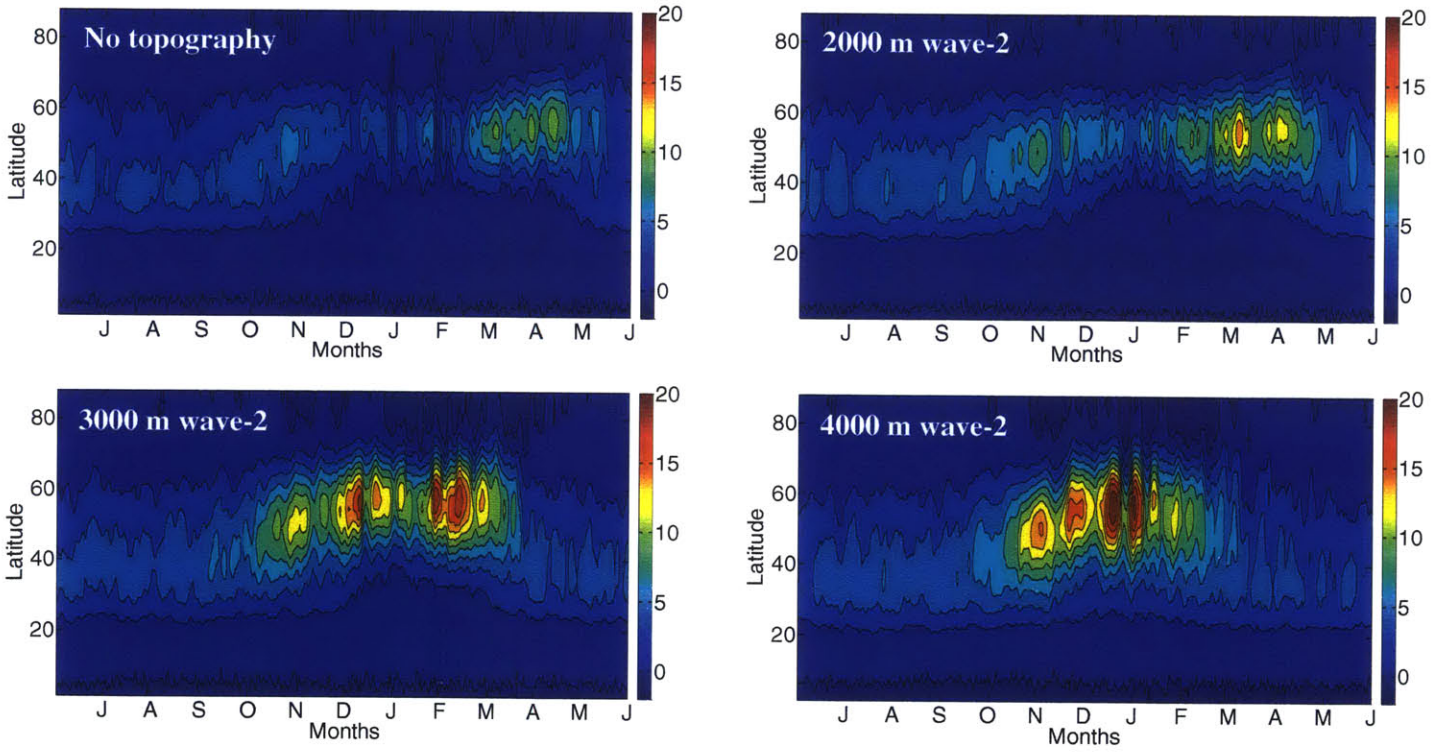

Figure 2-8: The seasonal cycle (calendar average) of 50 hPa heat fluxes (mKs^{-1}) for Experiments 1 (no topography, top row, left), 2 (2000 m wave-2, top row, right), 3 (3000 m wave-2, bottom row, left), and 4 (4000 m wave-2, bottom row, right).

SSW events

All of our experiments exhibit some level of wintertime variability. For our purposes we adopt the definition of Charlton and Polvani (2007), and define "major" SSWs as those involving a reversal of the zonal mean westerlies at 10 hPa and 60°. Events that occur within 20 days of the final warming (to be defined below) are excluded.

In observations, the Arctic vortex exhibits major SSWs about every other year on average (in the combined ERA40 (Uppala et al. 2006) +ERA Interim record from 1958-2013, there are 34 major SSWs, giving a mean frequency of 0.61 events per winter). Gerber and Polvani (2009) found that the most realistic frequency of such events (major SSWs every 200-300 days in their perpetual January integrations) occurred when their model was forced with 3000 m wave-2 topography. In our model, as seen in Table 1, the inclusion of wave-2 topography of modest amplitude leads to infrequent major SSWs (Experiments 2 and 3). The frequency of such events increases monotonically with h_0 (in the range explored here). We find that major SSWs occur with a realistic Northern Hemisphere-like frequency when h_0=4000 m (Experiment 4, for which the average occurrence is 0.62 per winter).

We now examine both 'weak' and 'strong' vortex events from Experiment 4. We identify weak and strong vortex events based on 1σ and 2σ annular mode anomalies (anomalies of the principal component time series corresponding to the first EOF of geopotential height at 10 hPa which exceed 1 or 2 standard deviations). For each year, we identify the largest annular mode anomalies, i.e. we count at most one weak vortex event and one strong vortex event every year. Among this set of 'largest' weak and strong vortex events, we group them into 1σ and 2σ events. In the 50 model years, there were 50 weak vortex events that met the 1σ criterion, amongst

which 30 events also met the 2σ criterion. There were fewer strong vortex events -- 41 events met the 1σ criterion, amongst which only 6 events also met the 2σ criterion. The top row of Figure 2-9 shows composites of geopotential height anomalies normalized by their standard deviations for a 60 day period centered on the 20 weak vortex events that met the 1σ criterion (but not the 2σ criterion) in the left panel and the 30 2σ weak vortex events in the right panel. The 2σ events result in both a stronger and a more persistent impact at the surface than the 1σ events. The bottom row of Figure 2-9 shows the heat flux anomalies at 95 hPa normalized by their standard deviations and composited on all 50 weak vortex events. There is a burst of poleward heat flux anomalies just prior to the weak vortex events, followed by equatorward heat flux anomalies just after. The wavenumber-2 component accounts for most of these heat flux anomalies.

Figure 2-10 shows geopotential height anomalies normalized by their standard deviations for a 60 day period centered on the 41 strong vortex events, with their associated heat flux anomalies at 95 hPa, also normalized by their standard deviations. Composites of 2σ strong vortex events are not shown, because of their small numbers. Just as in the case of weak vortex events, we see anomalously equatorward/poleward heat flux anomalies just before and after strong vortex events. Our analysis of weak and strong vortex events can be compared with the studies of Baldwin and Dunkerton (2001) and Gerber and Polvani (2009). However, strong vortex cases were not analyzed in the perpetual winter configuration of the model by Gerber and Polvani (2009) because "events" were not well captured by any particular threshold; the vortex tended to slowly build up and decay, without a marked, event-like structure.

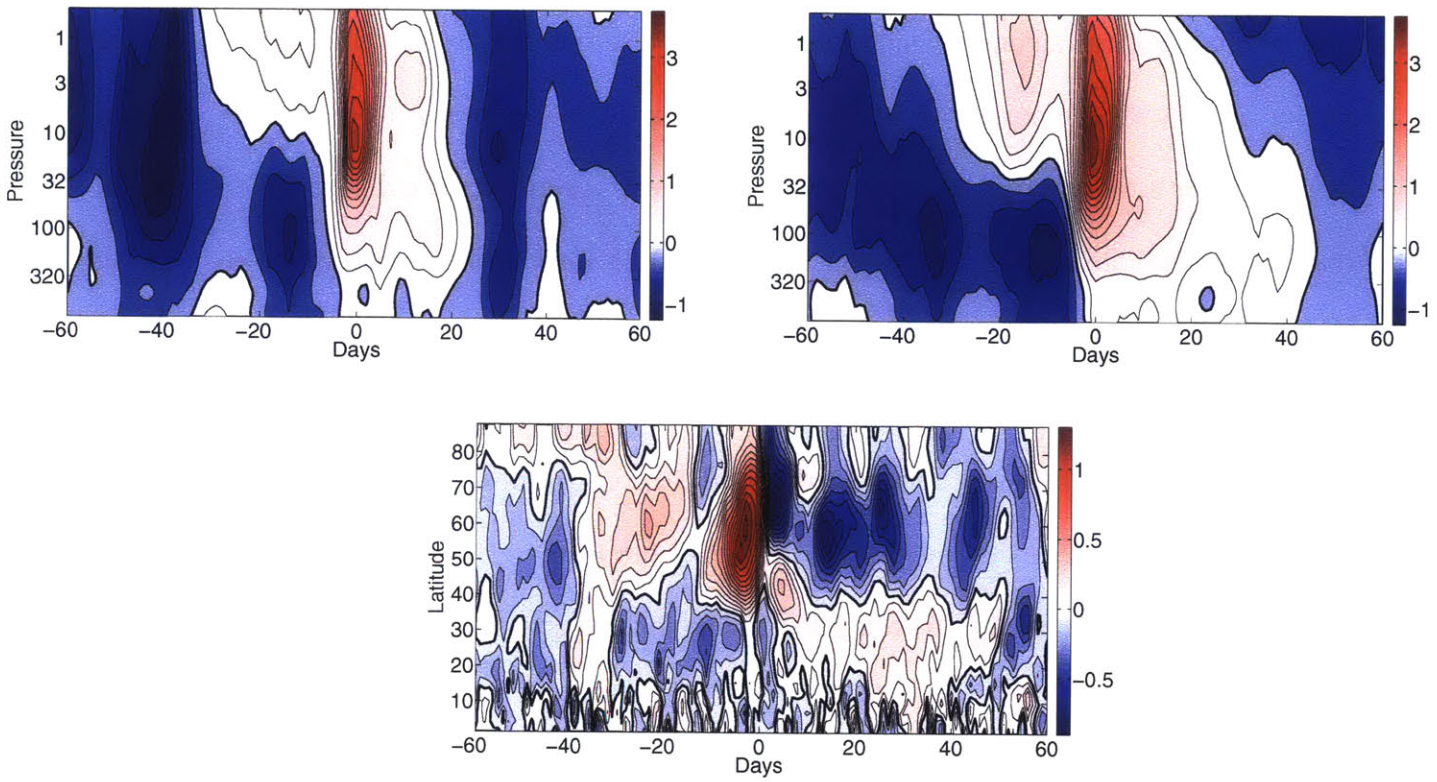

Figure 2-9: Evolution of weak vortex events, from Experiment 4 (4000 m wave-2). The top row shows geopotential height anomalies averaged from 65-90°N, normalized by their standard deviations and composited on weak vortex events. The left and right panels of the top row show events that are chosen based on 1σ and 2σ or greater annular mode anomalies at 10 hPa. The contour interval is .25. The bottom row shows heat flux anomalies at 95 hPa normalized by their standard deviations and composited on all 50 weak vortex events. The contour interval is 0.1. The zero level is shown by the heavy black contour in all panels.

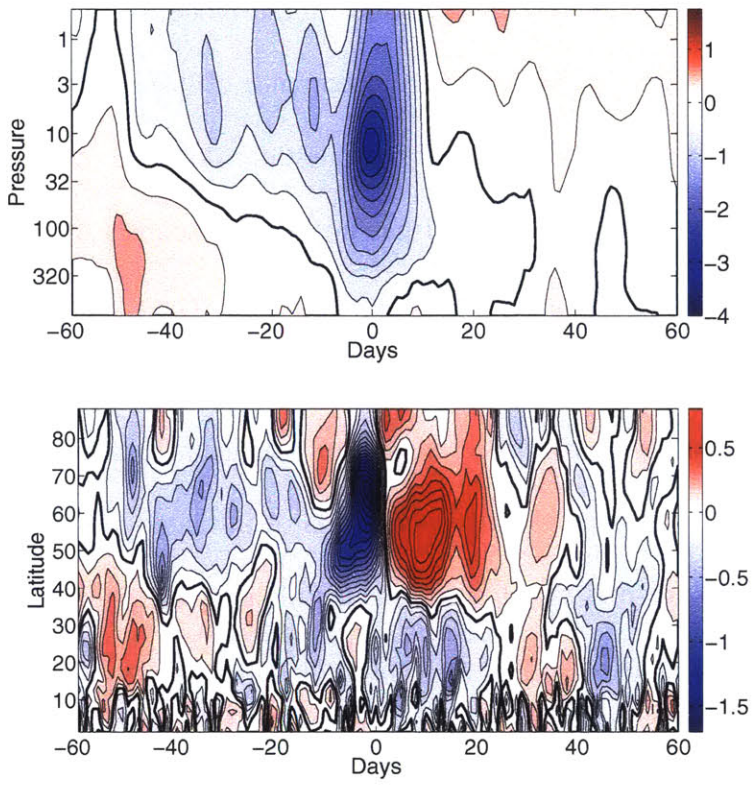

Figure 2-10: Evolution of strong vortex events from Experiment 4 (4000 m wave-2). The top panel shows geopotential height anomalies averaged from 65-90°N, normalized by their standard deviations and composited on strong vortex events, defined as 1σ annular mode anomalies at 10 hPa. The contour interval is 0.25. The bottom panel shows heat flux anomalies at 95 hPa, normalized by their standard deviations and composited on strong vortex events. The contour interval is 0.1. The zero level is shown by the heavy black contour in both panels.

Major SSW events do not occur every year, either in the model or in the observed Northern Hemisphere stratosphere. The distribution of the occurrence of these events, or, more generally, of winters that are highly disturbed, leads to the question: does the stratosphere retain some 'memory' of the previous winter? The model has no external sources of memory (such as sea surface or land conditions) but the tropical zonal winds may retain memory from year to year (the "low-latitude fly-wheel" effect; Scott and Haynes, 1998). In the 50 model years, there were 31 years in which the winter was disturbed enough to produce at least one major SSW. In the left panel of Figure 2-11, we compare the distribution of the interval between years in which there were major SSWs (shown as blue bars) to the distribution that results from a time series of 1 million randomly generated 0s and 1s with the probability of occurrence of a "1" fixed at 31/50=0.62 (shown as grey bars). With the random number generator we explicitly specify that there is no memory from one "year" to the next. We sample the randomly generated 0's and 1's in batches of 50 years to generate 20000 batches of 50 years (i.e. we use a Monte Carlo method), and plot the 95^{th} and 5^{th} percentiles of the distribution of intervals between 1's as grey dots in the left panel of Figure 10. For comparison, we follow a similar procedure for midwinter warming events identified from the ERA-40 Reanalysis (obtained from Charlton and Polvani, 2007) from 1958-2002, combined with those we identify from ERA-Interim data from 2003-2013; these results are shown in the right panel of Figure 2-11. The dearth of major SSWs in the 1990s (the interval of 8 years in the right panel of Figure 10) is the only potentially significant departure from a random process with no interannual memory; an 8 year gap occurs in only 2.7% of the random 56 year batches. In our idealized model, however, the occurrence of major SSWs shows no sign of being significantly different from the null hypothesis of events occurring at random

with a given probability. Thus, there is no evidence of winter-to-winter stratospheric memory in our model.

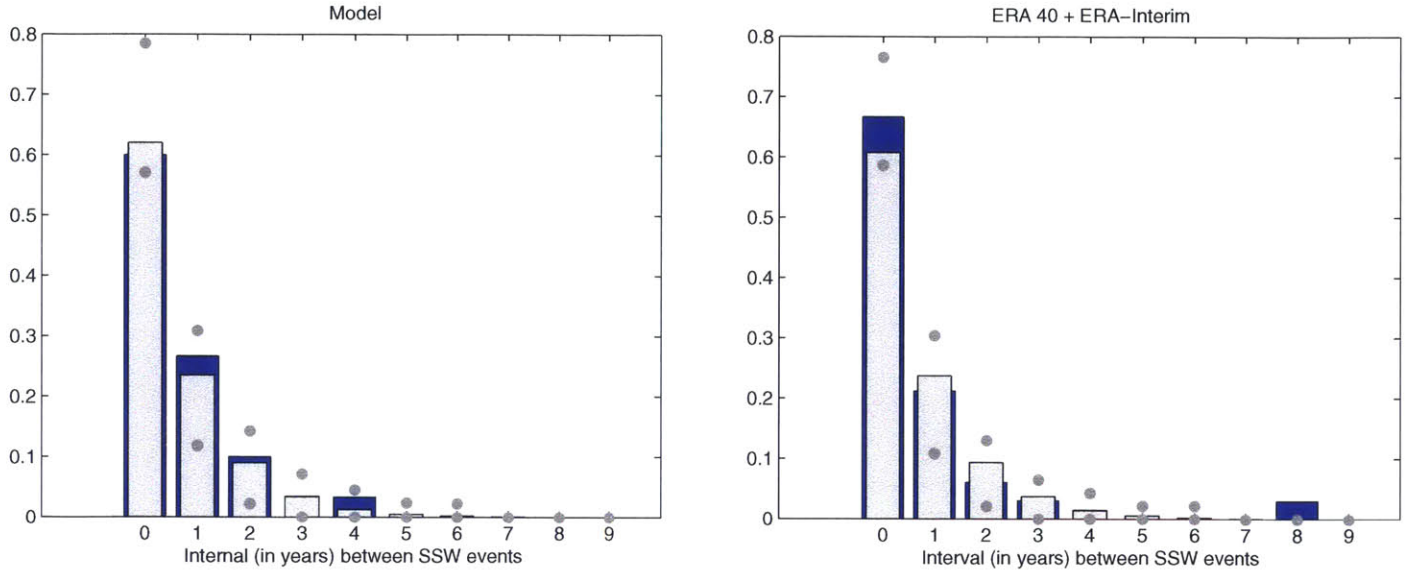

Figure 2-11: Histograms of the distribution of the interval (in years) between midwinter warming events from the idealized model (from the experiment with 4000 m wave-2 topography, which had a realistic Northern Hemisphere-like frequency of midwinter warming events) in the left panel and from the ERA Reanalyses in the right panel. Blue bars show the actual distribution of intervals between midwinter warming events in the model run/reanalysis. Grey bars show the distribution of intervals between midwinter warming events from the random time series of 0s and 1s with a given probability. The grey dots are the 95th and 5th percentiles of the samplings from the random sequences of 0s and 1s.

Final warming events

In our analysis of FW events in the model, we follow Black and McDaniel (2007a, b) in focusing attention on the 50 hPa level. Examining FW events in the Northern Hemisphere, Black and McDaniel (2007a) defined the timing of these events as the final time when the 50-hPa zonal mean zonal wind at 70°N drops below zero without returning to 5 ms^{-1} until the subsequent autumn. For southern hemisphere FW events, however, where the zonal wind may remain weakly westerly at 50hPa through the summer, they found it expedient to alter the definition as the final time that the zonal mean zonal wind at 50 hPa and 60°S reached the value of 10 m s^{-1} (Black and McDaniel 2007b). In our case, each choice of the height and wavenumber of topography results in a different stratospheric climatology in the model. In order to apply a uniform definition of FW events across all model experiments, we define the timing of these events as the day that the zonal mean zonal wind at 50 hPa and 60° falls below 25% of its annual maximum for the last time. For comparison, we apply the same definition to 30 years from ERA-Interim data (1979-2008) (shown for the Arctic and Antarctic vortices in the last two rows of Table 1).

As we have seen, Experiment 1 (with no topography) results in a Southern Hemisphere-like stratospheric seasonal variability with a relatively smooth seasonal cycle of zonal winds and no major SSW events[2]. FW events occur on the average shortly before summer solstice (*i.e.*, more than one radiative relaxation time constant after equinox). As seen in Table 1, there is a monotonic shift towards earlier final warming events with increasing h_0, consistent with the

[2] Kushner and Polvani (2005) reported the occurrence of one strong midwinter warming event in an 11000 day perpetual January integration in a model setup using the T_{eq} specifications of Polvani and Kushner (2002), with a lapse rate of 2 K/km and no topography. We did not see such an event in our 30 year integration.

results of Sun and Robinson (2009) and Sun et al. (2011). In Experiment 4 (with h_0=4000 m, for which we see Northern Hemisphere-like stratospheric variability) the FW happens 72 days earlier (compared to Experiment 1) on average, i.e. close to vernal equinox, although the FW date becomes more variable from year to year. However, more modest values of h_0 do not cause an increase in the variability in timing of FW events.

The synoptic evolution of final warming events from the experiments without topography and with different amplitudes of wave-2 topography is illustrated in Figure 2-12. Each row of Figure 2-12 shows a typical example of a final warming event from Experiments 1, 2 and 3 (Experiment 4 is similar to Experiment 3 in this respect and is therefore not shown). In the cases with no topography and 2000 m wave-2 topography, as the vortex goes through the final warming it weakens, wanders off the pole and disintegrates into multiple segments. With higher amplitudes of wave-2 topography, the final warming is always a split of the polar vortex, an example of which is shown in the third row of Figure 2-12.

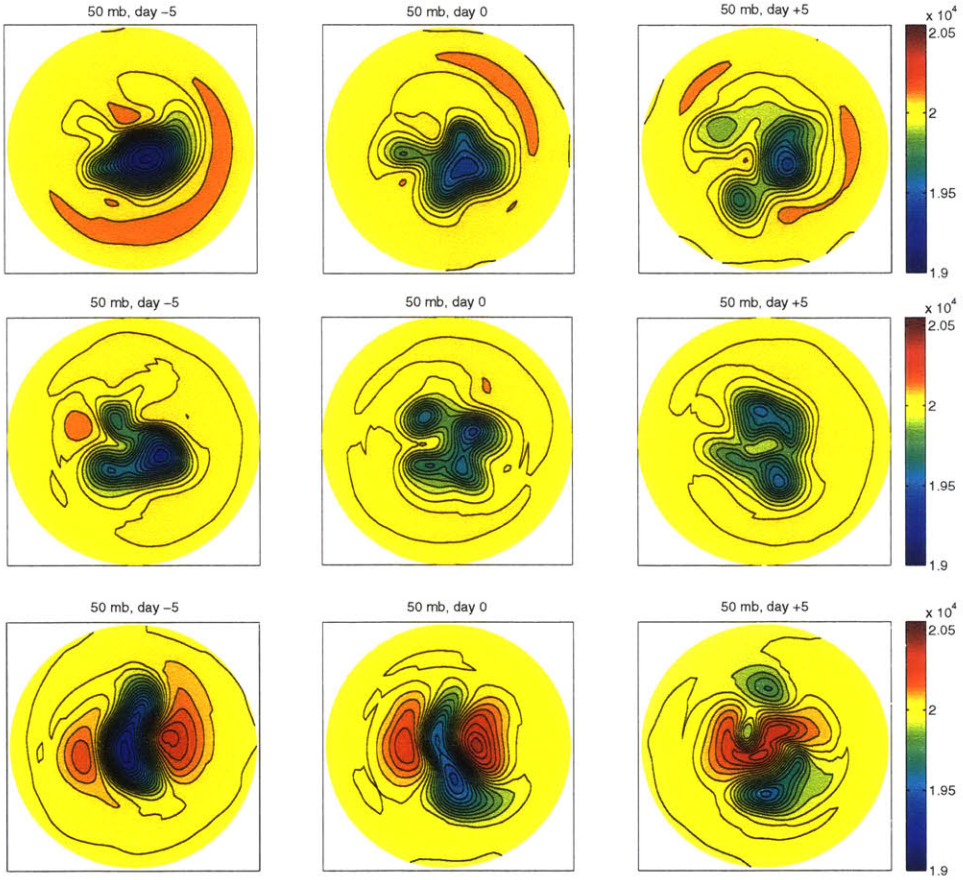

Figure 2-12: Examples of the evolution of 50 hPa geopotential height (m) leading up to and immediately after final warming events. 50 hPa geopotential height is shown 5 days before, the day of, and 5 days after the final warming. These are examples of final warming events from Experiment 1 (no topography, top row), Experiment 2 (2000 m wave-2 topography, second row) and Experiment 3 (3000 m wave-2 topography, bottom row). Experiment 4 (4000 m wave-2 topography) is similar to Experiment 3. The contour interval is 53 m.

Figure 2-13 shows the 50 hPa zonal mean zonal wind at 60°N for a 60 day period composited on FW events for Experiments 1-4 (the experiments without topography and increasing heights of wave-2 topography). The change in winds as the vortex goes through the final warming is larger for higher tropospheric wave forcing, with the exception of the 4000 m wave-2 case in which the vortex is already very weak as it approaches the final warming. The transition in winds as the vortex goes through the final warming is largest in the case of the 3000 m wave-2 topography. Both the cases with 3000 and 4000 m wave-2 topography result in weak easterlies following the final warming.

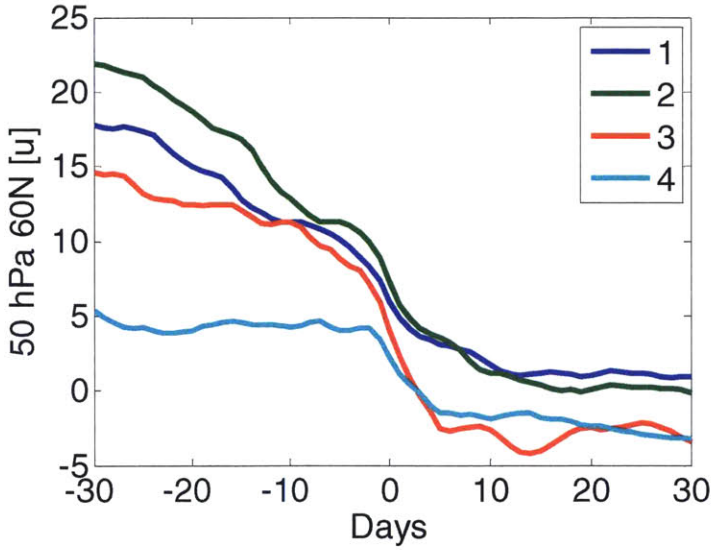

Figure 2-13: 50 hPa zonal mean zonal wind at 60°N (ms^{-1}) composited on the final warming for Experiments 1 (no topography), 2 (2000 m wave-2), 3 (3000 m wave-2), and 4 (4000 m wave-2).

Hu et al. (2014a), in their analysis of the timing of midwinter warming events and final warming events in the NCEP-NCAR reanalysis, suggested that late spring final warming events tend to be preceded by major SSWs, while early FW events do not. Similarly, in Experiment 4, we find that final warming events occur on the average 11 days later in years with major SSW events. This could be related to the transition to easterlies and the consequent suppression of wave propagation into the stratosphere following a major SSW. However, we note that this difference is less than half the standard deviation in the timing of FWs in this experiment.

The behavior of lower stratospheric heat fluxes during FWs is qualitatively similar across the model experiments. Figure 2-14 shows the seasonal cycle of $\overline{v'T'}$ at 50 hPa composited on final warming events for all the wave-2 model experiments. The heat fluxes become strong around the time when the lower stratospheric winds start to become variable, and remain strong until the final warming, when they collapse. The burst of heat fluxes at the final warming is more intense with increasing tropospheric wave forcing, but is less pronounced in Experiment 4, for which SSW events occur about every other year and for which the average zonal winds are weaker. The latitude of the maximum heat fluxes migrates slightly poleward up to the final warming, after which the planetary scale fluxes collapse, and smaller-scale waves (which maximize at lower latitudes) then dominate, leading to a sharp equatorward shift of the locus of maximum heat fluxes.

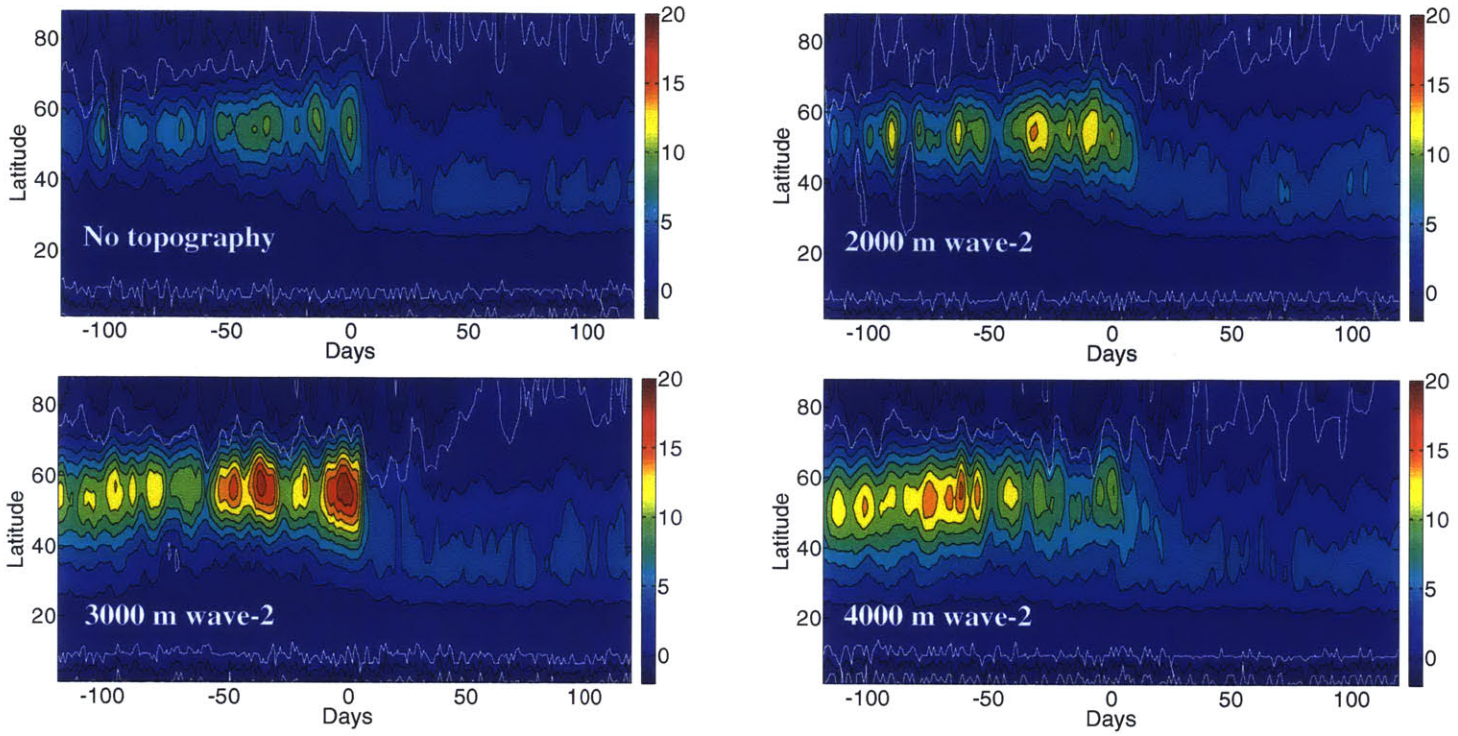

Figure 2-14: 50 hPa heat fluxes (mKs^{-1}) composited on final warming events for Experiment 1 (no topography, top row, left), 2 (2000 m wave-2, top row, right), 3 (3000 m wave-2, bottom row, left) and 4(4000 m wave-2, bottom row, right). The white contour indicates the 95% confidence interval for a two sided t-test.

2. 4. Stratospheric seasonal cycle in the presence of wavenumber-1 topography

Figure 2-15 shows the seasonal cycle and variability of zonal winds at 60°N, 10 hPa, for a range of forcing amplitudes with m=1 topography. As for the m=2 cases, for stronger forcing the model exhibits weaker mean winds, increased variability, and a general drift of these features towards earlier in the winter, although less markedly so than for the m=2 case. In fact, the evolution through the winter of wave amplitudes, shown in Figure 2-16 shows a slight discrepancy in late winter between cases with forcing below or above h_0=3000 m, but otherwise the timing of the seasonal evolution of wave amplitudes is insensitive to forcing amplitude. Just as in the m=2 case, geopotential height amplitudes at 10 hPa appear to saturate at values near 800 m with sufficiently large (3000 m) forcing amplitude. The one exception to this statement is for the case with h_0=5250 m, for which substantially larger amplitudes are reached in midwinter; with greater h_0, however, the magnitudes revert to the saturated values. We currently have no explanation for this non-monotonic behavior.

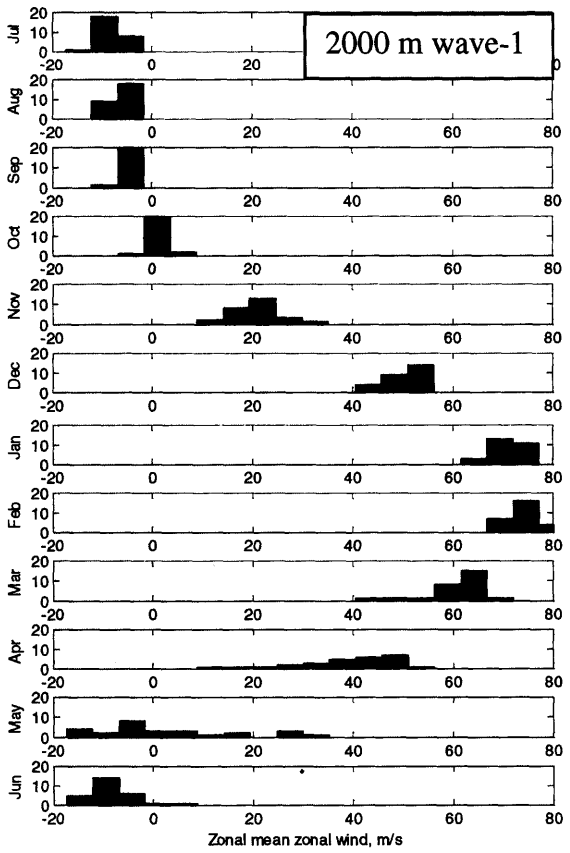
2000 m wave-1
Jul
Aug
Sep
Oct
Nov
Dec
Jan
Feb
Mar
Apr
May
Jun
Zonal mean zonal wind, m/s

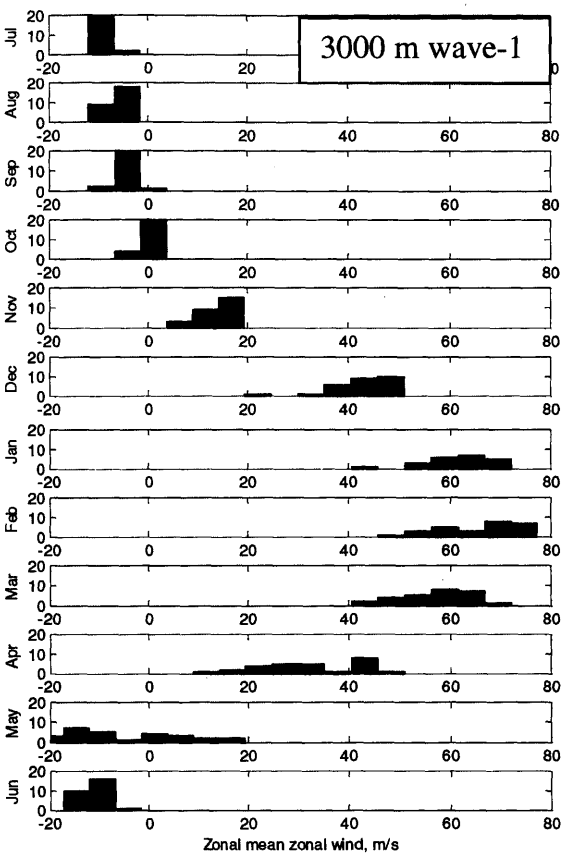
3000 m wave-1
Jul
Aug
Sep
Oct
Nov
Dec
Jan
Feb
Mar
Apr
May
Jun
Zonal mean zonal wind, m/s

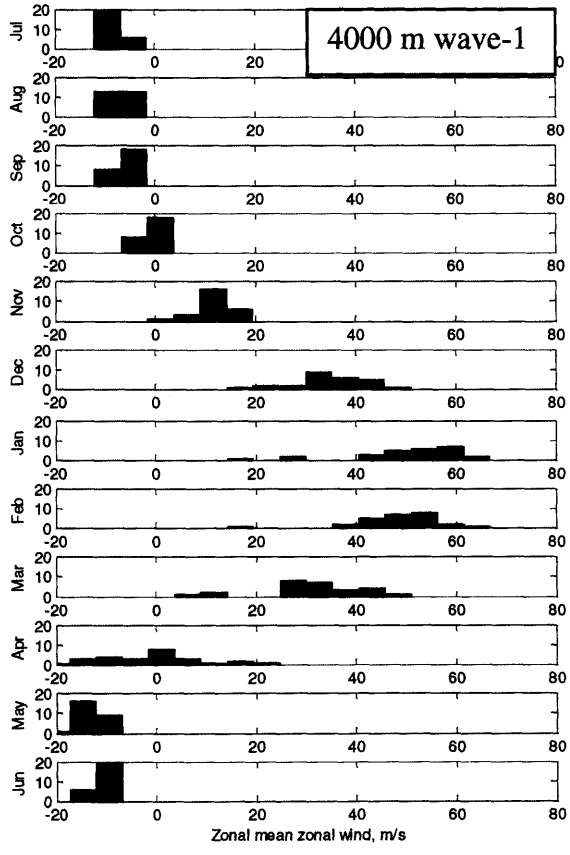
4000 m wave-1
Jul
Aug
Sep
Oct
Nov
Dec
Jan
Feb
Mar
Apr
May
Jun
Zonal mean zonal wind, m/s

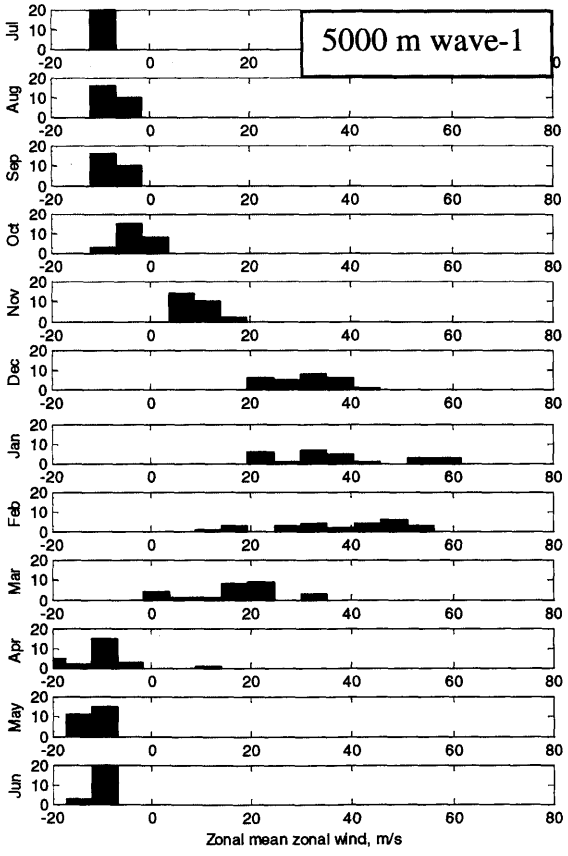
5000 m wave-1
Jul
Aug
Sep
Oct
Nov
Dec
Jan
Feb
Mar
Apr
May
Jun
Zonal mean zonal wind, m/s

Figure 2-15: Histograms of 10 hPa zonal mean zonal wind at 60°N for Experiments 5 (top left), 6 (top right), 7 (bottom left) and 8 (bottom right). The ordinate shows the number of occurrences of a specific value of zonal mean zonal wind.

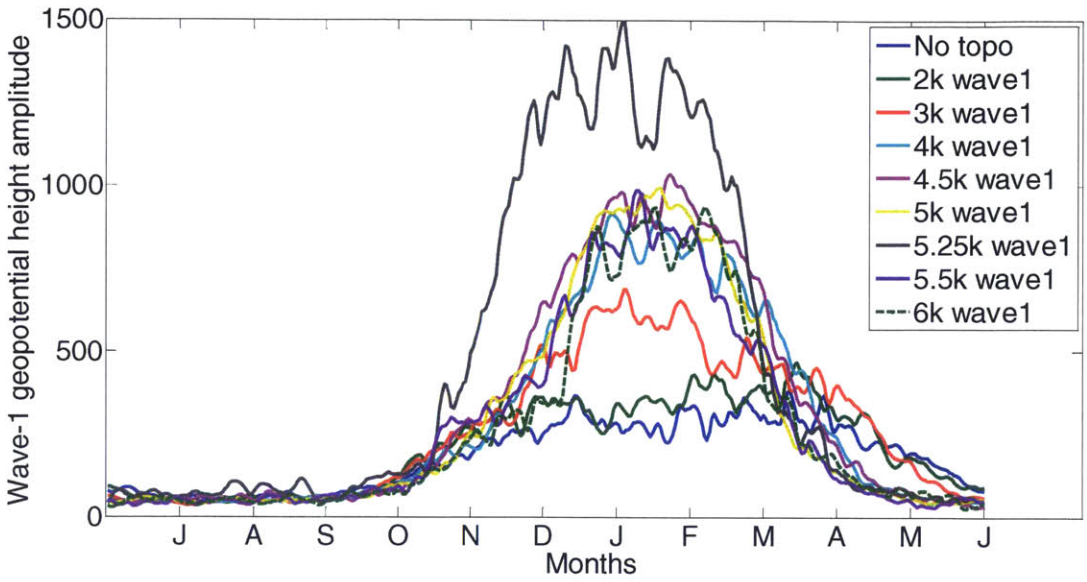

Figure 2-16: The climatological evolution of the wave-1 geopotential height amplitude (m) at 10 hPa, 60°N for Experiments 1 (no topography), 5 (2000 m wave-1), 6 (3000 m wave-1), 7 (4000 m wave-1), 4500 m wave-1, Experiment 8 (5000 m wave-1), 5250 m wave-1, 5500 m wave-1 and 6000 m wave-1.

Another significant difference between these experiments and those with m=2 forcing is that for m=1 forcing we are unable to find a regime with a realistic (northern hemisphere) frequency of major SSWs. This mirrors the inability of Gerber and Polvani (2009) to find any such events in their perpetual solstice experiments. We do find some events, however, for 4000 m $\leq h_0 \leq$ 5500 m, though with lower frequency --- no more than 0.3 events per year --- than observed in northern winter. Some of these are 'displacement' and others 'splitting' events, with more displacements than splits. Strangely, we find no major SSWs for even stronger forcing $h_0 \geq$6000 m; in such cases the stratospheric state at 10 hPa exhibits a very high degree of

interannual variability --- in some winters the vortex never becomes strong --- with violent midwinter disturbances which, however, fail to meet the 'major' SSW criterion of a wind reversal at 60°N. This fact may just be an indication of the arbitrariness of this criterion (Coughlin and Gray, 2009), rather than having any more fundamental implications.

Reasonably realistic FW events are produced in these m=1 experiments. As is evident from Table 1, they happen about a month earlier for h_0=4000 m than for h_0=3000 m, though the shift towards earlier FWs is less dramatic than for the m=2 case, as is suggested by Figures 14 and 15. Figure 2-17 illustrates the synoptic evolution of FW events for h_0=3000 m (other experiments are similar), compared with the case without topography. The two are similar in showing no clear wavenumber preference after the event: in both cases, the vortex weakens, meanders off the pole, and disintegrates into multiple segments as it goes through the final warming.

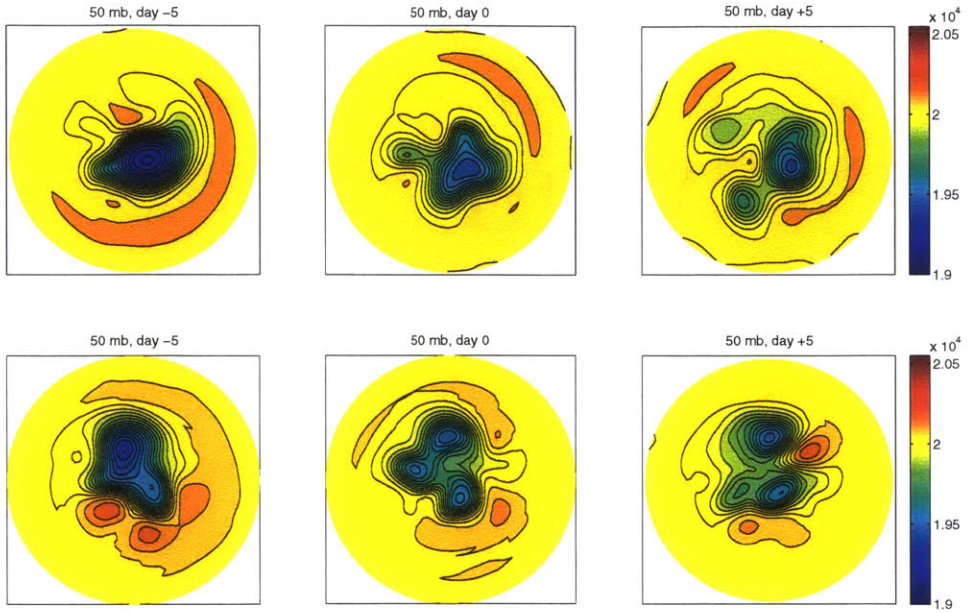

Figure 2-17: Evolution of 50 hPa geopotential height (m) leading up to and immediately after final warming events. 50 hPa geopotential height is shown 5 days before, the day of, and 5 days after the final warming. These are examples of final warming events from Experiment 1 (no topography, top row) and Experiment 5 (3000 m wave-1 topography, bottom row). Experiment 6 (4000 m wave-1 topography) is similar to Experiment 5 (not shown). The contour interval is 53 m.

2. 5. Impact of the stratospheric seasonal cycle on the troposphere

Figure 2-18 shows the seasonal variation of 515 hPa winds for Experiments 1 (no topography), 2 (2000 m wave-2), 3 (3000 m wave-2), 5 (2000 m wave-1) and 6 (3000 m wave-1) as climatological averages. Since (as noted in Section 2. 2) the seasonal cycle in imposed equilibrium temperature is confined to the stratosphere, any seasonal variations in the tropospheric circulation must be of stratospheric origin. At 515 hPa, the zonal flow is dominated by the model's subtropical jet near 30° latitude. In the absence of topography, however, the jet exhibits strong seasonal variation, shifting poleward by almost 10° and weakening in spring, evidently revealing a strong seasonal coupling from the stratosphere. As Figure 2-18 shows, this seasonal variation becomes substantially weaker with increasing surface topography.

It seems that this behavior arises because of the impact of topography on the time scale τ of the model's annular mode, which is shown on each frame of the figure for each experiment. (We determined the annular mode as the first EOF of daily zonal mean zonal wind at 850 hPa. The time scale τ was then defined from the principal component autocorrelation function, as the best least squares fit to an exponential decay.) Increasing the topography produces a marked reduction in τ, consistent with the arguments of Gerber and Vallis (2007). In turn, this leads us to expect a significant reduction in the sensitivity of the tropospheric jet to perturbation from the stratosphere, since Ring and Plumb (2008) and Gerber et al. (2008) found that the response of the tropospheric jet to external forcing increases with τ, as suggested by the fluctuation-dissipation relationship.

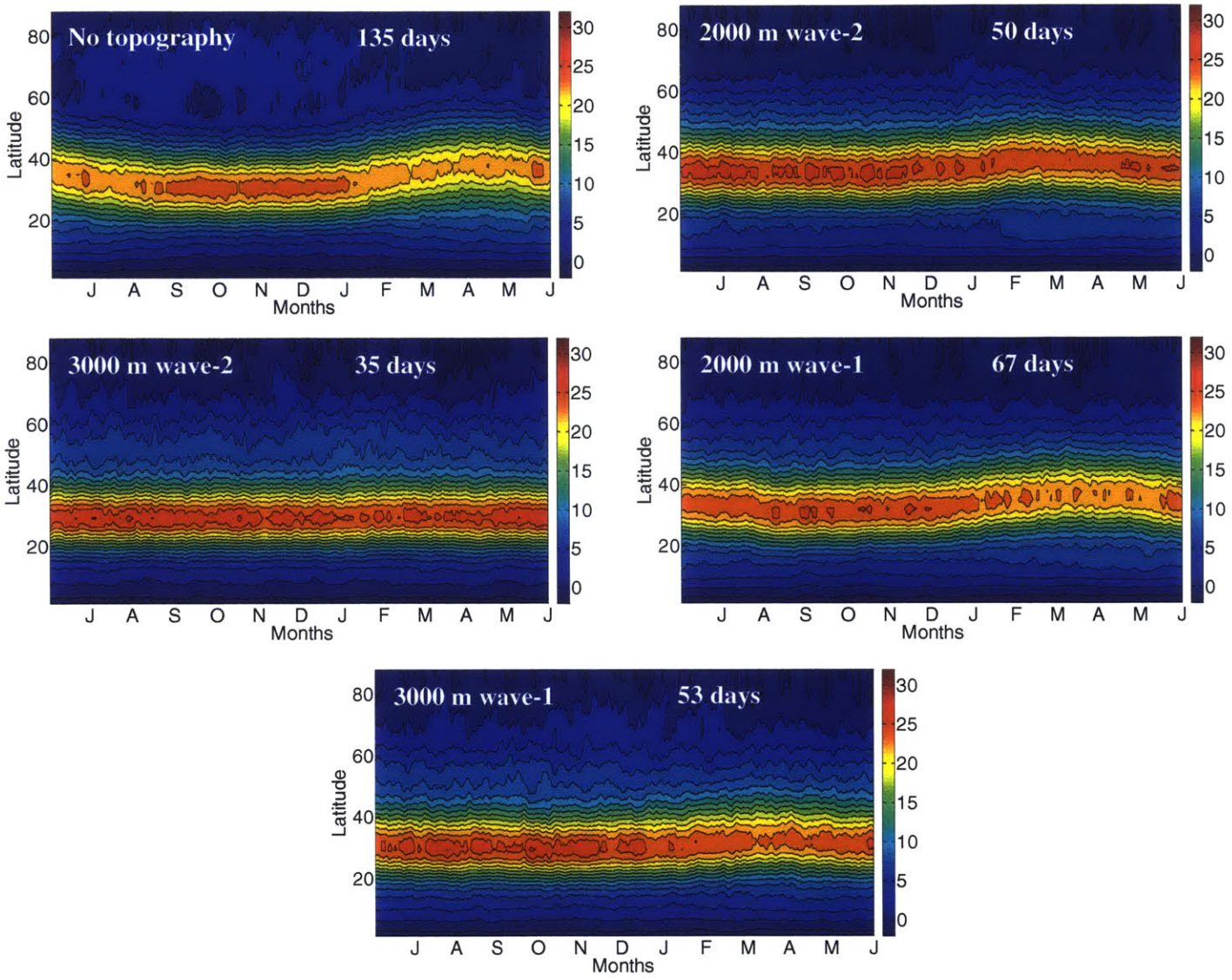

Figure 2-18: Seasonal cycle of 515 hPa winds (ms^{-1}) from Experiments 1 (top row, left, no topography), 2 (top row, right, 2000 m wave-2), 3 (middle row, left, 3000 m wave-2), 5 (middle row, right, 2000 m wave-1) and 6 (bottom row, 3000 m wave-1) shown as calendar averages. The tropospheric annular mode timescale for the experiment is also indicated. Experiments with higher heights of topography of both wavenumbers are similar to Experiment 3 (not shown).

Our interpretation of this behavior as a consequence of decreasing τ, rather than as a direct consequence of the presence of topography, is supported by experiments in which, following Chan and Plumb (2009), we fix topography but change τ by altering the distribution of equilibrium temperature in the troposphere; results (not shown here) show the same reduction in tropospheric seasonality with reduced τ. The seasonal jet shift (the difference between the most equatorward and the most poleward locations of the maximum winds) varies from 1-3° for the lowest values of τ that we were able to obtain in this model (20-40 days) to 8-12° for the cases with τ in the range of 130-150 days. The shift is about 5° for intermediate values of τ (40-100 days). Note from Figure 2-18 that, even in the presence of large topography, the time scale τ exceeds values appropriate to the observed atmosphere by a factor of 2 or 3, implying that even for these cases the potential for coupling with the stratospheric seasonal cycle is likely exaggerated compared with the real atmosphere.

2. 6. Conclusions

One of the more surprising outcomes of these experiments is the different response of the model's stratosphere to wave-1 and wave-2 forcing. With wave-2 forcing, the response evolves smoothly from southern-hemisphere-like behavior, with strong midwinter westerlies and with eddy heat fluxes and zonal wind variability that peak in spring, to a northern-hemisphere-like state in which zonal winds are much reduced on average, and both eddy heat fluxes and zonal wind variability maximize in midwinter, as the wave forcing (in the form of imposed surface topography) is increased. This behavior is similar to that found, using wave-1 forcing, by Taguchi and Yoden (2002). Given sufficiently strong forcing (topographic height of 4000 m) the model produces a realistic frequency of major warmings (as compared with the observed

northern hemisphere). All of these major warming events take the form of vortex splits, which is not surprising, given the wave-2 forcing. We do not, however, find a climatological springtime amplification of the wave geopotential magnitude (as opposed to the heat flux) with weak forcing, in contrast both to Taguchi and Yoden's results and to observed behavior in the southern hemisphere. One striking characteristic of our results is that the stratospheric wave amplitudes saturate, in the sense that increasing topographic height beyond a modest magnitude does not lead to increased geopotential wave amplitude in the middle stratosphere; there are suggestions of the same behavior in Taguchi and Yoden (2002; their Figure 3). Unlike the wave-1 experiments of Scott and Haynes (2002), we find no suggestion of threshold behavior in the response of the system to different levels of topographic forcing, nor of resonant behavior in early winter when the topographic forcing is weak.

The behavior of the model stratosphere's response to wave-1 forcing is rather different. The zonal winds do weaken, and the pattern of their variability shifts somewhat earlier in the winter, as topography is increased, but less markedly so than with wave-2 forcing. More strikingly, the dependence on topographic forcing is non-monotonic. For peak topography h_0 up to about 5000 m, the winter vortex becomes increasingly disturbed, and some major warmings occur (in contrast to Gerber and Polvani (2009) who were unable to find any such events in an almost identical model run in perpetual solstice mode) but never with the frequency observed in the northern hemisphere. However, their frequency then *decreases* with further increases in forcing, although the winter vortex remains highly disturbed. Our difficulty in reproducing the observed frequency with wave-1 forcing is curious, since about half of the observed midwinter warming events in the Northern Hemisphere are displacement events (Charlton and Polvani 2007). When

major warmings do occur in the runs with wave-1 forcing, some are displacement events, while some are splits.

Since we are considering a model setup in which the seasonal cycle in equilibrium temperatures is confined to the stratosphere, we were able to study stratosphere-troposphere coupling on seasonal timescales. We found that the stratospheric seasonal cycle induces a seasonal tropospheric jet shift, the magnitude of which increases with the model's tropospheric annular mode timescale. This suggests that full GCMs will tend to overestimate stratospheric influences on the tropospheric circulation (and, indeed, tropospheric circulation responses to any external forcings) unless their tropospheric annular mode timescale matches observations (most GCMs have tropospheric annular mode timescales that are larger than those in the observed atmosphere).

Full GCMs tend to underestimate the wave forcing in the Northern Hemisphere, but slightly overestimate the wave forcing in the Southern Hemisphere (Eyring et al., 2010, Chapter 4), while many such models underestimate the frequency of major warming events (Charlton et al., 2007). Reaching an adequate understanding of the dependence of the modeled stratosphere on tropospheric forcing should help in understanding the behavior of climate models; however, while progress is being made, more clearly remains to be done.

3. Does the delay in Antarctic polar vortex breakdown explain recent trends in surface westerlies?[3]

3. 1. Introduction

In both hemispheres, stratospheric polar vortices form in the fall, reach maximum strength in midwinter, and decay in late winter-spring. The breakdown of these vortices is known as the Stratospheric Final Warming (SFW). Observational and modeling evidence suggests that fluctuations in the polar stratospheric vortices in both hemispheres have an effect on the troposphere (e.g. Baldwin and Dunkerton, 2001, Thompson and Solomon, 2002, Polvani and Kushner, 2002, Gillett and Thompson, 2003). Various studies linking the strength of the Northern Hemisphere winter stratospheric polar vortex to tropospheric climate (e.g. Baldwin and Dunkerton 2001, Thompson and Wallace 2000, Thompson et al., 2005), indicate that a stronger stratospheric polar vortex is associated with stronger tropospheric westerlies in the vicinity of 60^0N.

Black et al. (2006) in their exploratory study of SFW events in the Northern Hemisphere reported that these events provide a strong organizing influence upon the large-scale circulation of the stratosphere and troposphere during the period of spring onset and Black and McDaniel (2007a) studied the dynamics of these events in the Northern Hemisphere. Black and McDaniel (2007b) investigated the organizing influence of SFW events on the circulation of the Southern Hemisphere. They found that part of the annual weakening of the high-latitude circumpolar

[3] This chapter is based on Sheshadri, A., R. A. Plumb, and D. I. V. Domeisen, 2014: Can the delay in Antarctic polar vortex breakup explain recent trends in surface westerlies? *J. Atmos. Sci.*, **71**, 566-573.

westerlies in the uppermost troposphere and stratosphere occurs within a short time surrounding SFW onset, and that a coherent annular circulation change occurs during SFW onset with zonal decelerations (accelerations) observed at high (low) latitudes. These studies used reanalysis data and in an attempt to filter out other factors that influence tropospheric circulation and focus on the relatively short-term signal around final warming events, considered circulation anomalies from an average seasonal cycle defined by the first six Fourier harmonics. From these studies, it also emerged that the tropospheric circulation response to stratospheric final warming events is structurally distinct from the annular mode in both hemispheres.

A tendency towards an increase in the positive phase of the Southern Annular Mode (SAM) has been reported in the Southern Hemisphere (e.g. Thompson et al., 2000 and Fogt et al., 2009). This positive phase of the SAM is associated with a poleward shift of the Southern Hemisphere midlatitude jet and storm tracks (Archer and Caldeira, 2008). It has been suggested that stratospheric ozone depletion is the cause of these changes (e.g. Thompson and Solomon, 2002, Polvani et al., 2011 and Thompson et al., 2011). Polvani et al. (2011) suggest that Southern Hemisphere tropospheric circulation changes in austral summer over the second half of the twentieth century have been caused primarily by polar stratospheric ozone depletion, and, in particular, that ozone depletion leads to a poleward jet shift that extends all the way to the surface. Waugh et al. (1999) and Black and McDaniel (2007b) have noted a trend in the timing of Southern Hemisphere SFW events, with the warming occurring later in recent years. This trend could be a response to the radiative effects of Antarctic ozone depletion (Thompson et al. 2011). Therefore, in this paper we investigate the question of whether the observed changes in surface westerlies could be due to this delay in SFW timing.

We begin our analysis by demonstrating explicitly that stratospheric final warming events have an impact on the troposphere. We do this by investigating final warming events in a simplified general circulation model. In reanalysis data, unambiguous separation of the tropospheric response to stratospheric final warming events from the internal seasonal cycle of the troposphere is difficult. Therefore, we use a model setup that enables the tropospheric response to be attributable explicitly to seasonal changes in the stratosphere. As will be described in Section 2, the model is forced by relaxation towards an equilibrium temperature distribution that varies seasonally within the stratosphere, but not in the troposphere. Thus, seasonal variations in the tropospheric circulation, including those occurring around the time of the breakdown of the stratospheric polar vortex in spring, are unambiguously stratospheric in origin. In the model configuration used here, a surface topography of zonal wavenumber 2 is included in one hemisphere only, in order to force quasi-stationary waves. This makes this hemisphere similar to the observed northern hemisphere in its wintertime stratospheric behavior. Even without topography, the model generates enough long-wave activity to make the final warming quite variable in its timing, though it does not produce strong midwinter warming events. We analyze here the model hemisphere with topography. Our interest in this part of the paper is to demonstrate, in a general sense, unambiguous stratospheric influence on the troposphere during the time of the final warming. It is not intended that the results from this component of the research should be interpreted as being especially applicable to the southern hemisphere of the real atmosphere. Our model results in Section 2 also resemble that of Black and McDaniel (2007a and 2007b) in that the tropospheric response to final warming events is structurally distinct from the annular mode.

Having demonstrated in Section 2 that stratospheric final warming events do impact the circulation of the troposphere, we proceed in Section 3 to use NCEP/NCAR Reanalysis data to investigate the question of whether the observed changes in surface westerlies could be due to this delay in SFW timing. To do this, we examine differences between years of large ozone depletion and the pre-ozone-hole years.

3. 2. SFW events in the simplified model

a. Model description

The model we use is similar to that of Kushner and Polvani (2006). The model is dry and hydrostatic, solving the global primitive equations with T42 resolution in the horizontal and 40 levels in the vertical. Linear damping of the horizontal winds is applied in the planetary boundary layer and in a sponge above 0.5 mb. The bottom boundary in one hemisphere only includes wave-2 topography (identical to run 9 in Gerber and Polvani, 2009), centered on 45^0S and 3000 m high. Newtonian relaxation forces temperatures toward a zonally symmetric equilibrium-temperature field T_{eq}. Within the stratosphere, a seasonal cycle in T_{eq} is prescribed using the specification of Kushner and Polvani (2006, their equations (1) and (2)), with the lapse rate fixed at 4K/km. This produces a winter stratosphere in the hemisphere with topography that is qualitatively similar to that of the Northern Hemisphere (Gerber and Polvani, 2009). Within the troposphere (below 100 mb), there is no imposed seasonal variation; T_{eq} is specified as in Polvani and Kushner (2002) with the parameter $\varepsilon = -10K$ providing an asymmetry between the Northern and Southern Hemispheres. T_{eq} varies smoothly from tropospheric to stratospheric specifications across 100 mb.

b. Model results

33 final warmings were simulated in the model run. Five years in the model in which sudden warming events occurred that took more than ten days to recover were excluded from the analysis. Black and McDaniel (2007a) who used NCEP/NCAR Reanalysis data to examine SFW events in the Northern Hemisphere identified SFW events as the final time when the 50 mb zonal mean zonal wind at 70°N drops below the value of zero without returning to 5 m/s until the

subsequent autumn. The same authors (Black and McDaniel ,2007b), used ERA-40 data to analyze Southern Hemisphere SFW events and based their definition for the timing of these events on when the zonal mean zonal wind at 50 mb and 60°S reached the value of 10 m/s. The criterion used in this study for the model run was based on the day on which the zonal mean zonal wind at 50 mb and 60°S reaches the value of 2 m/s. This yields a final warming date for the model at approximately the same phase of the zonal wind cycle of the model as that used by Black and McDaniel (2007a and 2007b) for the ERA-40 and NCEP/NCAR Reanalysis data. Varying this definition did not change our results significantly.

Figure 3-1 shows the timing of SFW events for the 28 years analyzed from the model run. A similar run with no topography does not produce sudden warmings (Gerber and Polvani 2009) but the variability in the timing of final warmings is not profoundly different from the case with topography reported here.

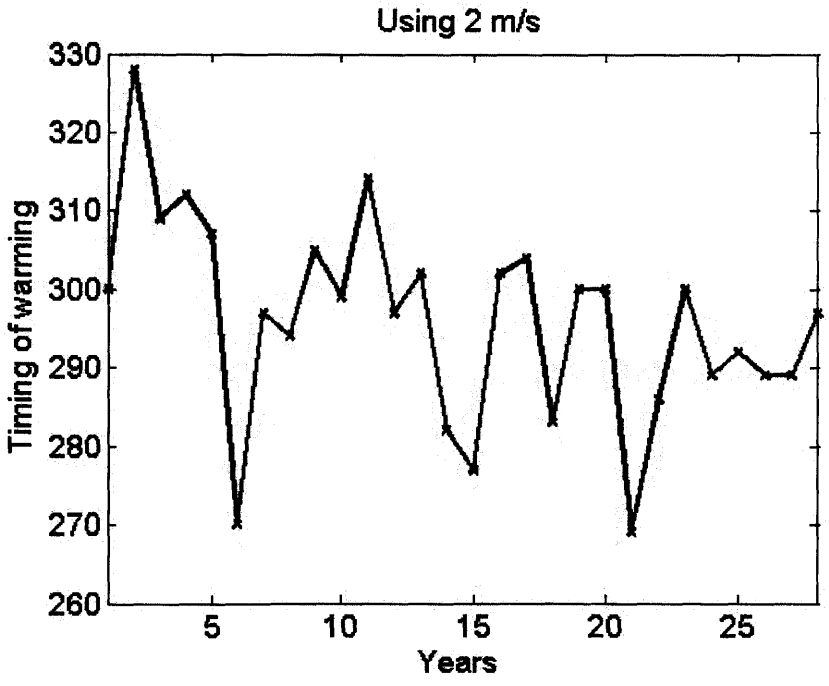

Figure 3-1: Timing of SFW events from the 28 years simulated in the model run.

The top panel of Figure 3-2 shows the zonal mean zonal wind averaged from 60^0S-70^0S over a 60 day period centered on final warming events and averaged over the 28 years that were analyzed from the simplified GCM run. We see a clear transition from westerlies to easterlies in the stratosphere and a weakening of the westerlies below. The bottom panel of Figure 3-2 is similar, but now presents the time evolution of zonal mean zonal winds averaged from 60^0S-70^0S relative to day -30. We see from the bottom panel of Figure 3-2 that SFW events in the model have a statistically significant impact that extends to the surface after day 0. Since there is no imposed seasonal cycle in the troposphere, these surface effects are unambiguously of stratospheric origin.

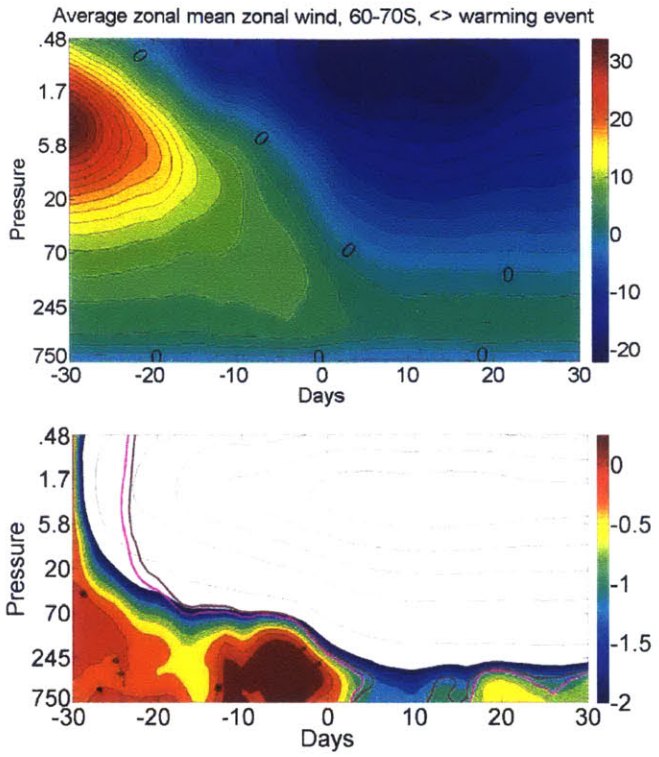

Figure 3-2: Top panel: Transition in zonal mean zonal wind averaged from 60°S to 70°S for a 60 day period centered on SFW events for 28 years from the GCM run. The contour interval is 2 m/s. Bottom panel: Time evolution of zonal mean zonal wind averaged from 60°S to 70°S for a 60 day period centered on SFW events for 28 years from the GCM run, as differences from day -30. The contour interval is 0.25 m/s up to -2 m/s (shown as filled colored contours) and 5 m/s thereafter (shown as unfilled black contours). Magenta and brown contours denote the 90% and 95% confidence intervals for a two-sided t test.

The latitude-pressure structure of the change in zonal mean zonal winds between days +10 and -10 is seen in panel a of Figure 3-3. A dipole structure can be seen in the stratosphere, with the winds being decelerated southwards of about 40^0S. This dipole extends downwards into the troposphere and all the way to the surface, in qualitative agreement with the analysis of Black and McDaniel (2007b). Also in agreement with Black and McDaniel (2007b) is the fact that the zonal mean tropospheric wind anomaly, though dipolar, does not match the structure of the model's annular mode. To illustrate this, we define the model EOF in two ways. In the first, shown in panel b of Figure 3-3, we consider the first EOF of zonal mean zonal wind at 585 mb, which is the first model level above the extent of the topography. This peaks at 23.7^0S and 36.7^0S, whereas the tropospheric dipole in Figure 3a is displaced significantly poleward of this. The dipole structure in Figure 3-3a also does not match the latitude structure of vertically integrated anomalous tropospheric (from the surface to 200 mb) horizontal momentum flux divergence over the same time period (shown in panel c of Figure 3-3). Nor does it match the structure of the vertically integrated tropospheric horizontal momentum flux divergence regressed on the first EOF of zonal mean zonal wind at 585 mb (shown in panel d of Figure 3-3).

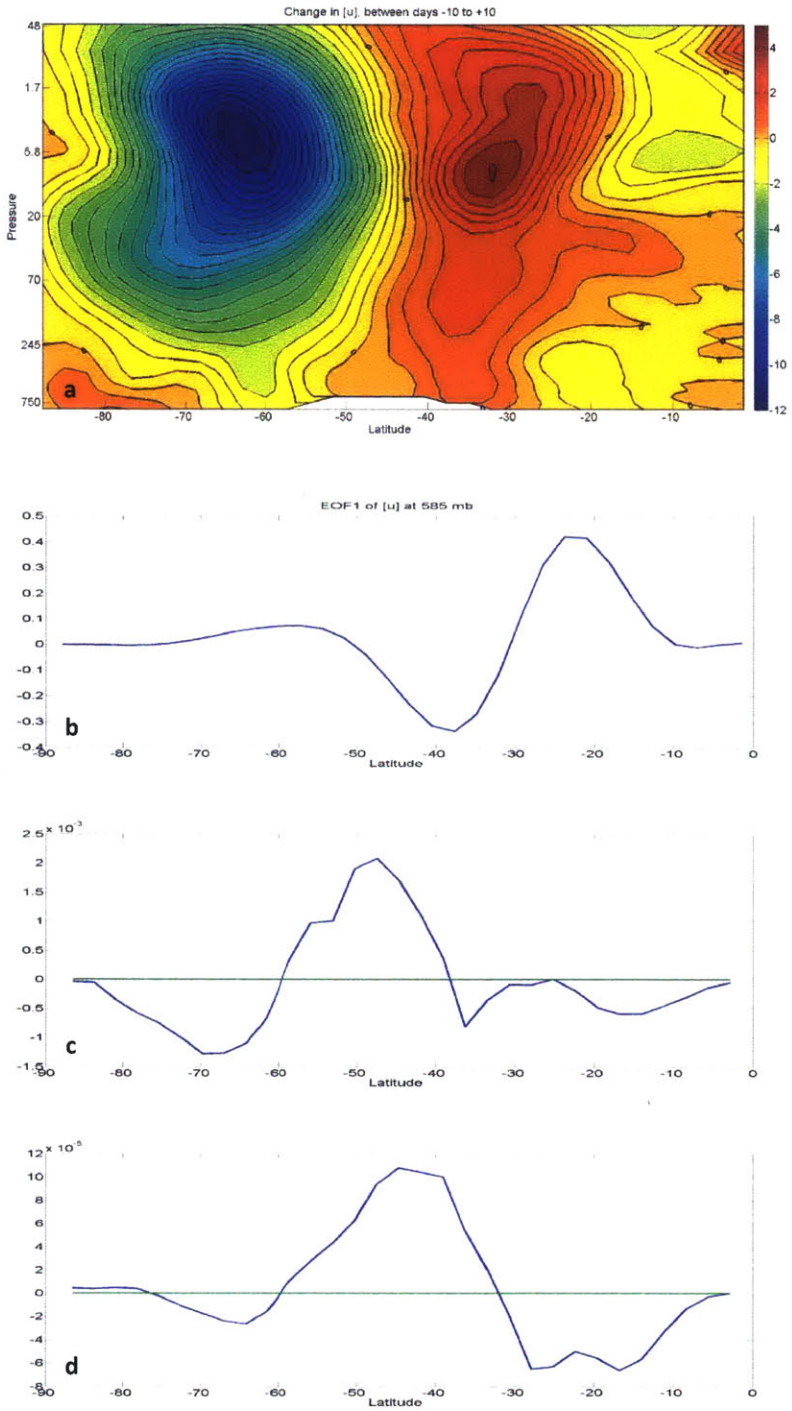

Figure 3-3: Panel a: Latitude-pressure structure of the change in zonal mean zonal winds between days -10 and +10. The contour interval is 0.5 m/s. Panel b: First EOF of zonal mean zonal winds at 585 mb. Panel c: Vertically integrated tropospheric (from the surface to 200 mb) horizontal momentum flux divergence as anomalies from the climatology averaged over a 21 day

period centered on the final warming (same time period as shown in panel a). Panel d: Vertically integrated tropospheric (from the surface to 200 mb) horizontal momentum flux divergence regressed on the first EOF of zonal mean zonal winds at 585 mb. These figures are from the model run, and the white patch in the top panel shows the extent of the bottom topography.

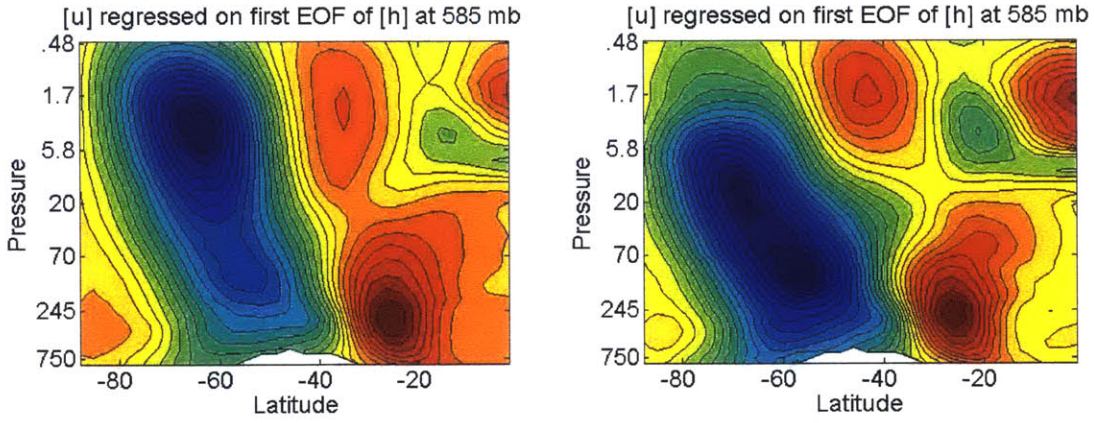

Figure 3-4: Latitude pressure structure of the zonal mean zonal wind regressed on the first EOF of geopotential height at 585 mb (the first model level above the extent of the topography). Latitude pressure structure shown for all data in the left panel and for a 90 day period centered on final warming events in the right panel. These figures are from the model run, and the white patch at the bottom of both figures shows the extent of bottom topography.

To confirm that this conclusion is not based on this definition of the annular mode, we show in Figure 3-4 the structure of zonal mean zonal wind regressed on the principal component time series corresponding to the first EOF of 585 mb geopotential height. The left panel of Figure 3-4 shows the structure of the regression for all data. The right panel shows the structure of the regression using the first EOF of 585 mb geopotential height computed using springtime data only (a 90 day period centered on the final warming event). By either definition of the annular mode, the tropospheric response to the final warming is shifted poleward of the annular mode. Indeed, the lower latitude lobe of the dipole of the tropospheric SFW signal (Figure 3-3a) almost coincides with the node of the dipole seen in Figure 3-4.

3. 3. SFW events in the NCEP/NCAR Reanalysis

a. Data and Methods

We use daily data from the NCEP/NCAR Reanalysis. We study the years 1960-2009, with the exception of 2002, because of the unusual nature of the stratospheric winter in this year (in late September 2002 the Southern Hemisphere underwent its first recorded sudden warming event, see, e.g. Krüger et al., 2005, Newman et al., 2005 and Baldwin et al., 2003). We use the term 'late years' to refer to the years of large ozone depletion (taken to be 1995-2009 with the exception of 2002) and the term 'early years' to refer to the pre-ozone-hole years (which we take to be 1966-1979). The average annual cycle of zonal mean zonal wind at 50 mb and 60°S had a maximum of 55 m/s. The criterion for the timing of SFW events was based on the day on which the zonal mean zonal wind at 50 mb and 60°S reaches the value of 10 m/s (this is a stage in the vortex breakup that is similar to the 2 m/s criterion in our model). Again, changing this definition did not affect our results significantly.

b. Results

Figure 3-5 shows the timing of all SFW events from 1960-2010 with the exception of the anomalous event in 2002, determined from NCEP/NCAR Reanalysis data. The slope[4] of a least squares linear fit for the timing is 0.383 days/year and it is statistically different from 0 at the 99% confidence level, using a Student's t-test. The late years (years of large ozone depletion) and early years (the pre-ozone hole years) are indicated. The timing of SFW events is later on average in the years of large ozone depletion as compared to the pre-ozone-hole years (the ozone

[4] This value is less than half that reported by Black and McDaniel (2007b) over the period 1978-2000, but is consistent with the same change in timing over the longer period analyzed here. Thus, the change over the full period is more akin to a step change, rather than a sustained linear trend.

hole cools the polar stratosphere, leading to stronger westerlies in the polar vortex and thus delaying SFW events, see, e.g. Thompson et al. 2011).

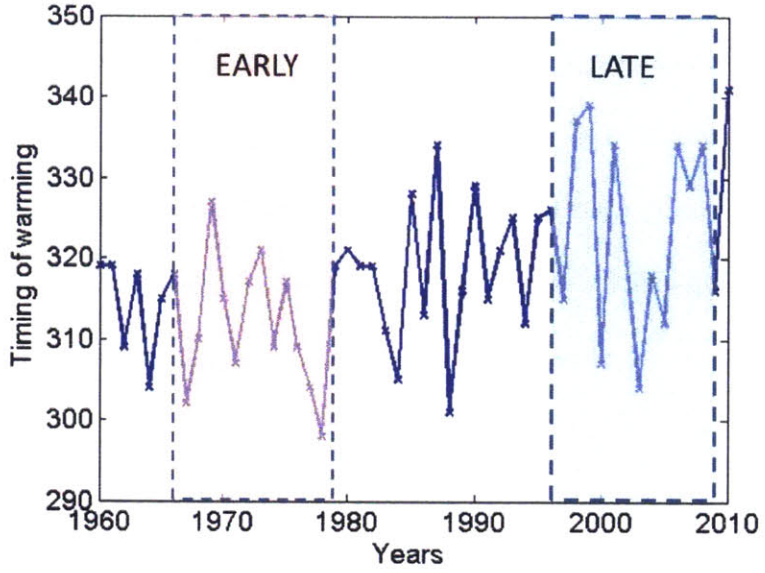

Figure 3-5: Timing of warming for SFW events from 1960-2010, determined from NCEP/NCAR Reanalysis data.

Figure 3-6 shows the transition in zonal mean zonal wind anomalies (from NCEP/NCAR Reanalysis data) averaged from 60^0S-70^0S 30 days before and after SFW events. Zonal mean zonal wind anomalies are calculated as anomalies from an average seasonal cycle (defined as the sum of the first six Fourier harmonics of a seasonal cycle derived from an annual time series of long-term daily averages; this is also the method used in Black and McDaniel, 2007b). We note that this method does not eliminate the effects of seasonal changes in annular mode decorrelation timescales (see, e.g. Baldwin et al., 2003). The top panel of Figure 3-2 and Figure 3-6 are qualitatively similar. Figure 3-6 can also be compared with Figure 3a from Black and McDaniel (2007b), noting that this study used ERA-40 Reanalysis data and analyzed 24 SFW events from 1978-2001. In both the top panel of Figure 3-2 and Figure 3-6, the contours slope downwards as the criterion is met first in the stratosphere, after which the effects progress downwards with time.

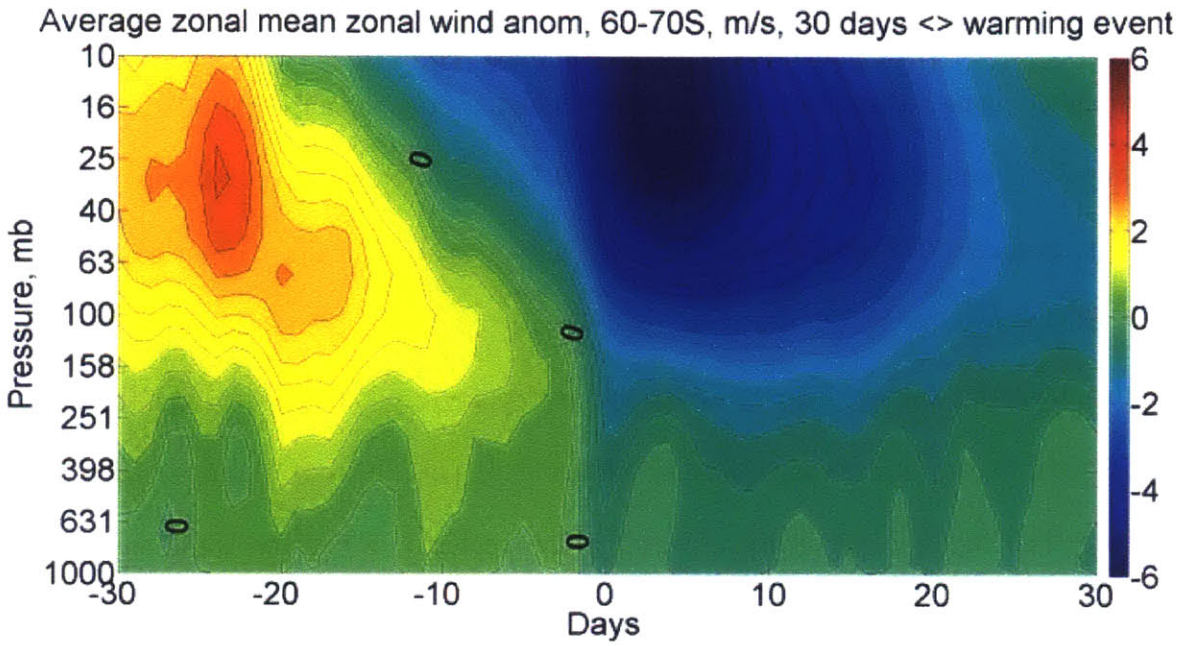

Figure 3-6: Transition in zonal mean zonal wind anomalies averaged from 60°S to 70°S for a 60 day period centered on SFW events, averaged for 49 SFW events from the NCEP/NCAR Reanalysis data. The contour interval is .3 m/s.

To address the question of whether the influence of stratospheric ozone depletion on surface westerlies is through the delay in timing of SFW events, we examine differences between the years of large ozone depletion and the pre-ozone-hole years. The ozone hole cools the polar stratosphere, changing the north-south temperature gradient, and extending the persistence of the polar vortex (Thompson et al. 2011), leading to SFW events being delayed. Therefore, on the average, SFW events are later in the years of large ozone depletion.

Figure 3-7 shows composite differences in geopotential height between the late and early years. Here geopotential height is shown as anomalies from an average seasonal cycle, as defined earlier in this section. Figure 3-7a is centered on the average day of occurrence of SFW events

for all years, and Figure 3-7b has all the years centered on the SFW event day of that year. Daily data smoothed using a centered moving average which averaged data 15 days before and after a given day were used to make this plot. In Figure 3-7a, the difference in the geopotential anomaly is strongly negative following day 0 and these contours extend all the way to the surface up to two months after the mean warming day. Decreases in the geopotential height indicate strengthening of the eastward flow in the polar vortex (corresponding to the high-index polarity of the SAM). Figure 3-7a is qualitatively similar to Figure 1b from Thompson et al. (2011), noting that their figure is terminated at 30 mb and is centered on January, while day 0 in Figure 3-7a is November 14 (the average day of occurrence of SFW events). If these signals seen in Figure 3-7a are caused purely because of the delayed timing of the final warming, they would disappear in composites where every year is centered on the day where the criterion for SFW is met. The similarity between figures 7a and 7b after day 0 leads us to conclude that the tropospheric signal is not being caused by the difference in the timing of final warming events alone.

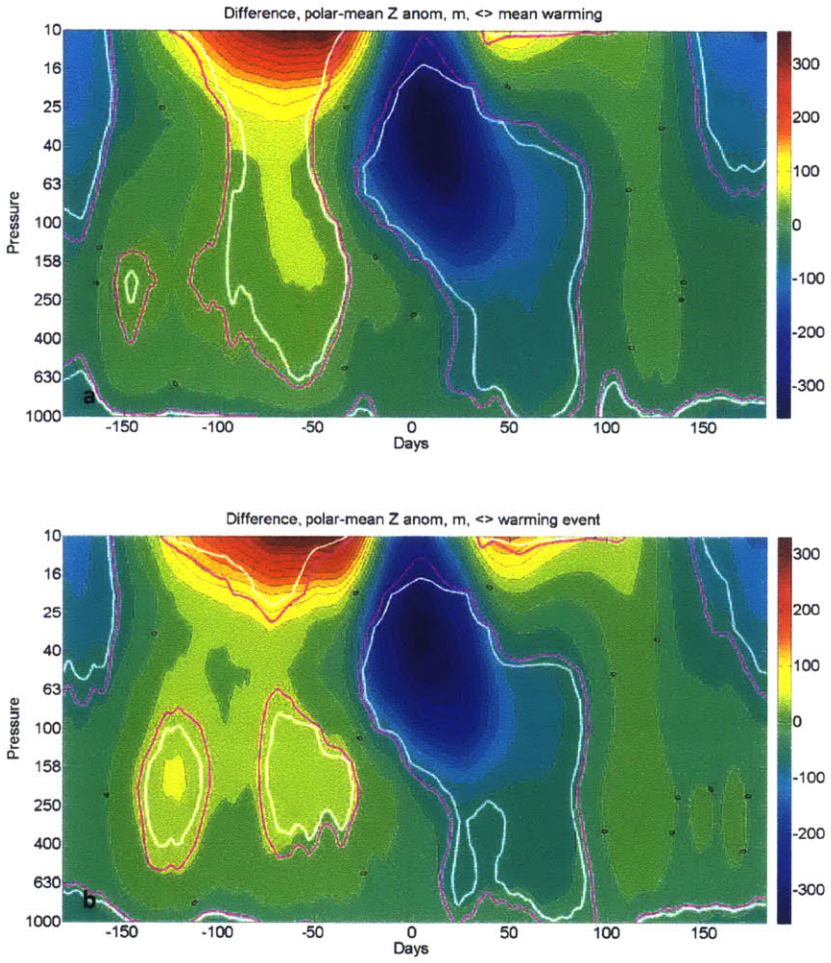

Figure 3-7: Polar mean (averaged from 65°S-90°S) geopotential height, shown as anomalies from an average seasonal cycle (defined as the sum of the first six Fourier harmonics of a seasonal cycle derived from an annual time series of long-term daily averages), difference between the late and early years, centered on the mean warming day in panel a and on the SFW event in panel b. The contour interval is 30 m. Magenta and white contours denote the 90% and 95% confidence intervals for a two sided t test.

This conclusion is reinforced in Figure 3-8. Figure 3-8 shows the difference in the 850 mb zonal mean zonal wind (smoothed as in Figure 3-7) at 60^0S (in Figure 3-8a) and 40^0S (in Figure 3-8b) between the late and early years, centered on the mean warming day (solid line) and the SFW event for each year (dashed line).

The zonal flow is more westerly at 60^0S in the late years than in the early years, which corresponds to the high-index polarity of the SAM. Figure 3-8b shows that the difference is negative at 40^0S after the warming (smaller eastward flow). These figures clearly indicate that the difference in surface winds between the late and early years does not change significantly because of the delay in SFW timing.

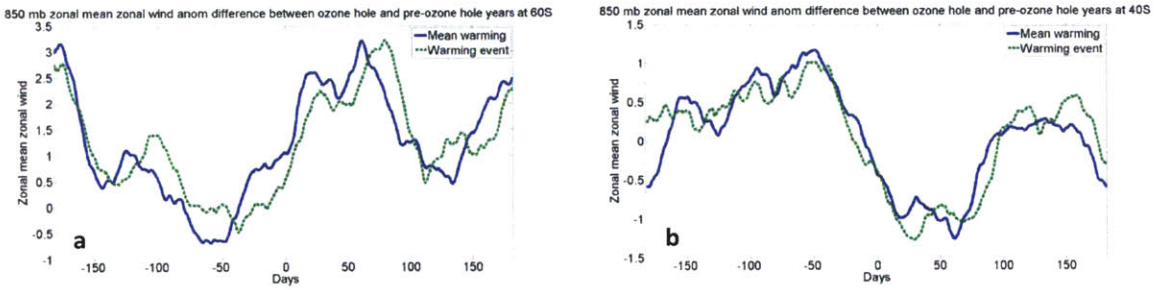

Figure 3-8: Difference between the late and early years 850 mb zonal mean zonal wind anomaly from time mean at a) 60^0S and b) 40^0S.

3. 4. Summary

In the model experiments described here, the imposed seasonal cycle of equilibrium temperature was, by design, confined to the stratosphere. Thus, the tropospheric signal evident in the model is unambiguously of stratospheric origin, and there reinforces the conclusions of Black and McDaniel (2007b) that the tropospheric signal seen in observations is similarly a response to stratospheric events.

Our analysis of data from the NCEP/NCAR Reanalysis confirms that there has been a statistically significant shift towards later final warming events in the Southern Hemisphere over the last five decades. This shift, widely attributed to the impact of springtime ozone depletion in the Antarctic lower stratosphere, has been largely coincident with the observed trends in surface winds, which themselves have been attributed to ozone depletion (e.g. Polvani et al., 2011 and Thompson et al., 2011). The results of Black and McDaniel (2007b), as well as our simplified model study, indicate that the lower tropospheric response to final warming is evident for relatively short time-scales (of the order of 10 days), indicating a dynamical response to stratospheric changes rather than a radiative one. These ideas led to the hypothesis that it is the delay in the final warmings that has led to the surface trends. However, since composites made with respect to the variable final warming date show a tropospheric trend that is little changed from those made with respect to calendar date, our results indicate that the surface trends cannot be explained as being caused simply by the trend in the timing of final warming events – i.e., it is not simply a matter of the delay of an otherwise unchanged tropospheric response to stratospheric events. That is not to say, of course, that the behavior of the final warming is not responsible for the surface trends: the warmings themselves may have changed in ways other

than mere timing (and there is some evidence for this). The point is that the trend in the tropospheric signal is not simply a matter of timing.

4. Responses of an idealized AGCM to ozone depletion-like polar stratospheric cooling

4. 1. Introduction

In the previous chapter, we found that the trends in surface westerlies over the second half of the twentieth century could not be explained as a direct consequence of the delay in the timing of stratospheric final warming events. To clarify the mechanisms by which stratospheric circulation changes brought about by ozone depletion are communicated to the troposphere and to the surface, in this chapter we consider circulation responses of the idealized model (described in Chapter 2, section 2) to imposed polar stratospheric cooling that mimics the effects of ozone depletion. We will begin by describing the form of the imposed cooling in section 4. 2, and then consider responses of the idealized model to this cooling and its dependence on the tropospheric annular mode timescale. Recent work involving full GCMs (e.g. Sigmond and Fyfe's recent analysis of 6 CMIP5 models with ozone-only forcing, 2014) reports some inconsistencies in model responses to imposed ozone depletion. In Section 4.3 we test whether this could possibly be explained by the timing of their imposed ozone depletion and its relation to their model's dynamics.

4. 2. Form of the imposed polar stratospheric cooling

We use the idealized model setup in 2.2, but use pure sigma co-ordinates instead of a hybrid vertical co-ordintae. Following the steady-state cooling used by Butler et al. (2010) and the time-dependent cooling used by Sun et al. (2014), to mimic the effects of ozone depletion, we impose diabatic cooling in the polar stratosphere as follows:

$$Q(\phi,\sigma,t) = q_0 \exp\left[-\left\{\frac{(\phi-\phi_0)^2}{2\sigma_\phi^2} + \frac{(-7000\ln\sigma + 7000\ln\sigma_0)^2}{2\sigma_\sigma^2} + \frac{(t-t_0)^2}{2\sigma_t^2}\right\}\right] \quad (1)$$

With

$q_0 = -0.5K/day$

$\phi_0 = -\frac{\pi}{2}$

$\sigma_\phi = 0.28$

$\sigma_0 = 0.05$

$\sigma_\sigma = 4000$

$t_0 = 231$ (This day corresponds to October 20, but will be varied over the course of the analysis.)

$\sigma_t = 20$

where ϕ_0, σ_ϕ, σ_0, and σ_σ define the spatial pattern and t_0 and $\sigma_t = 20$ days define the peaking time and persistence. Figure 4-1 shows the horizontal and vertical extents of the imposed diabatic cooling, peaking October 20.

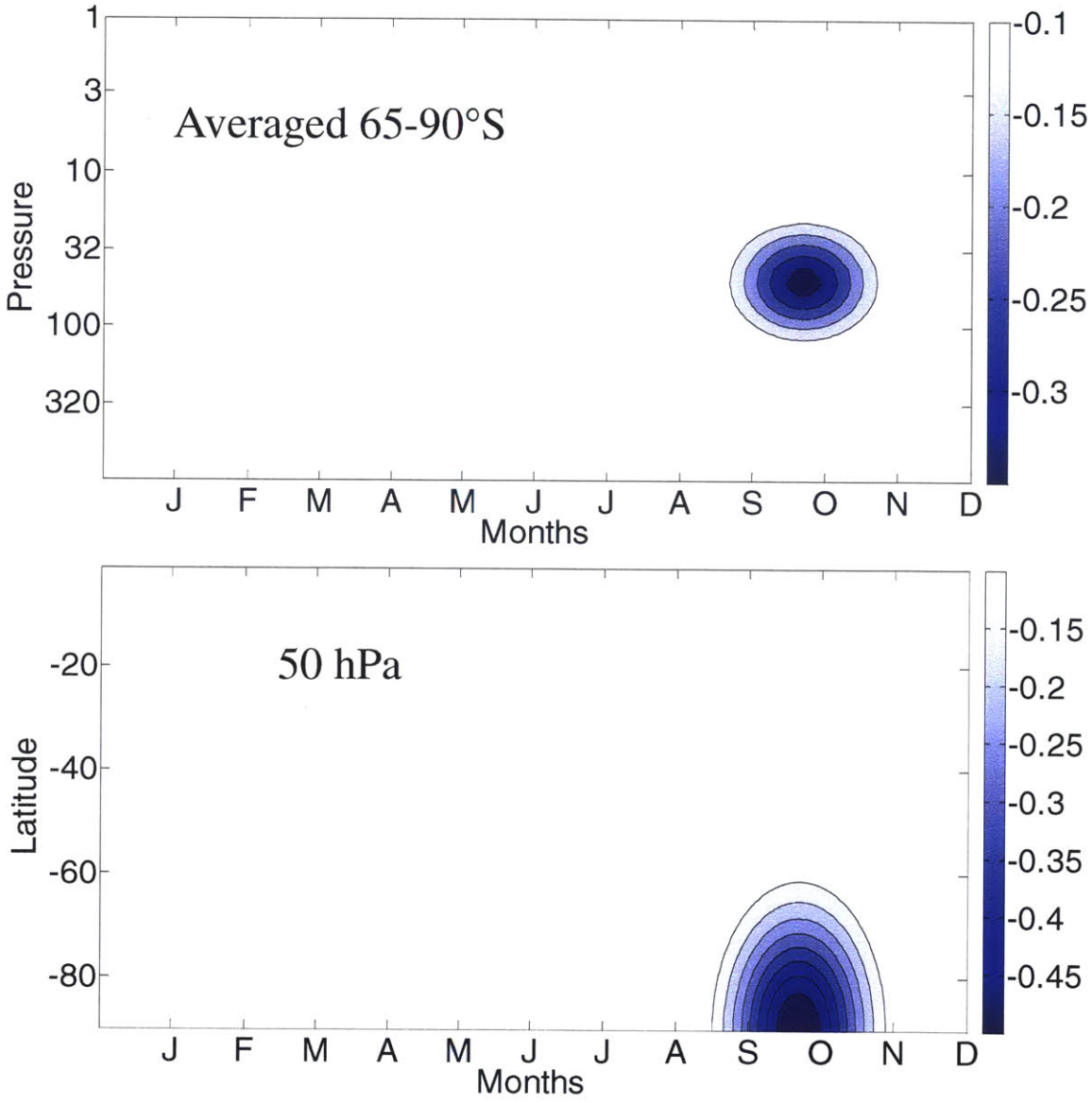

Figure 4-1: The vertical and horizontal extents of the imposed polar stratospheric diabatic cooling (K day^{-1}). (Top) vertical extent shown averaged over the polar cap (65-90°S), and (Bottom) latitudinal cross-section at 50 hPa.

4. 3. Responses to imposed polar stratospheric cooling

When the model is used in the configuration described in Chapter 2, section 2, (with the tropospheric asymmetry factor ε set to 10K), the tropospheric annular mode timescale is unrealistically long (135 days). This results in exaggerated responses of the tropospheric jet to external forcings. To avoid this issue, we swept through a range of values of ε, and investigated tropospheric responses to imposed polar stratospheric cooling in a model configuration with the minimum annular mode timescale that we found (in the range of values of ε considered). The temperature response of the idealized model to the applied polar stratospheric cooling is shown in Figure 4-2. A statistically significant negative temperature response is evident in the stratosphere, which extends to the end of January. As expected, the imposed cooling also leads to an extension of the lifetime of the Antarctic vortex in the model. In the control run, the mean date of the final warming was day 340 (December 10), which is delayed to a mean date of day 365 (January 5) is the perturbed run. Additionally, the standard deviation in the timing of final warming events increases (this is also evident in the observations, when one compares variability in the final warming date in the years with and without large ozone depletion). Figures 4-3 and 4-4 show the corresponding changes in winds and geopotential height for the same time period. Also as expected, the polar vortex strengthens and extends downwards into the troposphere in the summer – positive zonal mean zonal wind anomalies are evident at the surface from 40-60°S until the end of March. The model's responses are qualitatively consistent with both observations and results from fully coupled chemistry climate models (cf. Keeble et al. 2014). Quantitatively, the imposed cooling leads to changes in the model that are smaller than is evident in observations of composite differences between the years of large ozone depletion and the pre-ozone hole years

(cf. Thompson et al. 2011). The model shows about a 25 m reduction in geopotential height at the surface over the polar cap, about 60% of the 40 m difference evident in Figure 1 of Thompson et al. Figure 4-5 shows the surface geopotential height response in December. There are decreases in geopotential height over the polar latitudes up to 45°S, and increases between 45°S and 15°S. It is evident that the surface response extends well beyond the polar latitudes. The apparent wave-6 structure of the response in Figure 4-5 is due to single years and is not robust across the years. This structure would presumably disappear in a longer model integration, as there is no source of zonal asymmetry in the model setup.

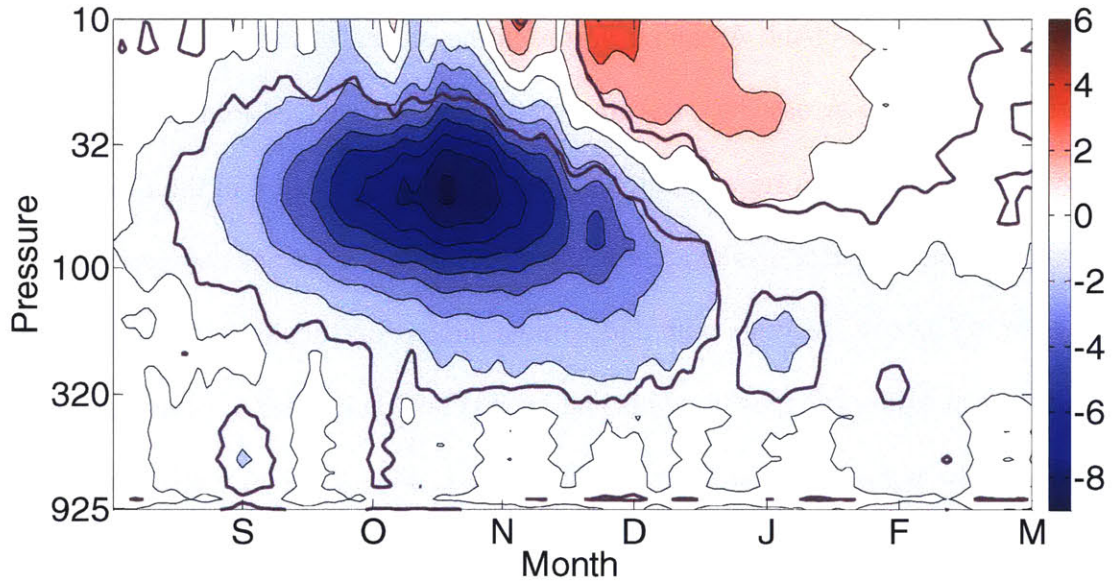

Figure 4-2: Temperature response to the imposed polar stratospheric cooling averaged over the polar cap (65-90°S). The magenta contour denotes 95% statistical significance. The contour interval is 1 K.

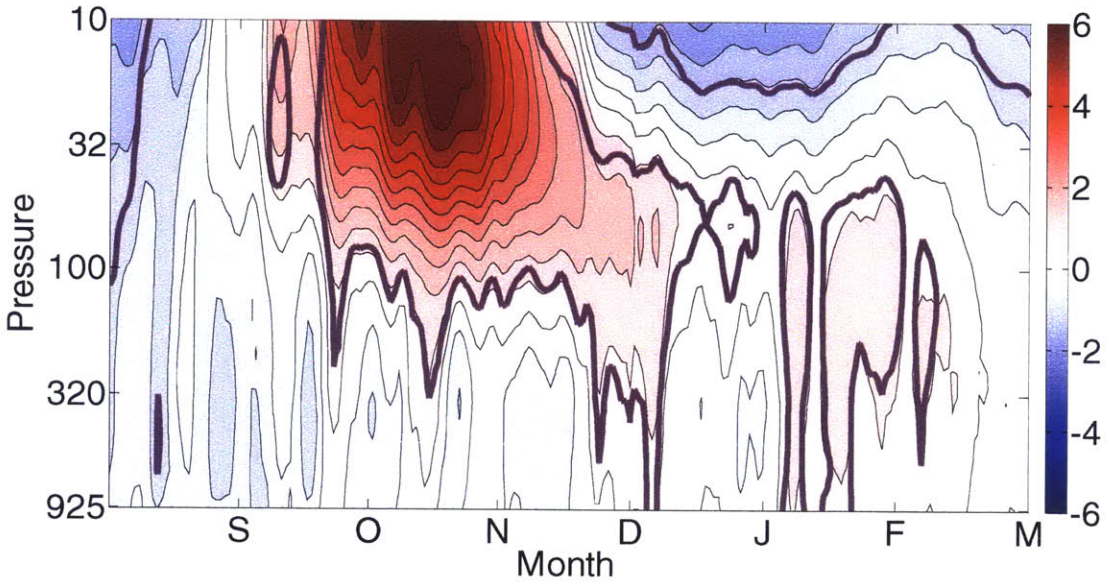

Figure 4-3: Zonal mean zonal wind response to the imposed polar stratospheric cooling averaged over 40-60°S. The magenta contour denotes 95% statistical significance. The contour interval is 1 m/s.

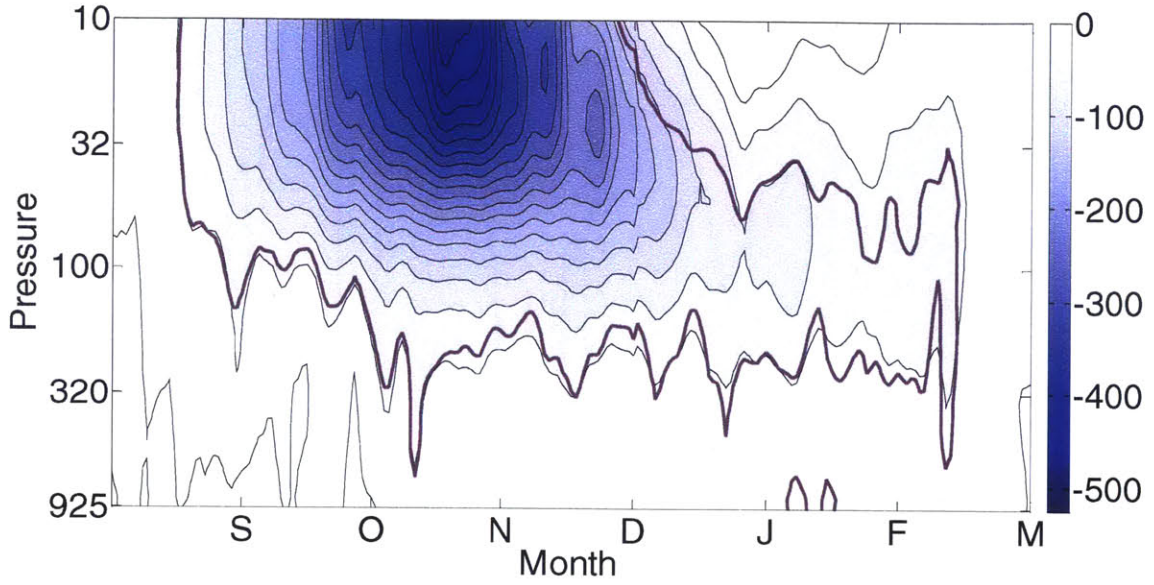

Figure 4-4: Geopotential height changes averaged over the polar cap (65-90°S). The magenta contour denotes 95% statistical significance. The contour interval is 25 m.

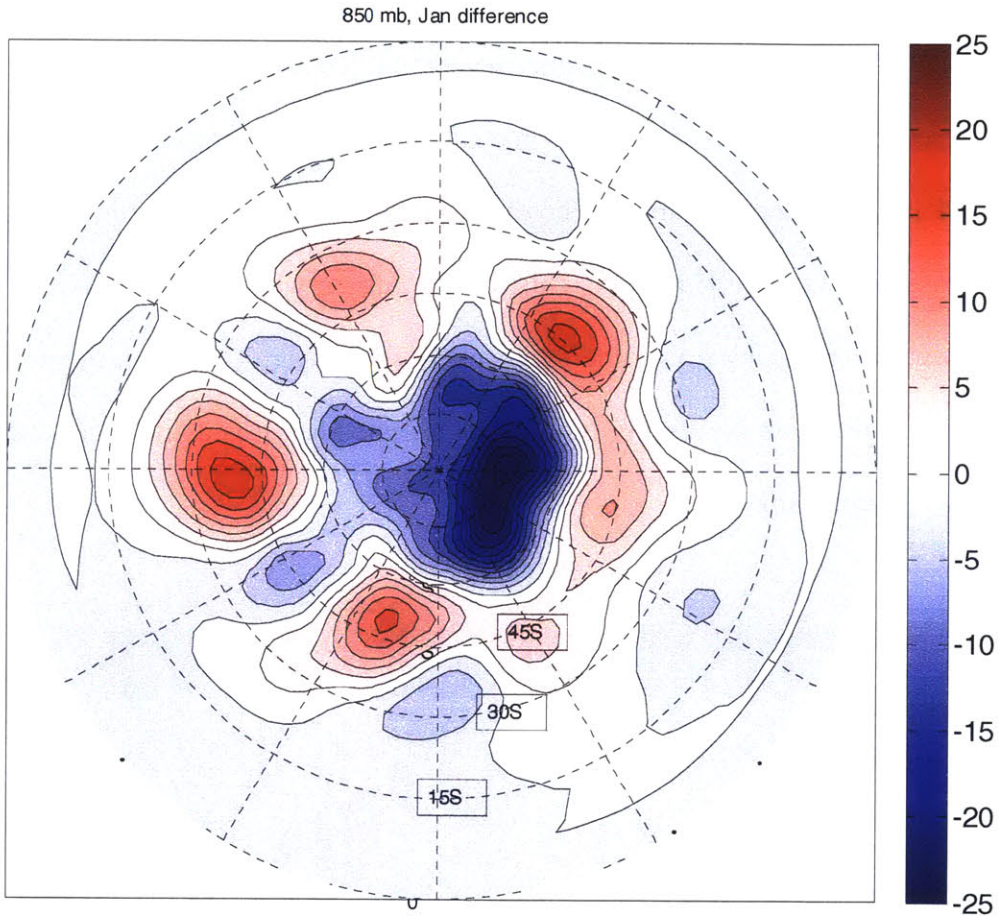

Figure 4-5: Polar plot of the December changes in geopotential height at 850 hPa.

Figure 4-6 shows the changes in eddy heat fluxes $\overline{v'T'}$ at 95 hPa, a measure of the upward propagating planetary wave activity entering the stratosphere. Since the imposed polar stratospheric cooling increases the persistence of the Antarctic vortex in the model (the final warming is delayed by about a month), there are westerlies in the perturbed run at a time when there were easterlies in the control run. This, in accordance with the Charney-Drazin criterion, now permits wave propagation into the stratosphere for longer. Therefore, there are increased heat fluxes at 95 hPa from November through to March. Also, it is evident that the heat fluxes have now moved poleward.

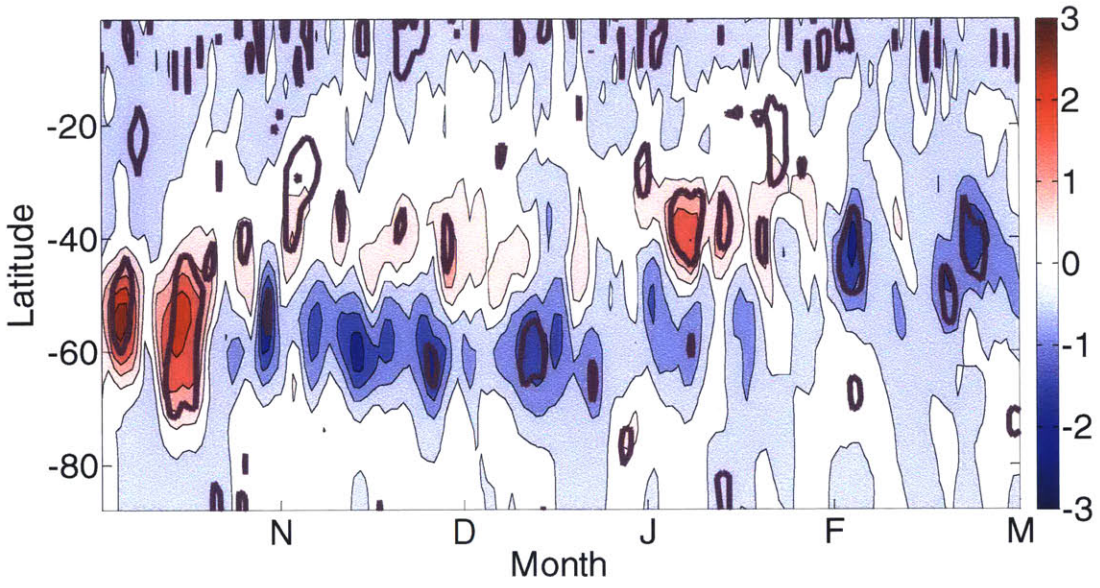

Figure 4-6: Change in eddy heat fluxes (Km/s). The magenta contour denotes 95% statistical significance. The contour interval is 0.5.

The 850 hPa wind responses are shown in the left panel of Figure 4-7. These wind changes are smoothed using a moving centered 20 day average. The response consists of a dipole (decreases in zonal mean zonal winds in the vicinity of 20°S and increases around 40°S) that matches the latitudinal structure of the model's annular mode (first EOF of zonal mean zonal winds at 850 hPa, shown in the right panel of Figure 4-7).

Figure 4-7 reinforces the conclusion drawn from Chapter 3, that the surface westerly wind trends that are evident in observations are not related to the tropospheric response to the stratospheric final warming. In Chapter 3 we concluded that the tropospheric response to stratospheric final warming events does not match the latitudinal structure of the model's annular mode (Figures 3-3a and 3-3b). However, the model's response to the imposed diabatic cooling (the left panel of Figure 4-7) matches the latitudinal structure of the model's annular mode (the first EOF of zonal mean zonal winds, shown in the right panel of Figure 4-7).

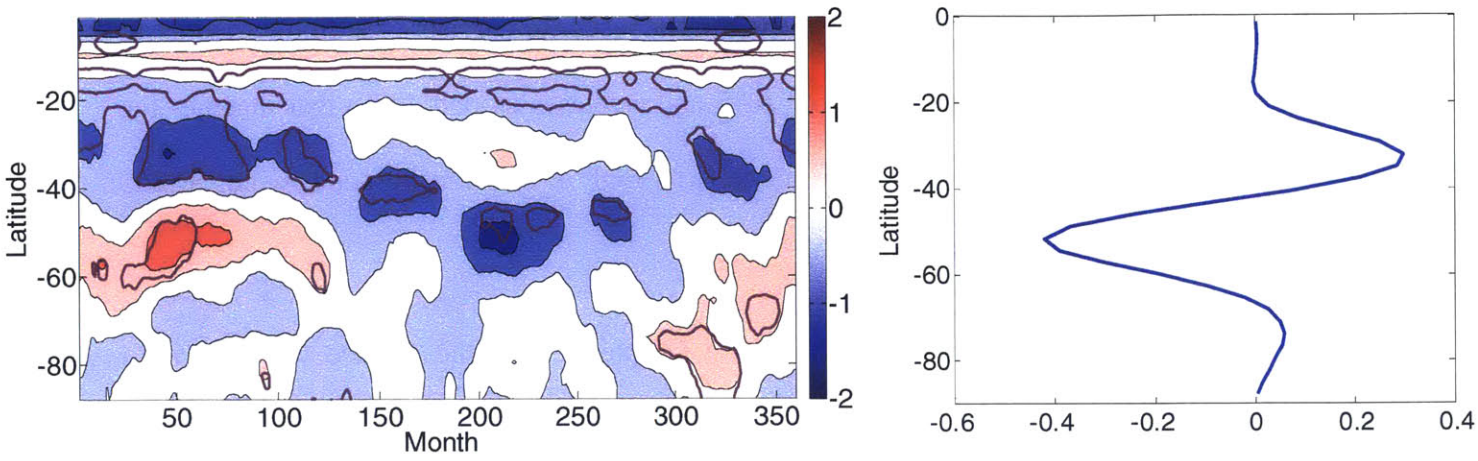

Figure 4-7: (Left panel) 850 hPa zonal mean zonal wind response. The magenta contour denotes 95% statistical significance. The contour interval is 0.5 m/s. (Right panel) First EOF of zonal mean zonal winds at 850 hPa.

To summarize, when an imposed polar stratospheric cooling is applied in the model, the polar stratospheric cooling leads to stratospheric temperature and circulation responses that are consistent with observations. The stratospheric changes are also consistent with those seen in fully coupled chemistry climate models (e.g. Keeble et al. 2014). There is a statistically significant negative temperature anomaly in the lower stratosphere, which in turn causes a strengthening of the polar vortex, and delays its breakdown (the final warming) by about a month. These changes to the zonal wind structure alter the propagation of planetary waves, which increase in magnitude and move poleward through December, January, February, and March. Stratospheric changes result in tropospheric circulation changes that extend to the surface, and are also qualitatively consistent with observations in the austral summer. The magnitude of the surface response is smaller in the model than in observations.

a. Sensitivity of the surface response to the timing of polar stratospheric cooling

Those of the CMIP5 models that have output available from ozone-only forcing experiments show inconsistent responses to ozone depletion (Sigmond and Fyfe 2014). In this section, we examine the sensitivity of the surface response to imposed polar stratospheric cooling applied at different times of the year. We consider the responses to cooling that peaks August 20, September 20, November 20, and cooling that is applied uniformly all year round and compare them to those of the run in which cooling peaked on October 20 (in which the temperature and circulation responses match the observed trends). Figures 4-8 to 4-11 show the smoothed 850 hPa change in zonal mean zonal winds for each of these model experiments.

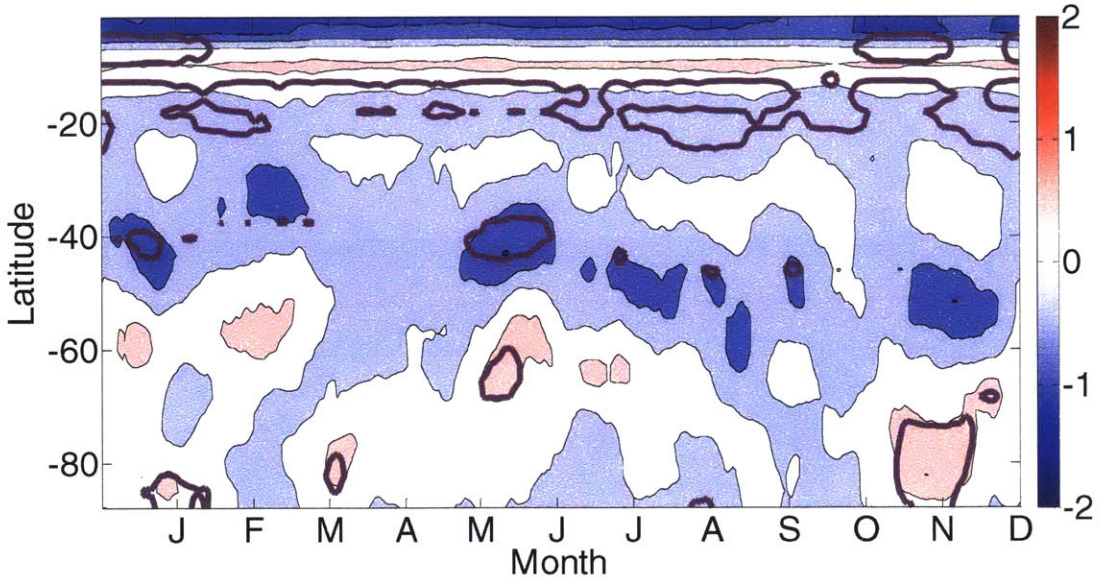

Figure 4-8: 850 hPa zonal mean zonal wind response for polar stratospheric cooling that peaks August 20. The magenta contour denotes 95% statistical significance. The contour interval is 0.5 m/s.

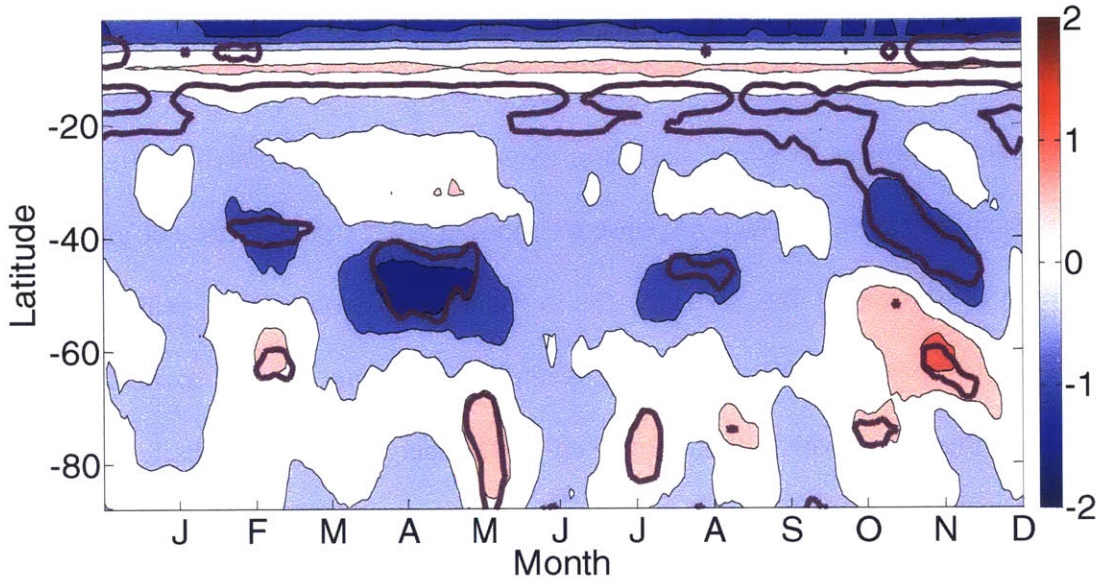

Figure 4-9: 850 hPa zonal mean zonal wind response for polar stratospheric cooling that peaks September 20. The magenta contour denotes 95% statistical significance. The contour interval is 0.5 m/s.

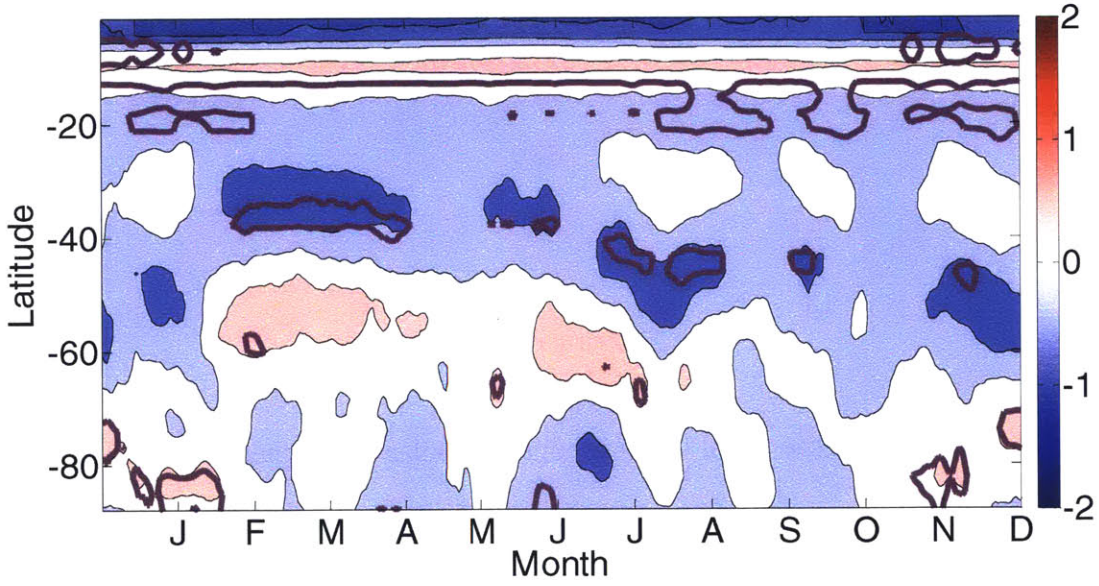

Figure 4-10: 850 hPa zonal mean zonal wind response for polar stratospheric cooling that peaks November 20. The magenta contour denotes 95% statistical significance. The contour interval is 0.5 m/s.

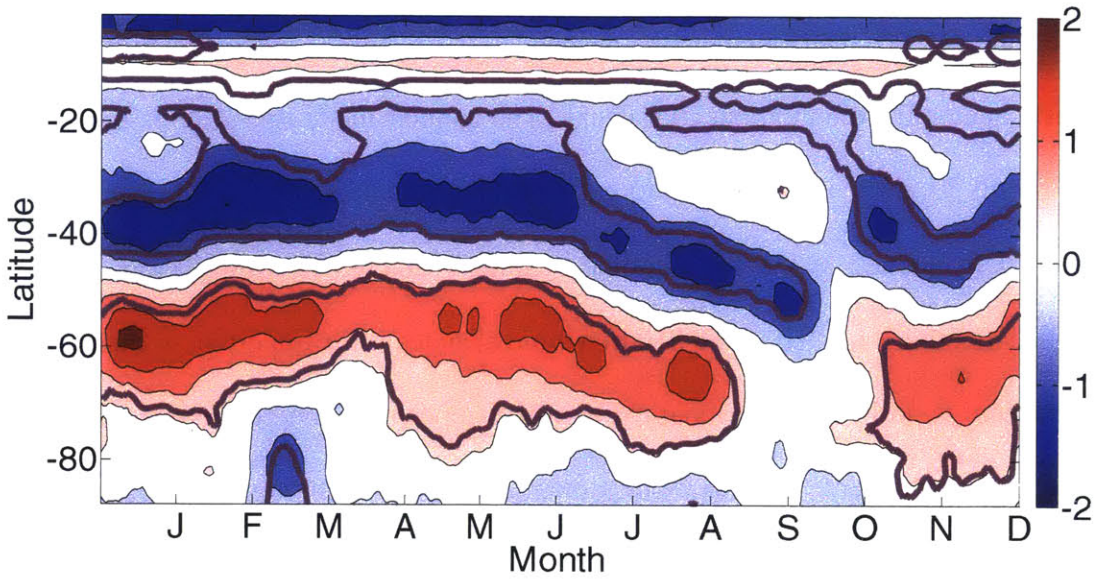

Figure 4-11: 850 hPa zonal mean zonal wind response for polar stratospheric cooling uniformly applied through the entire year. The magenta contour denotes 95% statistical significance. The contour interval is 0.5 m/s.

There is a complete lack of a statistically significant surface wind response in the case of the experiment with cooling peaking August 20. In the September 20 case, there is some statistically significant surface response in November and December, but its persistence is less than in the case of the cooling that peaks October 20. Similarly, the cooling that peaks November 20 results in small, less persistent, but statistically significant, changes in March and April. In the experiment with cooling applied uniformly through the year, the maximum surface wind response is early in the year, with very much smaller responses in September and October.

There appear to be two factors that are playing a role in setting these responses. The first is that there is a seasonal cycle of tropospheric annular mode timescales, shown in Figure 4-12. We calculate the annular mode timescale on a given day by using the principal component time series corresponding to the first EOF of zonal mean zonal wind for a period of 90 days centered on the day of interest. We then calculate the decorrelation time of the autocorrelation function as the best least squares fit to an exponential decay. The annular mode timescale is then averaged on that day for all 30 years of model data to get a mean seasonal cycle of 850 hPa annular mode timescales τ. Daily values of τ were smoothed using a centered moving average of 20 days (similar to the smoothing applied to the 850 hPa wind changes). It is important to note that in our model setup, there is no internal seasonal cycle in the troposphere, and therefore these seasonal variations in the tropospheric annular mode timescale are set by stratospheric variability. The seasonal cycle is somewhat similar to the results of Baldwin et al. (2003), keeping in mind that the final warming is delayed in this model in comparison to the observed Antarctic vortex breakup. The 850 hPa annular mode timescales are around their minimum values from July through October, and get larger towards December, January and February. The peak tropospheric annular mode timescale corresponds to the timing of the maximum variance in the annular mode around 200 hPa.

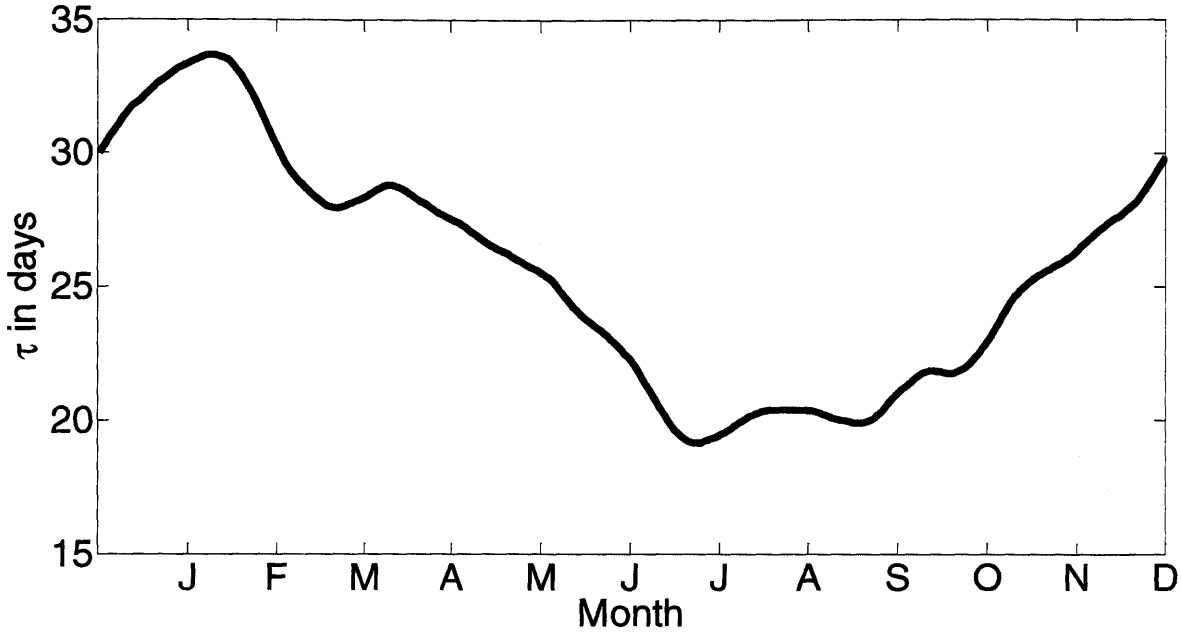

Figure 4-12: The seasonal cycle of 850 hPa annular mode timescale (days).

If the stratospheric cooling attempts to cause a tropospheric response at a time when the annular mode timescale is at its annual minimum, it is unlikely to evoke a response that is either large in magnitude or persistent in time. In the model experiment with cooling applied uniformly through the year (Figure 4-11), the smaller responses in October and November might be related to the lower tropospheric annular mode timescales at this time. For a response to be sustained for a period of three months (as is seen in observations in December, January and February), the response might need to be at a time that coincides with the annual maximum of tropospheric annular mode timescales in the spring. This would also be a factor in the complete lack of a statistically significant surface response in the case of a polar stratospheric cooling that peaks August 20 (Figure 4-8). Figure 4-12 shows only about a 30% increase of the tropospheric

annular mode timescale at any time from its minimum value. However, the responses in Figure 4-11 vary through the year by larger amounts.

The other factor that could be playing a role in setting the surface response is the delay in Antarctic polar vortex breakdown. We have established earlier that the delayed tropospheric response to the stratospheric final warming does not explain observed surface trends. However, if the polar stratospheric cooling causes weak westerlies to exist at a time when easterlies were prevalent in the control run, according to the Charney-Drazin theorem, planetary scale waves are now permitted to propagate into the stratosphere for an additional period of time. This then permits EP flux divergence in the stratosphere to influence the tropospheric circulation for longer than in the control run. If the cooling due to ozone depletion makes the vortex stronger at its peak, rather than at the end of its lifetime, the increased westerlies, again in accordance with the Charney-Drazin theorem, might become strong enough to inhibit wave propagation. In the case of the run with cooling that peaks August 20, this factor might also play a role in the lack of a statistically significant surface response, since in this case the final warming is only delayed on the average by 6 days.

b. Responses to doubled cooling

In this section we present the model's responses to polar stratospheric cooling that is similar to equation (1), but now with $q_0 = -1K/day$, i.e. with double the magnitude of imposed cooling. All the previous model experiments (polar stratospheric cooling that peaks August 20, September 20, October 20, November 20 and with the cooling uniformly applied through the year) were run for 30 years with the doubled cooling. In this case, the temperature perturbations were sufficiently high to delay the final warming in all cases (as in shown in plots of the seasonal

cycle of 50 hPa zonal mean zonal winds comparing the control run to the perturbed runs in Figure 4-13). The model's 850 hPa zonal mean zonal wind responses are shown in Figures 4-14 to 4-18 for these runs.

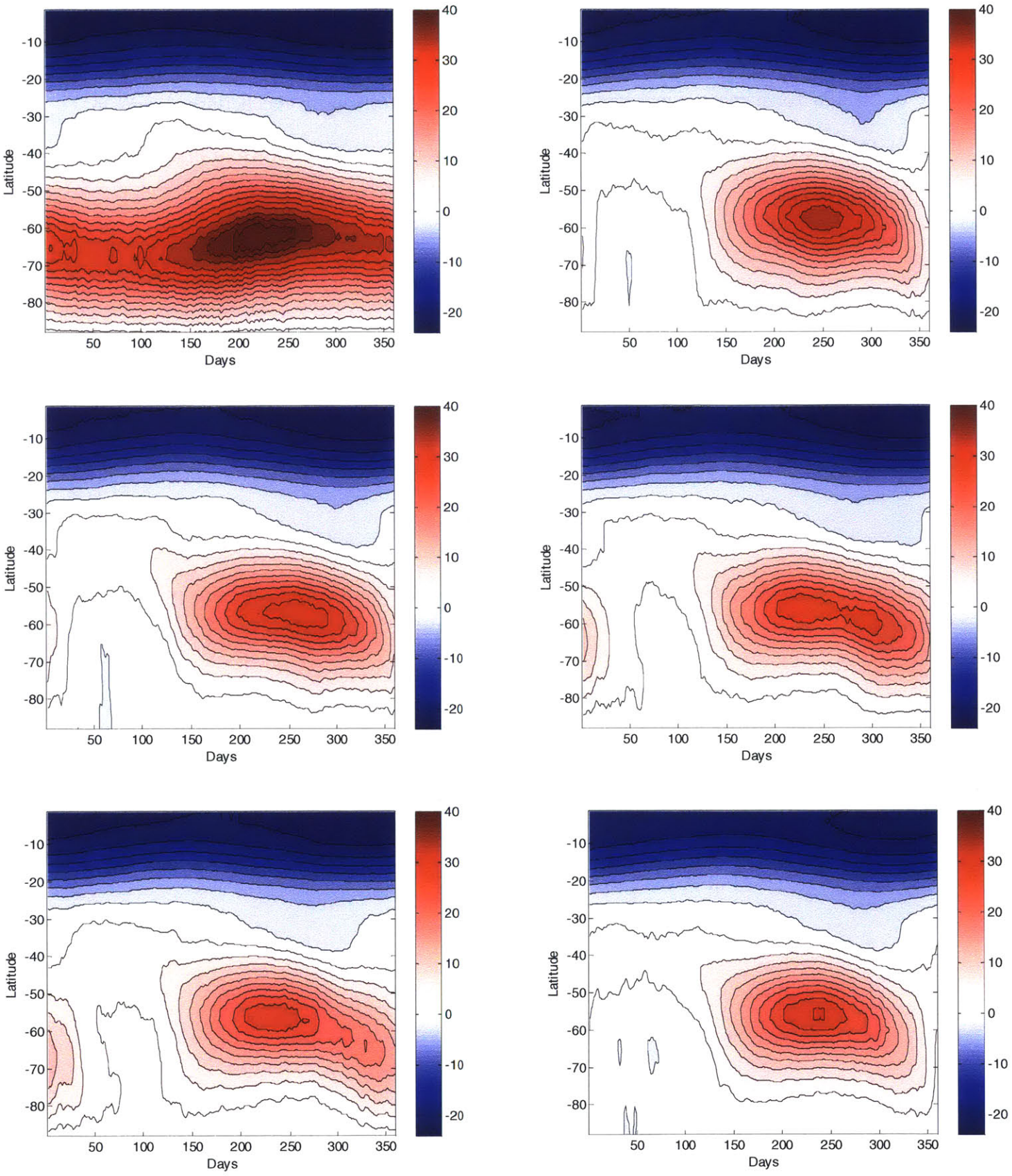

Figure 4-13: The seasonal cycle of 50 hPa zonal mean zonal winds for the model experiment with doubled cooling peaking (top row, left) all year around, (top row, right), August 20, (middle

row, left) September 20, (middle row, right), October 20, and (bottom row, left), November 20. The control run is shown in the right panel of the bottom row for comparison. The final warming is delayed in all the perturbed runs.

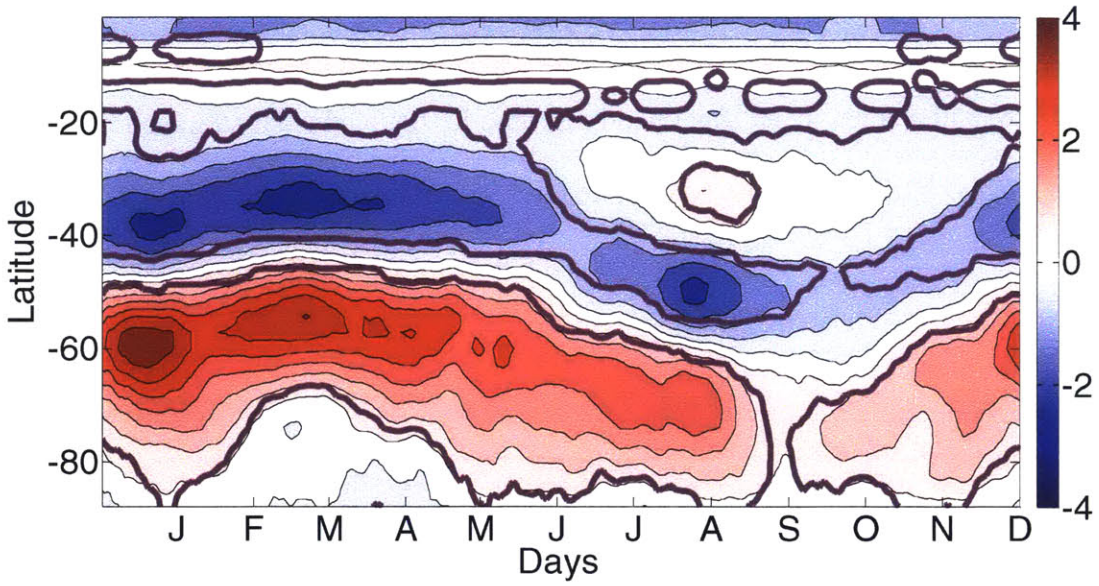

Figure 4-14: 850 hPa zonal mean zonal wind response for doubled polar stratospheric cooling uniformly applied through the entire year. The magenta contour denotes 95% statistical significance. The contour interval is 0.5 m/s.

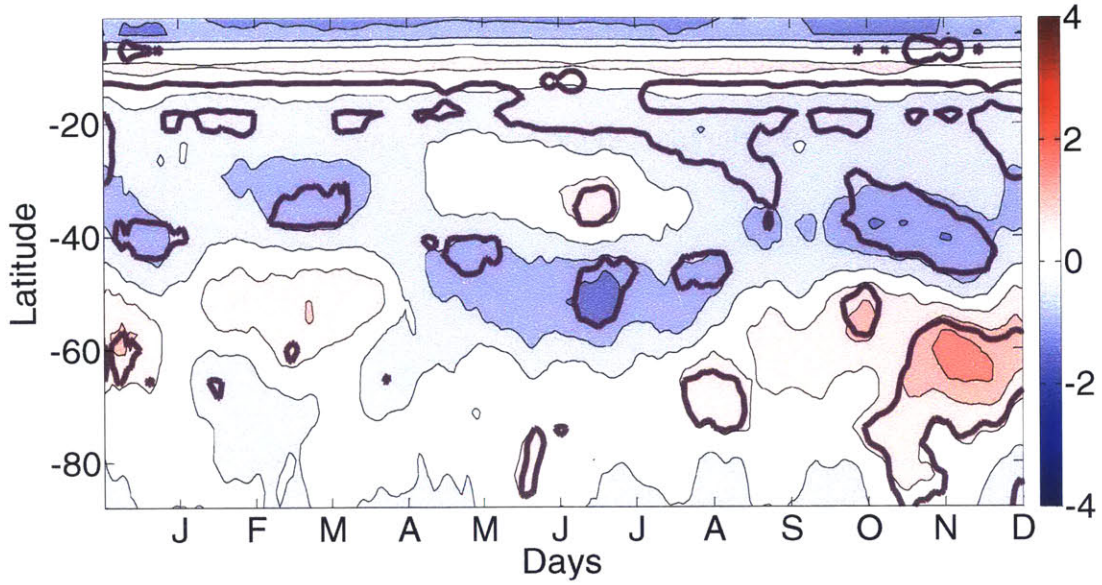

Figure 4-15: 850 hPa zonal mean zonal wind response for doubled polar stratospheric cooling that peaks August 20. The magenta contour denotes 95% statistical significance. The contour interval is 0.5 m/s.

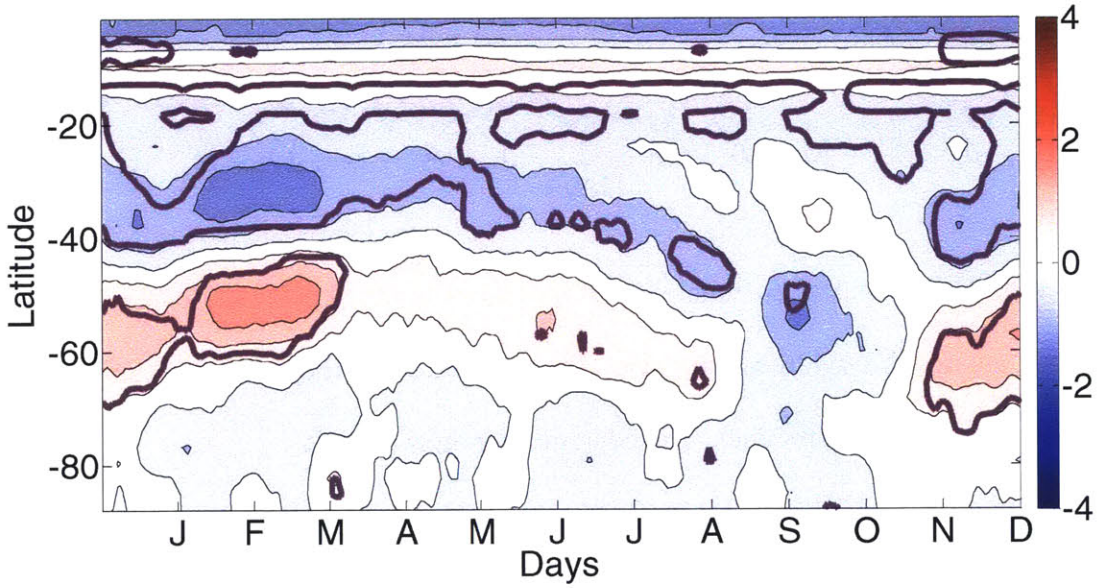

Figure 4-16: 850 hPa zonal mean zonal wind response for doubled polar stratospheric cooling that peaks September 20. The magenta contour denotes 95% statistical significance. The contour interval is 0.5 m/s.

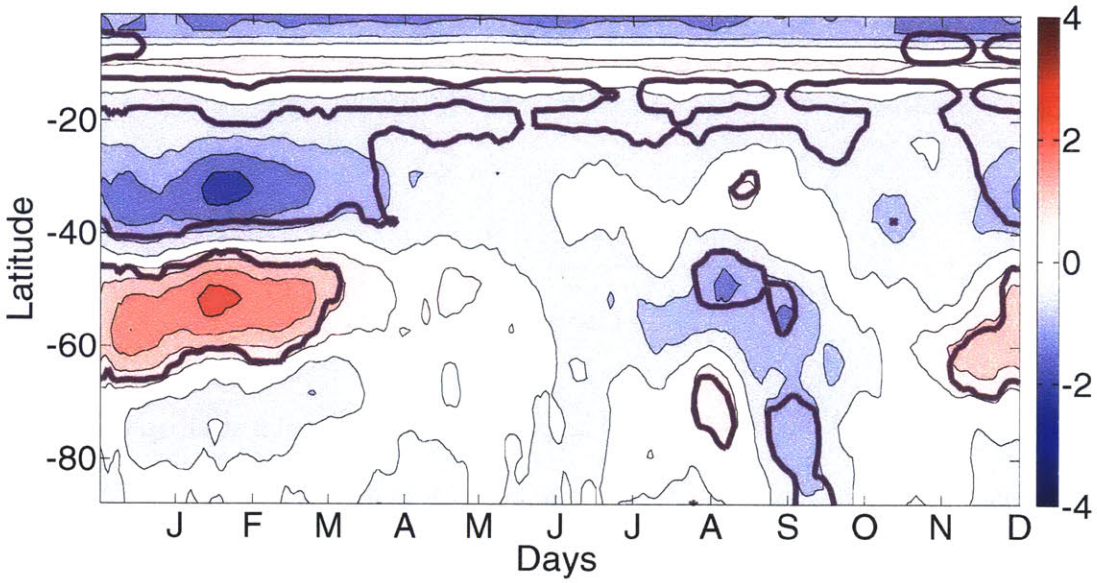

Figure 4-17: 850 hPa zonal mean zonal wind response for doubled polar stratospheric cooling that peaks October 20. The magenta contour denotes 95% statistical significance. The contour interval is 0.5 m/s.

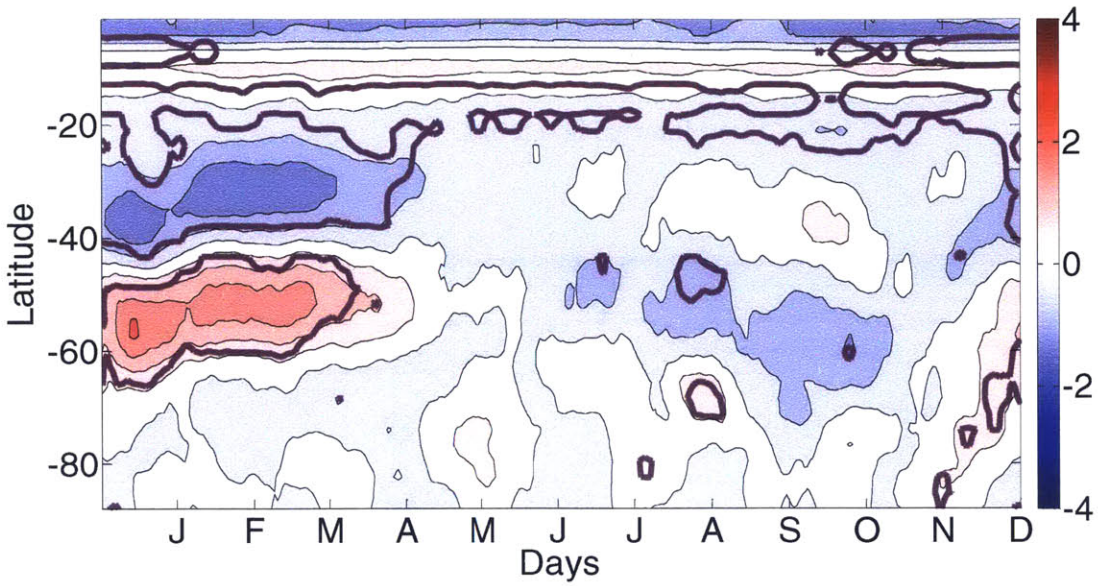

Figure 4-18: 850 hPa zonal mean zonal wind response for doubled polar stratospheric cooling that peaks November 20. The magenta contour denotes 95% statistical significance. The contour interval is 0.5 m/s.

Since the final warming is delayed in all cases, we would expect the surface response to be modified by the seasonal cycle of tropospheric annular mode timescales. There is a statistically significant 850 hPa wind response in all 5 cases. As we saw before, the surface response in the run with cooling applied uniformly through the year has a minimum corresponding to the annual minimum in tropospheric τ. In the cases with cooling peaking August 20, September 20, October 20, and November 20, the onset of the dipole surface response is delayed in time as the cooling peak shifts. In these model experiments as well, the minimum in τ might play a role in the lack of a surface response in the months of September and October. When the stratospheric cooling leads to a tropospheric response in the months of DJF (with the high annular mode timescales), we expect a larger and more persistent surface response. The statistically significant responses appear to terminate around April for the cases of cooling peaking September 20, October 20, and

November 20. The case with cooling all through the year appears to suggest that tropospheric responses to stratospheric cooling are somewhat linear – the changes in 850 hPa winds in Figure 4-14 are double the changes seen in Figure 4-11, and also have the same latitudinal structure.

4.4. Conclusions

We have used an idealized model to investigate the factors that play a role in setting surface responses to polar stratospheric cooling that is meant to mimic the radiative effects of polar stratospheric ozone depletion. We found that there are certain configurations of the model (determined by ε, the asymmetry parameter) in which the tropospheric annular mode timescale is so unrealistically long that any annually repeating lower stratospheric perturbation results in a tropospheric circulation change that lasts throughout the year. After carrying out a series of experiments sweeping through different values of ε, we found an 'optimal' value (in the range considered), that lowered the tropospheric annular mode timescale to one that is similar to what it is in the observed atmosphere. In this new model setup, we experimented with imposed polar stratospheric cooling that peaks at different times in the seasonal cycle of the polar vortex. We found that the surface response to polar stratospheric cooling can be related to the model's tropospheric annular mode timescale – a perturbation that tends to cause a response at times when τ is high produces a response that is both larger in magnitude and more persistent, and vice versa. We also found that there might be a potential link between the extended lifetime of the vortex and the surface response, not as a consequence of the delayed tropospheric response to the vortex breakdown, but simply because the polar stratospheric cooling causes westerlies to exist at a time when easterlies were prevalent, allowing wave propagation into the stratosphere. In such a situation, if the magnitude of the imposed cooling is increased, the tail of the cooling

might be sufficient to extend the vortex lifetime (i.e. there might be a threshold past which a surface response would be expected).

5. Summary and future work

In this thesis, I have studied a number of problems involving the variability of the stratospheric polar vortex and the effects of this variability on tropospheric weather and climate patterns on various timescales, ranging from weekly to intra-seasonal and interannual. In chapter 2, an improved idealized model setup that includes a seasonal cycle in equilibrium temperatures that is confined to the stratosphere was developed. This model setup enabled the study of stratosphere-troposphere coupling on seasonal timescales, without the complication of an internal tropospheric seasonal cycle. This setup was used with varying wavenumbers and heights of bottom topography to investigate the effects of changing tropospheric wave forcing on the seasonal variability in the strength of the polar vortex. With appropriate choices of the wavenumber and height of topography, the model is able to reproduce observed differences in the climatology and variability of the Arctic and Antarctic vortices. This setup also enabled us to establish that the stratospheric seasonal cycle has a continuous effect on the tropospheric jet, in addition to the more localized (in time) tropospheric impacts of 'events' such as sudden warming and final warming events. This model setup with a seasonal cycle also enabled the study of another aspect of the stratosphere – the question of whether it is any interannual, winter-to-winter memory. We found that while there might possibly be some evidence for interannual memory in the observed Arctic stratosphere, the model does not show any such evidence, indicating that such 'memory' might arise in the real stratosphere from factors that are external to the stratosphere, such as sea surface temperatures. An open question that might be a fruitful topic for future research is the distribution of the occurrence of sudden warming events, considered in Chapter 2. Why was there a 'hiatus' in sudden warming events in the 1990s (this hiatus might, however, be sensitive to how sudden warming events are defined – a definition

based on wind reversal at 65°N instead of 60°N does not lead to an 8 year gap without warmings in the 90s (Butler et al. 2015)), and are such long gaps without events present in full GCMs? Work intended to address these questions is planned in the immediate future.

This model setup is likely to prove a useful tool in the future to study the coupled stratosphere-troposphere system, and its response to forcing. Indeed, it is currently being used by two other students to study the problems of the relationship between the "age" of air and the residual circulation, and the communication of low latitude upper stratospheric temperature perturbations induced by the solar cycle to the tropospheric circulation and to the earth's surface.

In Chapters 3 and 4, a problem involving polar vortex variability on the timescale of decades and its impacts on tropospheric circulation trends was studied. The structure and dynamics of the Antarctic vortex enable the occurrence of temperatures that are low enough to allow for PSC formation, and ozone depletion. The Antarctic ozone hole is widely regarded as having been the primary driver of Southern Hemisphere tropospheric circulation trends over the last few decades, including effects on the atmosphere, ocean and sea ice. Changes to the variability of the Antarctic polar vortex are the first links in this chain of impacts on the climate system. Firstly, we have shown that the surface wind trends cannot be explained as being a simple consequence of the delay in Antarctic polar vortex breakdown. Secondly, we have shown that there are two potential factors that might play a role in setting a model's surface response to the polar stratospheric cooling induced by ozone depletion. The model's surface response at a given time of the year is determined by the model's tropospheric annular mode timescale at that time of year. Additionally, we found that the presence or absence of stratospheric westerlies might play a role in determining the surface response, not because of the delayed tropospheric response to the final warming, but simply because wave propagation is permitted when there are weak

westerlies. Therefore, if observed ozone depletion is put into a full GCM in which the vortex breakdown occurs later than in the observed Antarctic stratosphere (some models do exhibit this bias), the model might not show surface climate responses that match observations.

There is also a great deal of interest in how the polar vortices will respond to increasing concentrations of greenhouse gases, and would be a topic of possible future research. In addition, in the near future, the concentrations of ozone depleting substances are expected to decrease back to what they were around 1960, which would counteract the expected warming trends in the Antarctic polar stratosphere with ozone recovery. However, increases in greenhouse gas concentrations would lead to changes in tropospheric wave generation and propagation. Forcing the model with small differences in the equilibrium temperature distribution in the troposphere and stratosphere might lead to insights on the dynamical changes to the coupled stratosphere-troposphere system that this radiative forcing might bring about.

Martius et al. (2009) showed a close connection between atmospheric blocking and stratospheric sudden warming events. Hassanzadeh et al. (2014) showed the occurrence of atmospheric blocking in an idealized Held Suarez setup without a stratosphere. Future work is planned to study in our model (described in Chapter 2), the link between the strength and variability of the polar vortex and atmospheric blocking. This has implications for a stratospheric connection to midlatitude extreme weather events. In general, research has shown that variability in the polar stratospheric vortices, including SSWs is linked to wave activity, but the relative contributions from tropospheric, stratospheric, and coupled processes are not well understood. In addition, Esler and Scott (2005), and Esler et al. (2006) suggest that the resonant excitation of free modes, rather than upward propagating Rossby waves, play a major role in SSWs. This remains an open question.

Given the many outstanding issues, there is need for further research into what sets the dynamics and variability of the polar stratospheric vortices, and their representation in global climate models.

6. References

Ambaum, M. H. P., and B. J. Hoskins, 2002: The NAO troposphere– stratosphere connection, *J. Clim.,* **15**, 1969–1978.

Andrews, D. G., J. R. Holton, and C. B. Leovy, 1987: Middle Atmosphere Dynamics, 489 pp., Academic, San Diego, Calif.

Archer, C. L., and K. Caldeira, 2008: Historical trends in the jet streams, *Geophys. Res. Lett.,* **35**, L08803, doi:10.1029/2008GL033614.

Baldwin, M. P., and T. J. Dunkerton, 1999: Propagation of the Arctic Oscillation from the stratosphere to the troposphere, *J. Geophys. Res.*, **104**(D24), 30937–30946.

Baldwin, M.P. and T.J. Dunkerton, 2001: Stratospheric harbingers of anomalous weather regimes, *Science,* **244**, 581-584.

Baldwin, M. P., D. B. Stephenson, D. W. J. Thompson, T. J. Dunkerton, A. J. Charlton, and A. O'Neill, 2003: Stratospheric memory and skill of extended-range weather forecasts, *Science*, **301,** 636–640.

Baldwin, M., T. Hirooka, A. O'Neill, S. Yoden, A. J. Charlton, Y. Hio, W. A. Lahoz, and A. Mori, 2003: Major stratospheric warming in the Southern Hemisphere in 2002: Dynamical aspects of the ozone hole split, *SPARC newsletter,* **20**, 24-26.

Black, R. X., 2002: Stratospheric forcing of surface climate in the Arctic Oscillation, *J. Clim.*, **15**, 268–277.

Black, R. X., B. A. McDaniel, and W. A. Robinson, 2006: Stratosphere–Troposphere Coupling during Spring Onset. *J. Clim.*, **19**, 4891–4901.

Black, R. X. and B. A. McDaniel, 2007a: The Dynamics of Northern Hemisphere Stratospheric Final Warming Events. *J. Atmos. Sci.*, **64**, 2932–2946.

Black, R. X., and B. A. McDaniel, 2007b: Interannual variability in the Southern Hemisphere circulation organized by stratospheric final warming events. *J. Atmos. Sci.*, **64**, 2968–2974.

Black, R.X., B.A. McDaniel, and W.A. Robinson, 2006: Stratosphere–Troposphere Coupling during Spring Onset. *J. Clim.*, **19**, 4891–4901.

Butler, A. H., D. W. J. Thompson, and R. Heikes, 2010: The Steady-State Atmospheric Circulation Response to Climate Change–like Thermal Forcings in a Simple General Circulation Model. *J. Clim.*, **23**, 3474–3496.

Butler, A., D. Seidel, S. Hardiman, N. Butchart, T. Birner, and A. Match, 2015: Defining sudden stratospheric warmings. *Bull. Amer. Meteor. Soc.,* doi:10.1175/BAMS-D-13-00173.1, in press.

Chan, C. J., and R. A. Plumb, 2009: The response of the troposphere to stratospheric perturbations and its dependence on the state of the troposphere, *J. Atmos. Sci.*, **66**, 2107-2115.

Charlton, A. J., A. O'Neill, W. A. Lahoz, and A. C. Massacand (2004), Sensitivity of tropospheric forecasts to stratospheric initial conditions, *Q. J. R. Meteorol. Soc.*, **130**, 1771–1792.

Charlton, A. J. and L.M. Polvani, 2007: A new look at stratospheric sudden warmings. Part I. Climatology and modeling benchmarks, *J. Clim.*, **20**, 449-469.

Charlton, A. J., L.M. Polvani, J. Perlwitz, F. Sassi, E. Manzini, S. Pawson, J.E. Nielsen, K. Shibata, and D. Rind, 2007: A new look at stratospheric sudden warmings. Part II. Evaluation of numerical model simulations, *J. Clim.*, **20**, 470-488.

Chen, G., and I. M. Held, 2007: Phase speed spectra and the recent poleward shift of Southern Hemisphere surface westerlies, *Geophys. Res. Lett.*, **34**, L21805, doi:10.1029/2007GL031200.

Christiansen, B., 2000: A model study of the dynamical connection between the Arctic Oscillation and stratospheric vacillations. *J. Geophys. Res.*, **105**, 29 461–29 474.

Charney, J. G., and P. G. Drazin, 1961: Propagation of planetary-scale disturbances from the lower into the upper atmosphere, *J. Geophys. Res.*, **66**,83-109.

Coughlin, K., and L. J. Gray, 2009: A Continuum of Sudden Stratospheric Warmings. *J. Atmos. Sci.*, **66**, 531–540.

Dee, D. P., Uppala, S. M., Simmons, A. J., Berrisford, P., Poli, P., Kobayashi, S., Andrae, U., Balmaseda, M. A., Balsamo, G., Bauer, P., Bechtold, P., Beljaars, A. C. M., van de Berg, L., Bidlot, J., Bormann, N., Delsol, C., Dragani, R., Fuentes, M., Geer, A. J., Haimberger, L., Healy, S. B., Hersbach, H., Hólm, E. V., Isaksen, L., Kållberg, P., Köhler, M., Matricardi, M., McNally, A. P., Monge-Sanz, B. M., Morcrette, J.-J., Park, B.-K., Peubey, C., de Rosnay, P., Tavolato, C., Thépaut, J.-N. and Vitart, F. (2011), The ERA-Interim reanalysis: configuration and performance of the data assimilation system *Quart. J. Roy. Meteor. Soc.*, **137**: 553–597.

Eyring, V., T. G. Shepherd and D. W. Waugh (Eds.), 2010: SPARC CCMVal, SPARC report on the evaluation of chemistry climate models, SPARC report No. 5, WCRP-132, WMO/TD-No 1526.

Esler, J. G., and R. K. Scott, 2005: Excitation of Transient Rossby Waves on the Stratospheric Polar Vortex and the Barotropic Sudden Warming. *J. Atmos. Sci.*, **62**, 3661–3682.

Esler, J. G., L. M. Polvani, R. K. Scott, 2006: The Antarctic stratospheric sudden warming of 2002: A self-tuned resonance? *Geophy. Res. Lett.* **33,** L12804.

Fogt, R. L., J. Perlwitz, A. J. Monaghan, D. H. Bromwich, J. M. Jones, & J.G. Marshall, 2009: Historical SAM Variability. Part II: Twentieth-Century Variability and Trends from Reconstructions, Observations, and the IPCC AR4 Models. *J. Clim.*, **22**(20), 5346-5365.

Hartmann, D. L., J. M.Wallace, V. Limpasuvan, D.W. J. Thompson, and J. R. Holton, 2000: Can ozone depletion and global warming interact to produce rapid climate change?, *Proc. Nat. Acad. Sci. U. S. A.*, **97**, 1412–1417.

Holton, J. R., and C. Mass, 1976: Stratospheric vacillation cycles, *J. Atmos. Sci.*, **33**, 2218-2225.

Hu, J., R. Ren, and H. Xu, 2014a: Occurrence of Winter Stratospheric Sudden Warming Events and the Seasonal Timing of Spring Stratospheric Final Warming. *J. Atmos. Sci.*, **71**, 2319–2334.

Hu, J., R. Ren, Y. Yu, and H. Xu, 2014b: The boreal spring stratospheric final warming and its interannual and interdecadal variability, *Sci. China Ser. C.*, **57**, 710-718.

Gerber E. P. and G. K. Vallis, 2007: Eddy-zonal flow interactions and the persistence of the zonal index, *J. Atmos. Sci.*, **64**, 3296-3311.

Gerber, E. P., S. Voronin, and L. M. Polvani, 2008: Testing the annular mode autocorrelation timescale in simple atmospheric general circulation models. *Mon. Wea. Rev.*, **136**, 1523-1536.

Gerber, E.P. and L.M. Polvani, 2009: Stratosphere-troposphere coupling in a relatively simple AGCM: The importance of stratospheric variability, *J. Clim.*, **22**, 1920-1933.

Gillett, N., and D.W.J. Thompson, 2003: Simulation of recent Southern Hemisphere climate change. *Science*, **302**, 273-275.

Gray, L. J., Sparrow, S., Juckes, M., O' Neill, A. and Andrews, D. G., 2003: Flow regimes in the winter stratosphere of the northern hemisphere. *Quart. J. Roy. Meteor. Soc.*,**129**: 925–945.

Hardiman, S.C., et al. 2011: Improved Predictability of the troposphere using stratospheric final warmings, *J.Geophys. Res.*, **116**, D18113.

Hartley, D. E., J. T. Villarin, R. X. Black, and C. A. Davis, 1998: A new perspective on the dynamical link between the stratosphere and troposphere, *Nature*, **391**, 471–474.

Hassanzadeh, P., Z. Kuang, and B. F. Farrell, 2014: Responses of midlatitude blocks and wave amplitude to changes in the meridional temperature gradient in an idealized dry GCM, *Geophys. Res. Lett.*, **41**, 5223–5232, doi:10.1002/2014GL060764.

Haynes, P. H., C. J. Marks, M. E. McIntyre, T. G. Shepherd, and K. P. Shine, 1991: On the "downward control" of extratropical diabatic circulations by eddy-induced mean zonal forces, *J. Atmos. Sci.*, **48**, 651–678.

Hung, H. Y. and E. P. Gerber, 2013: An improved idealized atmospheric model for the study of the stratosphere-troposphere system, Poster at the 17th Conf. on the Middle Atmosphere, Newport, RI, *Amer. Meteor. Soc.*

Keeble, J., P. Braesicke, N. L. Abraham, H. K. Roscoe, and J. A. Pyle: The impact of polar stratospheric ozone loss on Southern Hemisphere stratospheric circulation and climate, *Atmos. Chem. Phys.*, **14**, 13705-13717, doi:10.5194/acp-14-13705-2014, 2014.

Kushner, P. J., and L.M. Polvani, 2004: Stratosphere-troposphere coupling in a relatively simple AGCM: The role of eddies, *J. Clim.*, **17**, 629-639.

Kushner, P.J. and L.M. Polvani, 2005: A very large, spontaneous stratospheric sudden warming in a simple AGCM: A prototype for the Southern-Hemisphere warming of 2002? *J. Atmos. Sci.*, **62**, 890–897.

Kushner, P. J. and L.M. Polvani, 2006: Stratosphere-troposphere coupling in a relatively simple AGCM: Impact of the seasonal cycle, *J. Clim.*, **19**, 5721-5727.

Kushner, P. J., 2010: Annular modes of the troposphere and stratosphere, in "The Stratosphere: Dynamics, Transport and Chemistry. A festschrift celebrating Alan Plumb's 60th birthday", L.M. Polvani, A.H. Sobel and D.W. Waugh, Eds., American Geophysical Union, Washington, D.C.

Krüger, K., B. Naujokat, K. Labitzke, 2005: The Unusual Midwinter Warming in the Southern Hemisphere Stratosphere, 2002: A Comparison to Northern Hemisphere Phenomena. *J. Atmos. Sci.*, **62**, 603–613.

Lindzen, R. S., and M. R. Schoeberl, 1982: A note on the limits of Rossby wave amplitudes. *J. Atmos. Sci.*, **39,** 1171–1174.

Limpasuvan, V., D. W. J. Thompson, and D. L. Hartmann, 2004: The Life Cycle of the Northern Hemisphere Sudden Stratospheric Warmings. *J. Clim.*, **17**, 2584–2596.

Limpasuvan, V., D. L. Hartmann, D. W. J. Thompson, K. Jeev, and Y. L. Yung, 2005: Stratosphere-troposphere evolution during polar vortex intensification, *J. Geophys. Res.*, **110**, D24101.

Manney, G. L., K. Kruger, J. L. Sabutis, S. A. Sena, and S. Pawson, 2005: The remarkable 2003-2004 winter and other recent warm winters in the Arctic stratosphere since the late 1990s, *J. Geophys. Res.*, **110**, doi: 10.1029/2004JD005367.

Martius, O., L. M. Polvani, and H. C. Davies, 2009: Blocking precursors to stratospheric sudden warming events, *Geophys. Res. Lett.*, **36**, L14806, doi:10.1029/2009GL038776.

Matsuno, T., 1970: Vertical propagation of stationary planetary waves in the winter northern hemisphere, *J. Atmos. Sci.*, **27**, 871–883.

Matsuno, T., 1971: A dynamical model of the stratospheric sudden warming, *J. Atmos. Sci.*, **28**, 1479-1494.

Matthewman, N. J., J. G. Esler, A. J. Charlton-Perez, and L. M. Polvani, 2009: A new look at stratospheric sudden warmings. Part III: Polar vortex evolution and vertical structure. *J. Clim.*, **22**, 1566–1585.

McIntyre, M. E., 1982: How well do we understand the dynamics of stratospheric warmings? *J. Meteorol. Soc. Japan.*, **60**, 37-65.

McIntyre, M. E., and T. N. Palmer, 1983: Breaking planetary waves in the stratosphere, *Nature*, **305**, 593-594.

McIntyre, M. E., and T. N. Palmer, 1984: The 'surf zone' in the stratosphere, *J. Atmos. Terr. Phys.*, **46**, 825-849.

Naujokat, B., 1981: Long-term variations in the stratosphere of the northern hemisphere during the last two sunspot cycles, *J. Geophys. Res.*, **86**(C10), 9811–9816.

Newman, P. A., E.R. Nash, 2005: The Unusual Southern Hemisphere Stratosphere Winter of 2002. *J. Atmos. Sci.*, **62**, 614–628.

Newman, P. A., 2010: Chemistry and dynamics of the Antarctic ozone hole, in "The Stratosphere: Dynamics, Transport and Chemistry. A festschrift celebrating Alan Plumb's 60th birthday", L.M. Polvani, A.H. Sobel and D.W. Waugh, Eds., American Geophysical Union, Washington, D.C.

O'Neill, A., and V. D. Pope, 1988: Simulations of linear and nonlinear disturbances in the stratosphere, *Q. J. R. Meteorol. Soc.*, **114**, 1063–1110.

Perlwitz, J., and N. Harnik, 2004: Downward coupling between the stratosphere and troposphere: The relative roles of wave and zonal mean processes, *J. Clim.*, **17**, 4902–4909.

Polvani, L.M. and P.J. Kushner, 2002: Tropospheric response to stratospheric perturbations in a relatively simple general circulation model, *Geophys. Res. Lett.*, **29**, doi: 10.129/2001GL014284.

Polvani L.M., and D. W. Waugh, Upward Wave Activity Flux as Precursor to Extreme Stratospheric Events and Subsequent Anomalous Surface Weather Regimes , *J. Clim.*, **17**, 3548-3554, 2004.

Polvani, L. M., Waugh, D. W., Correa, G. J. P. & Son, S-W, 2011: Stratospheric ozone depletion: The main driver of 20th century atmospheric circulation changes in the Southern Hemisphere. *J. Clim.*, **24**,795–812.

Plumb, R. A., 1981: Instability of the distorted polar night vortex: A theory of stratospheric warmings, *J. Atmos. Sci.*, **38**, 2514–2531.

Plumb, R. A., 1989: On the seasonal cycle of stratospheric planetary waves. *Pure Appl. Geophys.*, **130**, 233–242.

Plumb, R. A., 2010: Planetary waves and the extratropical winter stratosphere, in "The Stratosphere: Dynamics, Transport and Chemistry. A festschrift celebrating Alan Plumb's 60th birthday", L.M. Polvani, A.H. Sobel and D.W. Waugh, Eds., American Geophysical Union, Washington, D.C.

Ring, M. J., and R. A. Plumb, 2008: The response of a simplified GCM to axisymmetric forcings: applicability of the fluctuation-dissipation theorem, *J. Atmos. Sci.*, **65**, 3880–3898.

Rong, R. R., and D.W.Waugh, 2003: Vacillations in a shallow water model of the stratosphere, *J. Atmos. Sci.*, **61**, 1174–1185.

Scherhag, R., 1952: Die explosionsartigen Stratosparenerwarmungen des Spatwinters 1952. *Ber Det Wetterdienstes US Zone*, **38**, 51–63.

Schoeberl, M. R., 1982: Vacillation, sudden warmings, and potential enstrophy balance in the stratosphere. *J. Atmos. Sci.*, **39,** 1862–1872.

Scinocca, J. F., and Haynes, P. H., 1998: Dynamical forcing of stratospheric waves by tropospheric baroclinic eddies. *J. Atmos. Sci.*, **55**, 2361-2392.

Scott, R. K., and D. G. Dritschel, 2006: Vortex-vortex interactions in the winter stratosphere, *J. Atmos. Sci.*, **63**, 726–740.

Scott, R. K., and P. H. Haynes, 1998: Internal interannual variability of the extratropical stratospheric circulation: The low-latitude flywheel. *Quart. J. Roy. Meteor. Soc.*, **124**, 2149–2173.

Scott, R. K., and P. H. Haynes, 2000: Internal vacillations in stratospheric-only models, *J. Atmos. Sci.*,**57**,3233–3250.

Scott, R. K., and P. H. Haynes, 2002: The seasonal cycle of planetary waves in the winter stratosphere. *J. Atmos. Sci.*, **59**, 803–822.

Scott, R. K., and L.M. Polvani, 2004: Stratospheric control of upward wave flux near the tropopause, *Geophys. Res. Lett.*, **31**, L02115.

Scott, R. K., and L.M. Polvani, 2006: Internal variability of the winter stratosphere. Part I: Time-independent forcing, *J. Atmos. Sci.*, **63**, 2758-2776.

Sheshadri, A., R. A. Plumb, and D. I. V. Domeisen, 2014: Can the delay in Antarctic polar vortex breakup explain recent trends in surface westerlies? *J. Atmos. Sci.*, **71**, 566–573.

Sheshadri, A., R. A. Plumb, and E. P. Gerber, 2015: Seasonal variability of the polar stratospheric vortex in an idealized AGCM with varying tropospheric wave forcing, *J. Atmos. Sci.*, in press, doi: 10.1175/JAS-D-14-0191.1.

Sigmond, M., and J. C. Fyfe, 2014: The Antarctic Sea Ice Response to the Ozone Hole in Climate Models. *J. Clim.*, **27**, 1336–1342.

Son, S.-W., L. M. Polvani, D. W. Waugh, H. Akiyoshi, R. Garcia, D. Kinnison, S. Pawson, E. Rozanov, T. G. Shepherd, and K. Shibata, 2008: The impact of stratospheric ozone recovery on the Southern Hemisphere westerly jet, *Science*, **320**, 1486– 1489.

Song, Y., and W. A. Robinson, 2004: Dynamical mechanisms for stratospheric influences on the troposphere. *J. Atmos. Sci.*, **61**, 1711-1725.

Solomon, S., 1999: Stratospheric ozone depletion: A review of concepts and history, *Rev. Geophys.*, **37**, 275–316.

Sun, L., and W. A. Robinson, 2009: Downward influence of stratospheric final warming events in an idealized model. *Geophys. Res. Lett.*, **36**, L03819, doi:10.1029/2008GL036 624.

Sun, L., W. A. Robinson and G. Chen, 2011: The Role of Planetary Waves in the Downward Influence of Stratospheric Final Warming Events. *J. Atmos. Sci.*, **68**, 2826–2843.

Sun, L., W. A. Robinson and G. Chen, 2012: The Predictability of Stratospheric Warming Events: More from the Troposphere or the Stratosphere?, *J. Atmos. Sci.*, **69**, 768–783.

Sun, L., G. Chen, and W. A. Robinson, 2014: The role of stratospheric polar vortex breakdown in Southern Hemisphere climate trends, *J. Atmos. Sci.*, **71**, 2335-2353.

Taguchi, M., T. Yamaga, and S. Yoden, 2001: Internal variability of the troposphere–stratosphere coupled system simulated in a simple global circulation model. *J. Atmos. Sci.*, **58**, 3184–3203.

Taguchi, M., and S. Yoden, 2002: Internal Interannual Variability of the Troposphere–Stratosphere Coupled System in a Simple Global Circulation Model. Part I: Parameter Sweep Experiment. *J. Atmos. Sci.*, **59**, 3021–3036.

Thompson, D.W.J., and J.M. Wallace, 1998: The Arctic Oscillation signature in the wintertime geopotential height and temperature fields, *Geophys. Res. Lett.*, **25**, 1297-1300.

Thompson, D.W.J., and J.M. Wallace, 2000: Annular modes in the extratropical circulation. Part I: Month-to-month variability, *J. Clim.*, **13**, 1000-1016.

Thompson, D. W. J. & S. Solomon, 2002: Interpretation of recent Southern Hemisphere climate change. *Science,* **296**, 895–899.

Thompson, D.W.J., J.M. Wallace, and G. C. Hegerl, 2000: Annular modes in the extratropical circulation: Part II: Trends. *J. Clim.*, **13**, 1018-1036.

Thompson, D. W. J., M.P. Baldwin & S. Solomon, 2005: Stratosphere–troposphere coupling in the Southern Hemisphere. *J. Atmos. Sci.*, **62**, 708–715.

Thompson, D. W. J., J.C. Furtado, and T. G. Shepherd, 2006: On the Tropospheric Response to Anomalous Stratospheric Wave Drag and Radiative Heating. *J. Atmos. Sci.*, **63**, 2616–2629.

Thompson, D.W.J., S. Solomon, P.J. Kushner, M.H. England, K.M. Grise and D.J. Karoly, 2011: Signatures of the Antarctic ozone hole in Southern Hemisphere surface climate change. *Nature Geoscience* **4**(11), 741-749.

Tung, K. K., and R. S. Lindzen, 1979: A theory of stationary long waves. Part II: Resonant Rossby waves in the presence of realistic vertical shears, *Mon. Weather Rev.*, **107**, 735–750.

Uppala, S. M., KÅllberg, P. W., Simmons, A. J., Andrae, U., Bechtold, V. D. C., Fiorino, M., Gibson, J. K., Haseler, J., Hernandez, A., Kelly, G. A., Li, X., Onogi, K., Saarinen, S., Sokka, N., Allan, R. P., Andersson, E., Arpe, K., Balmaseda, M. A., Beljaars, A. C. M., Berg, L. V. D., Bidlot, J., Bormann, N., Caires, S., Chevallier, F., Dethof, A., Dragosavac, M., Fisher, M., Fuentes, M., Hagemann, S., Hólm, E., Hoskins, B. J., Isaksen, L., Janssen, P. A. E. M., Jenne, R., Mcnally, A. P., Mahfouf, J.-F., Morcrette, J.-J., Rayner, N. A., Saunders, R. W., Simon, P., Sterl, A., Trenberth, K. E., Untch, A., Vasiljevic, D., Viterbo, P. and Woollen, J. (2005), The ERA-40 re-analysis. *Quart. J. Roy. Meteor. Soc.*, **131**: 2961–3012.

Vallis, G. K., 2006: Atmospheric and Oceanic Fluid Dynamics, Cambridge University Press, 745 pp.

Waugh, D. W., 1997: Elliptical diagnostics of stratospheric polar vortices, *Quart. J. Roy. Meteor. Soc.*, **123**, 1725–1748.

Waugh, D.W. and L.M. Polvani, 2010: Stratospheric Polar Vortices, in "The Stratosphere: Dynamics, Transport and Chemistry. A festschrift celebrating Alan Plumb's 60th birthday", L.M. Polvani, A.H. Sobel and D.W. Waugh, Eds., American Geophysical Union, Washington, D.C.

Waugh, D.W., W. J. Randel, S. Pawson, P. A. Newman, and E. R. Nash, 1999: Persistence of the lower stratospheric polar vortices. *J. Geophys. Res.,* **104,** 27 191–27 202.

Waugh, D. W., and P. P. Rong, 2002: Interannual variability in the decay of lower stratospheric Arctic vortices, *J. Meteorol. Soc. Jpn.*, **80**, 997–1012.

Yoden, S., 1987: Dynamical aspects of stratospheric vacillations in a highly truncated model, *J. Atmos. Sci.,* **44**, 3683–3695.

Yoden, S., 1990: An Illustrative Model of Seasonal and Interannual Variations of the Stratospheric Circulation. *J. Atmos. Sci.*, **47**, 1845–1853.

Yoden, S., M. Taguchi, and Y. Naito, 2002: Numerical studies on time variations of the troposphere- stratosphere coupled system. *J. Met. Soc. Japan*, **80**, 811–830.